Shadows at the Galactic Center and at M87* as a tool to test gravity theories
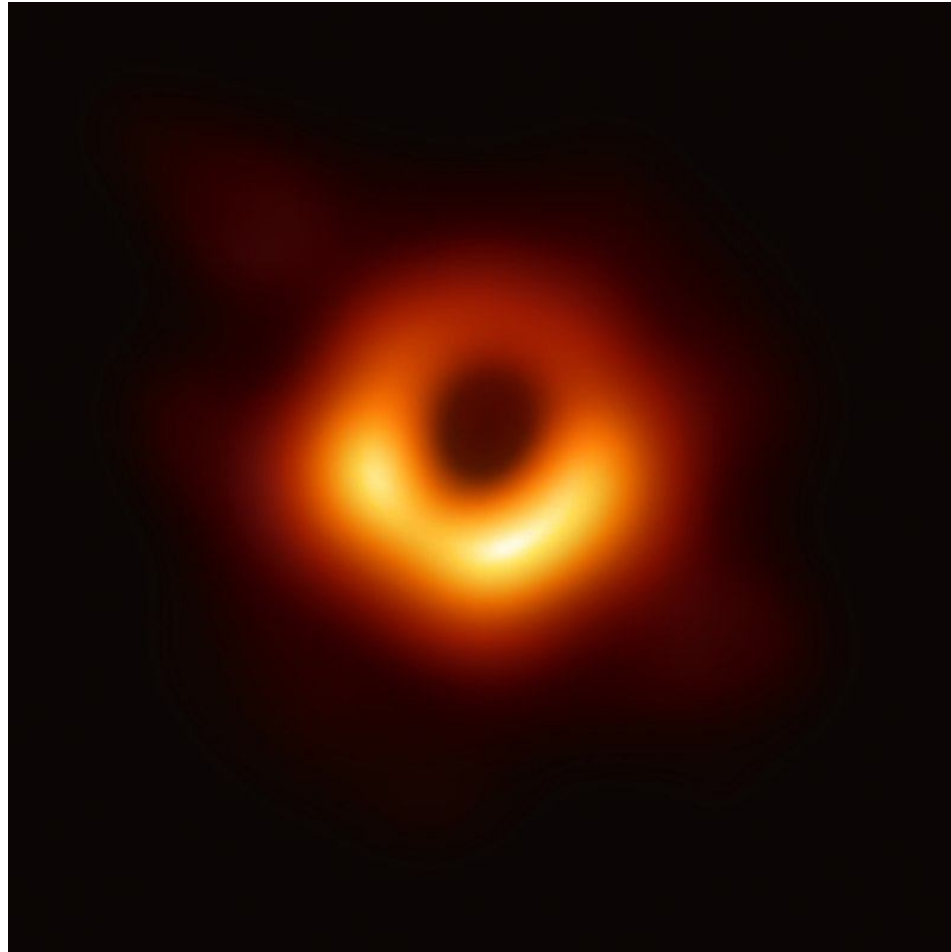
Александр Ф. Захаров (Alexander F. Zakharov)
E-mail: zakharov@itep.ru

Bogoliubov Laboratory of Theoretical Physics
Joint Institute for Nuclear Research, Dubna, Russia

05.11.2021

online ICRANet-Isfahan Astronomy Meeting

EHT shadow reconstruction for M87*

The EHT shadow as BH logo

Key References

- AFZ, F. De Paolis, G. Ingrosso, and A. A. Nucita, New Astronomy 10 (2005) 479.

- AFZ, F. De Paolis, G. Ingrosso, and A. A. Nucita, Astronomy & Astrophys. 442, 795 (2005).

- AFZ, F. De Paolis, G. Ingrosso, and A. A. Nucita, New Astronomy Reviews, **56**, 64 (2012).

- AFZ, Physical Reviews D **90**, 062007 (2014).

- AFZ, arxiv:2108.01533

Outline of my talk

- Introduction
- Shadows for Kerr metric as a tool to evaluate BH characteristics
- Shadows around Reissner-Nordstrom BHs
- The first image of shadow at M87*
- Dependence of shadow size on charge
- Conclusions

- Three basic pillars for M87* picture
- Synchrotron emission
- VLBI observations
- BH geometry (GR in a strong gravitational field)
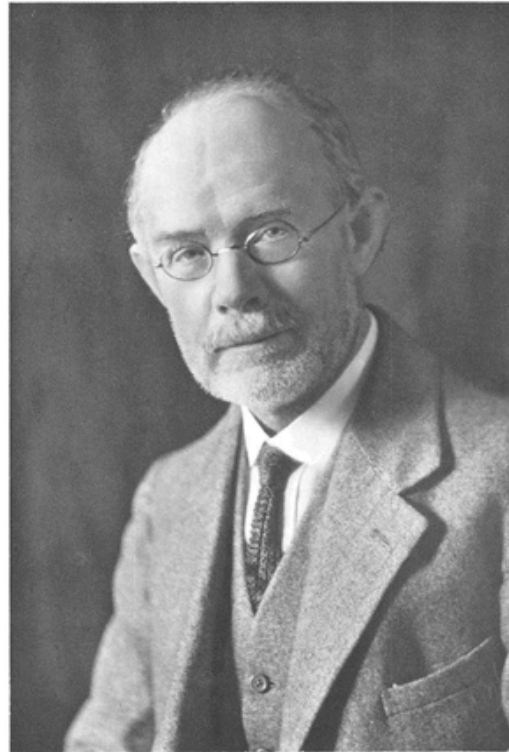
George A. Schott

ELECTROMAGNETIC RADIATION

AND THE MECHANICAL REACTIONS
ARISING FROM IT

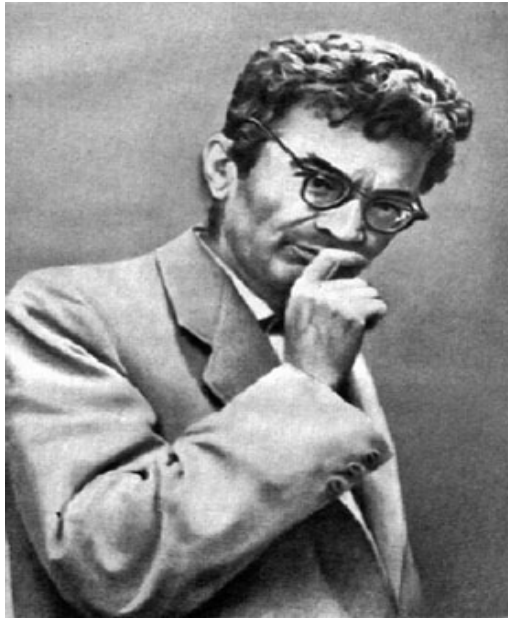BEING AN ADAMS PRIZE ESSAY IN THE
UNIVERSITY OF CAMBRIDGE

by

G. A. SCHOTT, B.A., D.Sc.

Professor of Applied Mathematics in the University College of Wales, Aberystwyth
Formerly Scholar of Trinity College, Cambridge

Cambridge :
at the University Press
1912

I. Pomeranchuk, The maximum energy that primary cosmic ray electrons can have on the Earth's surface due to radiation in the Earth's magnetic field, J. Phys. USSR, 2, 356 (1940)

D. Ivanenko and I. Pomeranchuk, On the Maximal Energy Attainable in a Betatron, Phys. Rev. 65, 343 (1944)

L.A. Artsimovich and I. Pomeranchuk, The maximum energy that primary cosmic ray electrons can have on the Earth's surface due to radiation in the Earth's magnetic field, J. Phys. USSR, 2, 267 (1945)

Elder, F. R., Gurewitsch, A. M., Langmuir, R. V., & Pollock, H. C. Radiation from Electrons in a Synchrotron. Physical Review, 71(11), 829 (1947)

In 1950 D. Ivanenko, A. A. Sokolov and I. Pomeranchuk were awarded the State prize of the second grade for works on synchrotron radiation, presented in book "Classical Field Theory"

Synchrotron radiation plays a key role in many astrophysical objects (including BH's)

Early VLBI in the USSR

L.I. Matveenko*

Space Research Institute RAN, Profsojuznaja 84/32, 117997 Moscow, Russia

This article gives story of interferometer with independent elements (Very Long Baseline Interferometer) in Russia. At the end of February 1962 the author discussed with G.Ya. Gus'kov, DSN Station, Evpatorija a new type of radio interferometer and proposed an experiment between two DSN stations. In September 1962 he reported the new method and proposed a VLBI experiment at seminar of Radio Astronomical Laboratory, Pushino, and then at a seminar of Astronomical Institute GAISH which recommended to take out a Patent. In December GAISH sent documents to the Patent Bureau. In summer 1963 the author discussed with B. Lovell in Evpatorija the VLBI method of and we signed memorandum an Ev-JB experiment at $\lambda = 32$ cm. In December 1963 the Patent Bureau permitted publication, and the paper was sent to Radiofizika. Really VLBI in the USSR began with the proposal of M. Cohen and K. Kellermann, February 1968, to do an experiment between 22-m antenna Pushino and 43-m Green Bank.

1 Introduction

Progress of technologies in the middle of the last century gave us atomic frequency standards, low-noise receivers, broad-band tape recorders, computers, and large antennas making possible modern radio astronomy. It was the epoch of great astronomical discoveries – synchrotron emission of radio sources, radio recombination lines, maser emission, quasars, pulsars, and planets. This was also the beginning of a new cosmic era, with direct studies of planets by space probes. For management of space flight it was necessary to have measurements with very high angular accuracy. For studies of the structure of compact radio sources it was necessary to have instrument with very high angular resolution too. Radio wavelengths are many thousands times larger than optical ones, so the size of radio telescopes would have to be very big. Radio astronomers proposed interferometer method, where angular resolution is determined by distance between antennas. Nobel laureate M. Ryle applied interferometer methods for studies of the structure of radio sources. The baseline size has technical limitations. The proposed method of "independent" interferometer removed the problems. The angular resolution of VLBI is thousands of times higher than that of optical telescopes and studies of the star-forming regions and AGN objects became possible. VLBI opened a new page of astronomy. If the Galileo's telescope opened the solar system, then VLBI opened all the surrounding cosmos. Radio astronomers of different countries and continents were joined and created a global VLBI network. This paper describes how this has happened.

2 Deep Space Network, Evpatorija

The history of VLBI is closely connected with space exploration. At the end of the 1950s first space vehicles (Lunniks) were launched. Radio astronomers of the Lebedev Institute constructed a radio interferometer near Simeiz in Crimea and measured trajectories of the space probes and point at which the package hit the Moon (Vitkevich et al. 1961). The results of measurements were highly praised by chief rocket designer S.P. Korolev. This technique enabled the detection of trajectories of the plasma flows leaving the Sun. The velocities of movements were higher than the escape velocity of the Sun and after several days the high-energy particles reached Earth causing a noise storm. Soon after the launch of the Lunniks the construction of the deep-space tracking station was started near Evpatorija, Crimea. The main instrument was an interferometer with 500-m baseline formed by two ADU-1000 antennas. Each of these antennas was composed of eight 16-m parabolic dishes, mounted on a naval gun turret (Fig. 1). The antennas were equipped with low-noise parametric preamplifiers at $\lambda = 32$ cm and masers at $\lambda = 8$ cm (Matveenko et al. 1965). The Lebedev Institute collaborated in the construction of the interferometer. The angular accuracy was to be 0.1 arcsec, a very high accuracy for that time. Bright compact reference radio sources were needed to calibrate the radio interferometer. We invited G. Khromov and G. Sholomitskii, aspirants of I.S. Shklovskii at GAISH, to select the reference radio sources.

*   Corresponding author: matveen@iki.rssi.ru

ika, Armenia, with a mixer receiver but the accuracy was insufficient. We measured parameters of the real system with parametric preamplifier, parameters of which were very critical for antenna adjusting. We knew from our measurements near Simeiz that during spring and autumn humidity is high and water vapor condenses in the cables. The same was expected to happen in antenna waveguides, increasing absorption. During the disconnecting of waveguides we discussed coordinate data, obtained by the method of the long baseline Doppler measurements. The frequencies of received signals were decreased by mixing with signals of atomic frequency standards (ammonia type) at each antenna, and written on a magnetic tape recorder, with a bandwidth of 100 kHz. Then the differential Doppler frequency of the signals was determined by computer. But the same principle could be applied to an interferometer to measure the differential phase of the signals. The coherence of intermediate frequency signals could be checked by pilot signals written on the tape from the same atomic standard. In this case the elements of the interferometer need not be physically connected and distances between antennas were not limited. The Earth size does not impose a limit, since an antenna can be placed in orbit. This interferometer had no problems with compensation of relative time delay. The tapes containing signals could be read later. We had only one problem – the narrow bandwidth of the tape recorder, which limited the sensitivity of the measurements. But big progress in recorder technology very soon overcome this problem. The Guskov Institute was actively developing a broadband tape recorder with rotating heads and the Basov laboratory developed hydrogen frequency standards. Gus'kov proposed for the beginning to use the DSN stations Evpatorija (ADU-1000) and Simferopol', Crimea (32 m antenna), which had the necessary equipment.

In autumn 1962 I had been in Pushino at a seminar of the Radio Astronomy Laboratory (Head V.V. Vitkevich) and reported about the proposal of the new type of radio interferometer with independent elements and suggested an experiment Evpatorija–Simferopol'; it was not supported. The opinion was: "It is impossible, because it is never possible"!? V.V. Vitkevich excused that the Laboratory cannot support publishing the paper or carrying out an experiment. I had only one possibility – my GAISH colleagues. After a few days the GAISH seminar, Director D.Ja. Martinov, recommended to take out a patent. This solution was a little strange for me – experimental methods should be accessible to all. In December 1962 GAISH sent to the Patent Bureau the VLBI proposal of L.I. Matveenko, N.S. Kardashev, and G.B. Sholomitskii.

In summer 1963 B. Lovell (Director of Jodrell Bank Radio Observatory) was a guest of M.V. Keldysh and visited the Evpatorija DSN station. The DSN director asked me to meet Prof. B. Lovell and explain the technical and scientific directions of DSN, including antennas, transmitter, atomic standards, low-noise receivers, and radio astronomical studies. To obtain more interest we invited I.S. Shklovskii and to
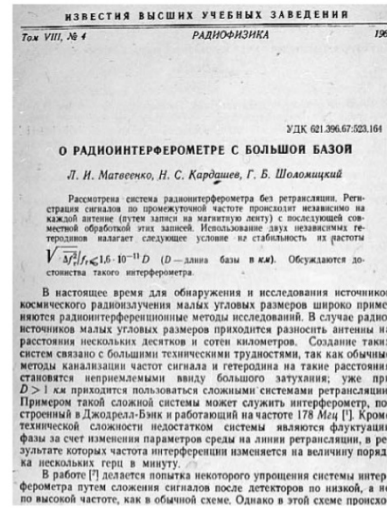

Fig. 4 The first VLBI publication in Radiofizika Vol. 4, p. 651, 1965.

translate we asked G.S. Khromov. They had been in Crimea Observatory for a summer school. I.S. Shklovskii proposed that I report about the VLBI method. However, I had to wait for the opinion of the Patent Bureau. B. Lovell agreed with the VLBI idea, but doubted the necessity of the very large resolution. Cas A or Tau A are the strongest radio sources because they have big angular size, but their brightness temperature is not very high $T_b \sim 10^7$ K. The radio emission of stars is weak because they have much smaller brightness temperature. I.S. Shklovskii remarked: "Maybe we do not know compact objects because we have no instruments to measure them". B. Lovell and I prepared a Memorandum concerning interferometer between Evpatorija and Jodrell Bank at $\lambda = 32$ cm. Jodrell Bank had equipment for collaboration on the Moon program. B. Lovell proposed to discuss details at Jodrell Bank and inform DSN and FIAN, but we did not receive an answer.

In the December 1963 the Patent Bureau agreed with the publication of the VLBI method and the paper was sent to the journal Radiofizika. After a long discussion with the referee, the dependence of interference fringes on the stability of the local oscillator was included and the paper published in 1965 (Fig. 4).

5 Proposal of M.H. Cohen and K.I. Kellermann

The first VLBI experiment was carried out in 1967 by two independent teams in the USA and in Canada. After finish-

HISTORY

The Jablonna conference on gravitation: a continuing source of inspiration

Marek Demianski

First of all I would like to welcome all of you at the main campus of the University of Warsaw—my University. Especially warmly I would like to welcome the youngest participants who for the first time participate in a big international conference. I do understand how you feel, I do understand your anxiety. Fifty one years ago I was able to observe the International Jablonna Conference on General Relativity and Gravitation, that later was classified as the GRG-3 conference. In June of 1962, I got my Master of Science degree in physics. My thesis advisor, Professor Leopold Infeld, was the Chairman of the Local Organizing Committee of the Jablonna conference. Professor Infeld asked me to help with such simple tasks as cleaning the blackboard, make sure that chalk was always available, but also—and this was really important—every morning to collect participants who were staying in hotels in Warsaw into a special coach and bring them in time to Jablonna, and in the evening bring them back to Warsaw. So that is how I ended up listening to all lectures and discussions and more. Now looking back from the perspective of half a century I think that the Jablonna Conference was the most important scientific conference that I attended so far.

The opening session of the Jablonna conference was held at the Staszica Palace in Warsaw, a short walk from where we are now. It is an easy recognizable building, in front of it is the famous monument of Copernicus (Fig. 1). The first talk was delivered by Professor J. L. Synge on "Relativistic interpretation and modification of Newtonian models". On Fig. 2 is Professor J. Synge delivering his talk and, in the first row (from the left) Professors L. Infeld, V. Fock, J. Anderson, T. Newman, R. Penrose and B. Hoffman, and on the far right Dr. Róza Michalska-Trautman. After the first talk,

M. Demianski (✉)
Institute of Theoretical Physics, Hoza 69, 00-681 Warsaw, Poland
e-mail: marek.demianski@fuw.edu.pl

Fig. 1   The Staszica Palace in Warsaw

Fig. 2   Professor J. Synge delivering the opening lecture

followed by a short discussion, the session was adjourned and all participants were transferred to Jablonna.

Jablonna is a small town about 20 km from Warsaw. In XVIII century a famous Polish aristocratic family of Poniatowski built there a summer palace and two adjacent buildings with several rooms for their guests and servants. The Palace was surrounded
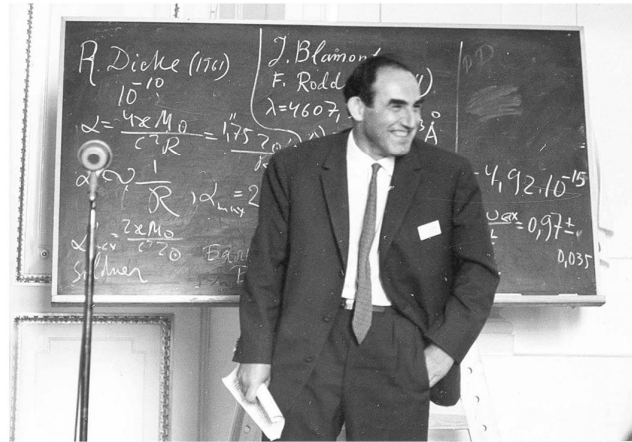
Fig. 7 Vitali Ginzburg delivering his lecture at the Jablonna conference
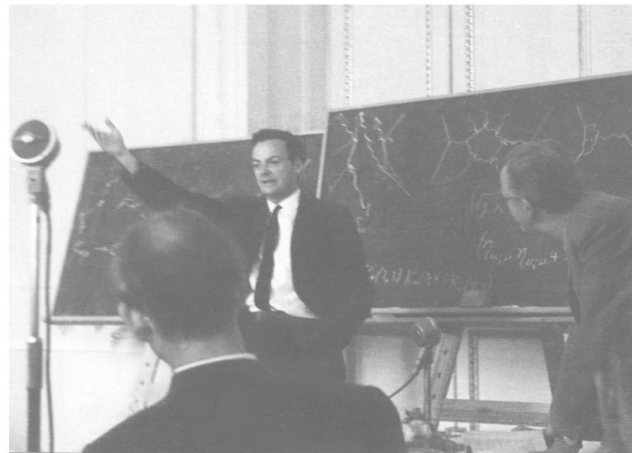

Fig. 8 Richard Feynman delivering his lecture at the Jablonna conference

"Incidentally, to give you some idea of the difference in order to calculate this diagram Fig. 4b the Young-Mills case took me about a day; to calculate the diagram in the case of gravitation I tried again and again and was never able to do it; and it was finally put on a computing machine—I don't mean the arithmetic, I mean the algebra of all the terms coming in, just the algebra; I did the integrals myself later, but the algebra of the thing was done on a machine by John Matthews so I couldn't done it by hand. In fact, I think it's historically interesting that it's the first problem in algebra that I know of that was done on a machine that has not been done by hand." Just for

Image of a Spherical Black Hole with Thin Accretion Disk

J.-P. Luminet

Groupe d'Astrophysique Relativiste, Observatoire de Paris, Section d'Astrophysique, F-92190-Meudon, France

Summary. Black hole accretion disks are currently a topic of widespread interest in astrophysics and are supposed to play an important role in a number of high-energy situations. The present paper contains an investigation of the optical appearance of a spherical black hole surrounded by thin accretion disk. Isoradial curves corresponding to photons emitted at constant radius from the hole as seen by a distant observer in arbitrary direction have been plotted, as well as spectral shifts arising from gravitational and Doppler shifts. By the results of Page and Thorne (1974) the relative intrinsic intensity of radiation emitted by the disk at a given radius is a known function of the radius only, so that it is possible to calculate the exact distribution of observed bolometric flux. Direct and secundary images are plotted and the strong asymmetry in the flux distribution due to the rotation of the disk is exhibited. Finally a simulated photograph is constructed, valid for black holes of any mass accreting matter at any moderate rate.

Key words: black holes – accretion disks – geometrical optics

1. Introduction

The aim of the present paper is to provide a reply to the question that many people ask themselves about the optical appearance of a black hole.

In order to be visible a black hole has of course to be illuminated, like any ordinary body. One of the simplest possibilities would be for the black hole to be illuminated by a distant localized source which in practise might be a companion star in a loosely bound binary system. A more interesting and observationally important possibility is that in which the light source is provided by an emitting accretion disk around the black hole, such as may occur in a tight binary system with overflow from the primary, and perhaps also on a much larger scale in a dense galactic nucleus. The general problem of the optical appearance of black holes is related to the analysis of trajectories in the gravitational field of black holes. For a spherical, static, electrical field-free black hole (whose external space-time geometry is described by the Schwarzschild metric) this problem is already well known (Hagihara, 1931; Darwin, 1959; for a summary, see Misner et al., 1973 [MTW]). In Sect. 2 we give only a brief outline of it with basic equations, trying to point out the major features which will appear later. All our calculations are done in the geometrical optics approximation (for a study of wave-aspects, see Sanchez, 1977). In Sect. 3 we calculate the apparent shape of circular rings orbiting a non-rotating black hole and the results are depicted in Figs. 5–6. In Sect. 4 we recall the standard analysis by Novikov and Thorne (1973) of the problem of energy release by a thin accretion disk in a general astrophysical context, focusing attention more particularly on the analytic solution for the surface distribution of energy release that was derived by Page and Thorne (1974) in the limiting case of a sufficiently low accretion rate. In terms of this idealized (but in appropriate circumstances, realistic) model, we calculate the distribution of bolometric flux as seen by distant observers at various angles above the plane of the disk (Figs. 9–11).

2. Image of a Bare Black Hole

Before analyzing the general problem of a spherical black hole surrounded by an emitting accretion disk, it is instructive to investigate a more simple case in which all the dynamics are already contained, namely the problem of the return of light from a bare black hole illuminated by a light beam projected by a distant source. It is conceptually interesting to calculate the precise apparent pattern of the reflected light, since some of the main characteristic features of the general geometrical optics problem are illustrated thereby.

The Schwarzschild metric for a static pure vacuum black hole may be written as:

$$ds^2 = -\left(1 - \frac{2M}{r}\right)dt^2 + \left(1 - \frac{2M}{r}\right)^{-1}dr^2 + r^2(d\theta^2 + \sin^2\theta\, d\phi^2) \quad (1)$$

where r, θ, and ϕ are spherical coordinates and the unit system is chosen such that $G = c = 1$. M is the relativistic mass of the hole (which has the dimensions of length). In this standard coordinate system the horizon forming the surface of the hole is located at the Schwarzschild radius $r_s = 2M$.

One can take advantage of the spherical symmetry to choose the "equatorial" plane $\theta = \pi/2$ so as to contain any particular photon trajectory under consideration. The trajectories will then satisfy the differential equation:

$$\left\{\frac{1}{r^2}\left(\frac{dr}{d\phi}\right)\right\}^2 + \frac{1}{r^2}\left(1 - \frac{2M}{r}\right) = 1/b^2. \quad (2)$$

The second term in the left member can be interpreted as an effective potential $V(r)$, in analogy with the non-relativistic mechanics. The motion does not depend on the photon energy E and on its angular momentum L separately, but only on the ratio $L/E = b$, which is the impact parameter at infinity.

Let the observer be in a direction fixed by the polar angle ϕ_0 in the Schwarzschild metric, at a radius $r_0 \gg M$. The rays emitted by a distant source of light and deflected by the black hole intersect the observer's detector (for example a photographic plate) at a
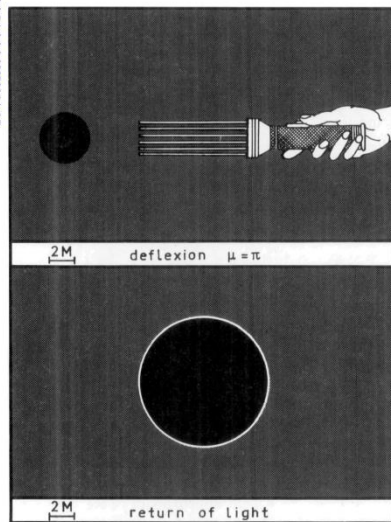
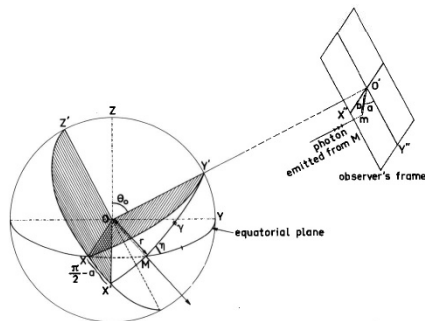**Fig. 2.** Return of light deflected by 180° from a bare black hole

Fig. 3. The coordinate system (see text)

on a Θ-direction. It follows from the above discussion that rays that reach the observer will give a picture consisting of a black disk of radius $b_c = 5.19695\,M$ surrounded by "ghost" rings of different radius and brightness. The exterior ring corresponds to the rays that have not described any circuit; as b approaches its critical value b_c, the rays describe more and more circuits, until in the limit $b_\infty = b_c$ (infinite circuits) the rays are captured.

The external ring is the brightest one; as we see from (8), the brightness decreases exponentially from the external ring to the internal ones.

One can ask for what values of $\Theta = \pi - \mu$ the rings are most visible. It is obvious that, if the observer is placed at an angle Θ

from the direction of incidence close to π, he will not see rings of brightness since almost all the observed photons at small deviations come from large impact parameter, for which circuiting does not take place. In fact, it is clear that the most favourable condition is $\theta = 0$, i.e. the rays are deflected by $\mu = \pi$. Figure (2) gives the corresponding image; the radius of the external ring is $b_1 = 5.341\,M$; this is already near the rim of the black disk of radius $5.197\,M$. The following rings fall at distances even closer, equal respectively to $0.00028\,M$, $0.000\,000\,56\,M$, $0.000\,000\,000\,1\,12\,M$, etc.

To conclude this section, the only ring practically distinguishable woud be the external one. This is not only a matter of brightness, but also a matter of resolution.

3. Image of a Clothed Black Hole

Let us now assume that the source of radiation is an emitting accretion disk orbiting around the black hole; the astrophysical properties of such an object will be briefly discussed in the next section. Let the thickness of the disk be negligible with respect to M, so that it is considered as lying in the equatorial plane of the Schwarzschild black hole. The coordinate system is chosen as in Fig. 3. The observer lies in the fixed direction θ_0, $\phi_0 = 0$ (plane YOZ) at a distance $r_0 \gg M$. We consider the disk as an assembly of idealized particles emitting isotropically. Starting from an emitting particle with Schwarzschild coordinates (r, ϕ), a typical trajectory whose asymptotic direction is the observer's direction OO' lies in the plane $OX''Y'$ and reaches the photographic plate (which is the plane $O'X''Y''$) at a point m, determined by its polar coordinates (b, α).

Assuming that the observer is practically at infinity and at rest in the gravitational field of the black hole, then the polar distance from m to $0'$ is precisely the impact parameter of the trajectory, and the polar angle α with the "vertical" direction $O'Y''$ is the complement of the dihedral angle between planes OXY' and $OX'Y'$. For a given coordinate r, varying ϕ from 0 to π (the figure being symmetric with respect to $O'Y''$-axis), we get the apparent shape $b(r) = b(r, \alpha)$ on the photographic plate of the circular ring orbiting the black hole at distance r.

As seen in the previous section, rays emitted from a given point M can circle around the black hole before escaping to infinity, giving an infinite series of images on the photographic plate; the same arguments indicate that only the secondary image (which corresponds to rays that have circuited once) has to be taken into account, images of higher order being almost exactly superposed at the critical value b_c. Thus, for a given emitter M, the observer will detect generally two images, a *direct (or primary) image* at polar coordinates $(b^{(d)}, \alpha)$ and a *ghost (or secundary) image* at $(b^{(g)}, \alpha + \pi)$.

Relationships between the different angles involved by the problem follow directly from the resolution of spherical triangles XMY' and XMX'' (Fig. 3). We get:

$$\cos \alpha = \cot \phi \, \cos \theta_0 / \sin \gamma = \cos \phi \, \cos \theta_0 (1 - \sin^2 \theta_0 \cos^2 \phi)^{-1/2} \tag{9}$$

so that α is a monotonic increasing function of ϕ.

We need also the relation

$$\cos \gamma = \cos \alpha (\cos^2 \alpha + \cot^2 \theta_0)^{-1/2}. \tag{10}$$

Calculation of curves $b^{(d)}(\alpha)$, $b^{(g)}(\alpha)$ at fixed r is performed with a computer. Nervertheless, prior to any precise drawing, we can foresee some characteristic features of the shape of our object by simply considering particular orbits in the plane $\{\phi = 0\}$ for strong inclination ($\theta_0 = 80°$; Fig. 4). Already we can point out that one of
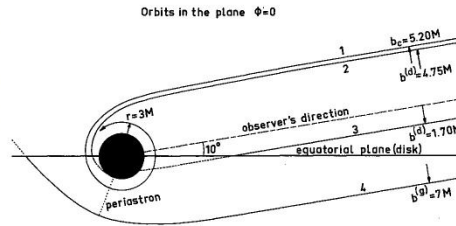
Orbits in the plane $\phi = 0$

Fig. 4. Illustrative orbits in the plane $\{\phi = 0\}$. Trajectory 1 has the critical impact parameter and circles infinitely around the black hole; trajectories 2 and 3 give direct images, trajectory 4 gives a secondary image

the main differences from the problem of the previous section is that not all orbits have necessarily a periastron, or equivalently an impact parameter greater than the critical value b_c. For example, the trajectory 2 is emitted outside the horizon, at a distance 2.60 M, and reaches the observer with an impact parameter $b^{(d)} = 4.75$ M, lesser than $b_c = 5.20$ M (in fact, this trajectory is only theoretically possible, but physically no photon will be emitted so near the horizon, see next section). More significant is the trajectory 3, which is emitted at $r = 9.80$ M from the center of the hole but gives a direct image at only $b^{(d)} = 1.70$ M. Clearly this is a pure projection effect, already encountered in a newtonian context when one observes Saturn's rings near the equatorial plane. Furthermore, the very small values of $b^{(d)}$ for trajectories emitted at relatively large r but small ϕ imply that the orbits are almost purely radial (indeed trajectory 3 is very close to a straight line); thus, we expect the part of accretion disk between the hole and the observer to give direct images with the aspects of newtonian ellipses which project onto the lower part of the black spot. Figure 4 shows another characteristic feature of the shape: the secondary image is not everywhere in direct juxtaposition to the black spot of radius b_c. In fact, trajectory 4 illustrates how, in order to reach the of radius b_c. In fact, trajectory 4 illustrates how, in order to reach the observer at strong inclination, a photon emitted behind the hole necessarily suffers a weak deviation, and hence has an orbit with large periastron and impact parameter; so, we can presume that the secondary image is really dropped forward the observer's direction (i. e. at relatively small values of ϕ), while on the opposite side it remains crushed around the black spot (at values of ϕ near π).

Now, to get more insight into the mathematics, it is interesting to write down explicitly some algebraic formulas for orbits having a periastron distance P. For the direct image, Eq. (3) leads to:

$$\gamma = \frac{1}{\sqrt{2M}} \int_0^{1/r} (G(x))^{-1/2} dx = 2(P/Q)^{1/2} \{ F(\zeta_r, k) - F(\zeta_\infty, k) \} \quad (11)$$

where

$$k^2 = \frac{Q - P + 6M}{2Q}, \ \sin^2 \zeta_\infty = \frac{Q - P + 2M}{Q - P + 6M}, \ \sin^2 \zeta_r$$

$$= \frac{Q - P + 2M + 4MP/r}{Q - P + 6M}. \quad (12)$$

We deduce:

$$\frac{1}{r} = -\frac{Q - P + 2M}{4MP} + \frac{Q - P + 6M}{4MP} \, sn^2 \left\{ \frac{\gamma}{2} \sqrt{P/Q} + F(\zeta_\infty, k) \right\}. \quad (13)$$

Given P, from (10) and (13) we get a relation $r = r(\alpha, P)$, and from (5) we obtain $b^{(d)} = b^{(d)}(r, \alpha)$ for a given angle θ_0.

We can thus draw the *isoradial* curves (corresponding to trajectories emitted at constant coordinate r from the hole) $b^{(d)} = b^{(d)}(\alpha)$ in polar coordinates.

In the newtonian limit, $b = P$ and $sn \sim \sin$, so that (13) reduces to $b^{(d)} = r \sin \gamma = r(1 + tg^2 \theta_0 \cos^2 \alpha)^{-1/2}$, which is obviously the equation of an ellipse of semi-major axis r along $O'X''$ and eccentricity $\sin \theta_0$.

More generally, for the $(1 + n)th$ order image, Eq. (11) must be replaced by $2n\pi - \gamma = 2(P/Q)^{1/2} \{ 2K(k) - F(\zeta_\infty, k) - F(\zeta_r, k) \}$ for orbits whose periastron is located between the point of emission and the infinity (that is the case for r slightly greater than $3M$). Of course, here, if the disk is optically thick, a photon whose trajectory intersects the disk would be reabsorbed and will not reach infinity. As we shall discuss later, the realistic physical situation *is* mostly optically thick.

Without taking account of absorption, redshift or physical emissive properties of the disk near the horizon, we have drawn in Figs. 5–6 the direct images of circular rings orbiting at $r = 2M$, $r = 6M$, $r = 10M$, $r = 20M$, $r = 30M$ and the secondary images for $r = 6M$, $r = 10M$, $r = 30M$ and $r = \infty$, for two values of the inclination angle θ_0.

The qualitative features foreseen above become clearly apparent, specially in Fig. 6; if we superpose newtonian ellipses for corresponding values of r, the curves fit perfectly up to fairly large values of α, of the order of 70°, the deformation becoming drastic only for the part of the ring behind the hole.

In practise, it is clear that, taking account of realistic physical properties of the accretion disk, what we would in fact observe through a telescope would be dramatically different from the mushroom of Fig. 6! The purpose of the following section is to study the actual distribution of flux that would really be observed.

## 4. Realistic Appearance of a Black Hole Accretion Disk

Until now we have considered the geometrical optics about a theoretical object consisting of a black hole surrounded by a thin accretion disk. It is appropriate at this stage to ask oneself what could be the relevance of such an object in astrophysics.

From an observational point of view, this problem is of importance: since a stationary black hole does not radiate either electromagnetic or gravitational waves, it could be detected only indirectly through its gravitational influence on the ambient medium.

Moreover, with recent discoveries of intense discrete X-ray sources with rapid variability, a considerable interest has focused upon gaz accretion onto compact objects such as neutron stars and black holes, and it is now currently admitted that accretion is probably the main process involved in a larger number of high-energy astrophysical situations, ranging from novae to quasars and other kinds of active galactic nuclei (see for instance Eardley and Press, 1975; Lightman et al., 1975).

Models of black holes with accreting medium are generally considered in the context of black holes in orbit about "normal" stars (binary systems) or supermassive black holes ($M \gtrsim 10^7 \, M_\odot$) which might reside at the centers of some active galactic nuclei (Lynden-Bell, 1969; Hills, 1975).

In both situations, the accreting matter is likely to have high specific angular momentum, so that the accretion would be far from spherical, but only axisymmetric with the matter flattened in the form of a more or less thin disk.
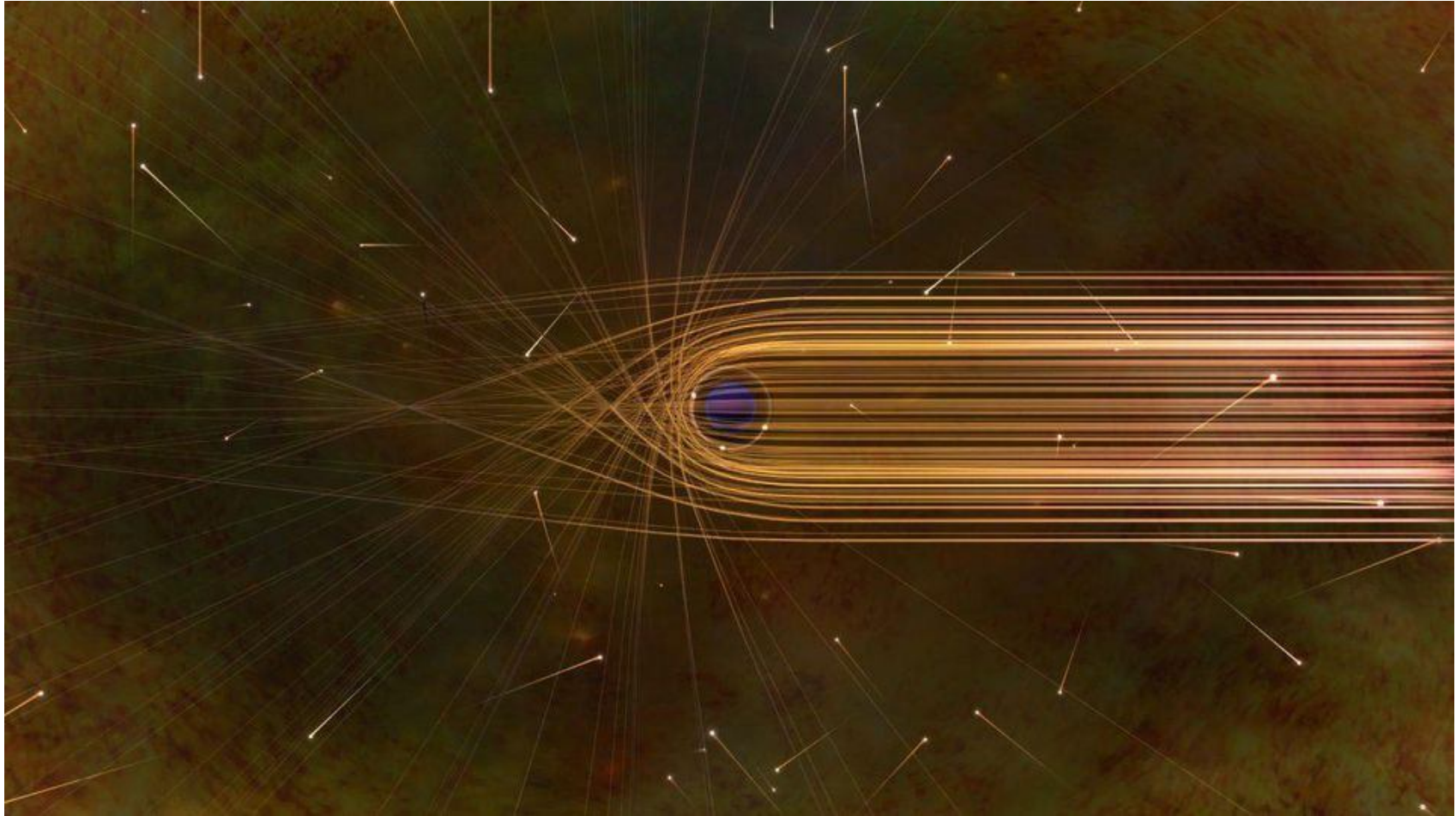
Falcke, Melia, Agol
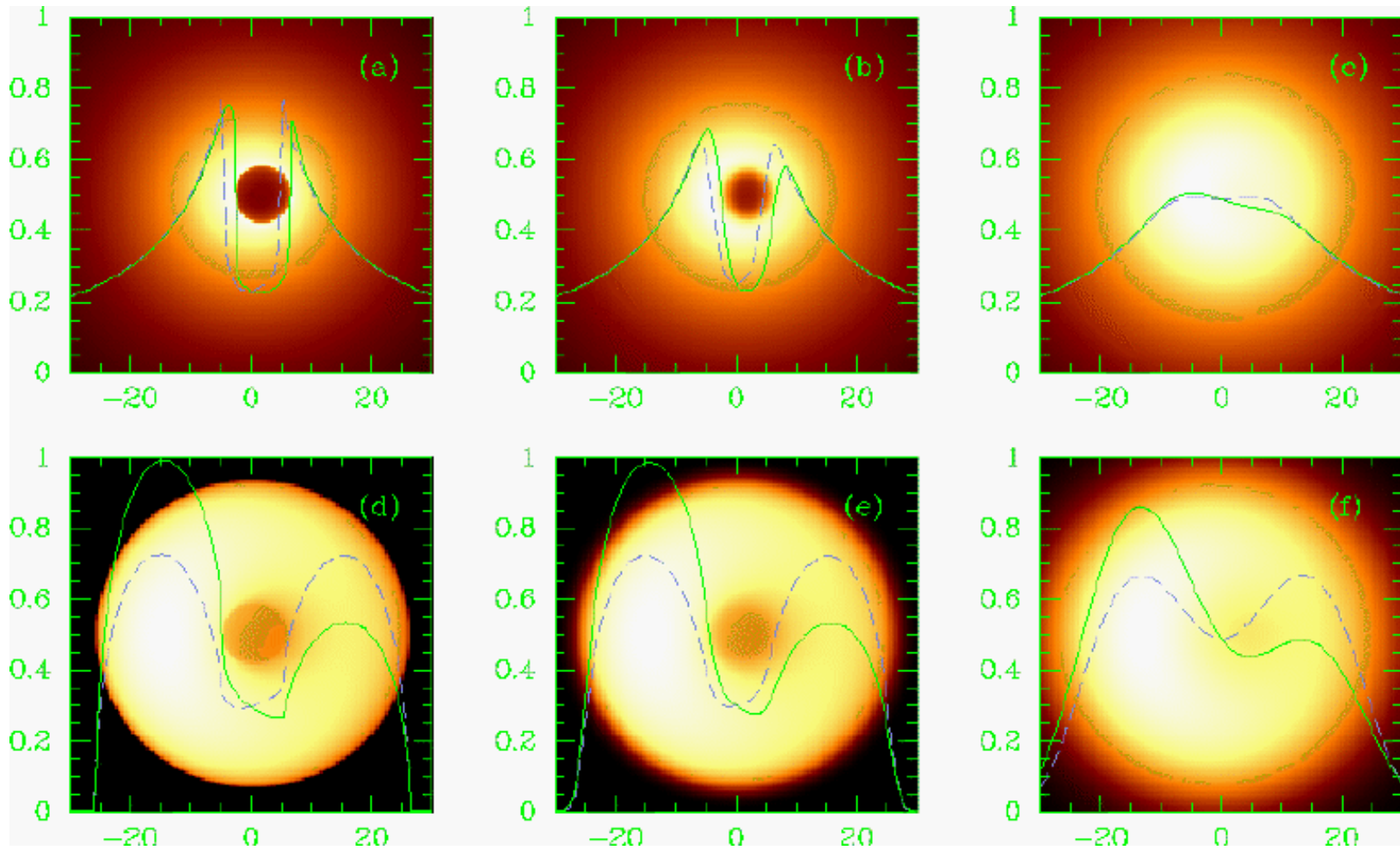
When Radioastron mission was under preparation N. S. Kardashev requested to analyse fundamental physics effects which could be observed with these facilities.

RADIO INTERFEROMETER MUCH LARGER THE EARTH

"SPECTR-R" (Mission "RadioAstron")

Main scientific tasks of the mission –

syntheses of high-precision images of various Universe objects, its coordinates measurements and search their variability with the time.
A fringe width of the system is up to 7 micro arc seconds.

Main characteristics of the space radio telescope

Spectral band:
* wavelength (cm) -   92;   18;   6.2;   1.19-1.63
* frequency (GHz) -   0,327; 1.66;   4.83;   18-26

Main organizations:
on scientific complex -   Astro Space Center of Lebedev Physical Institute of Russian Academy of Science;
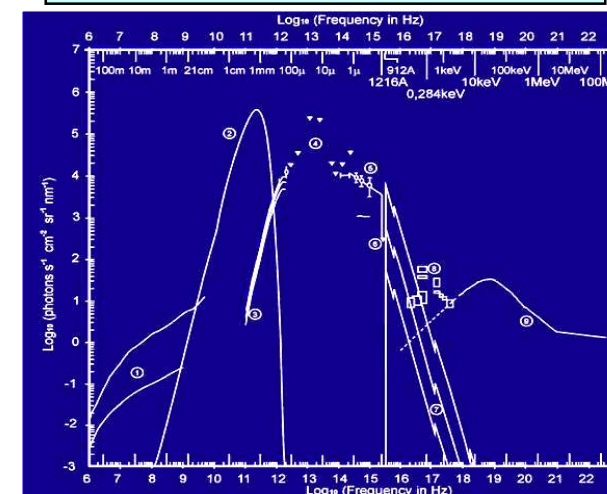*of spacecraft* -   Lavochkin Research Production Association   of Russian Space Agency.

The orbit of the mission :

apogee -	310 000 - 370 000 km
perigee -	10 000 - 70 000 km
declination -	51.6°
period variation -	7 - 10 days
Guarantied time of activity -	5 years
Scientific payload mass -	2100 kg
Pointing accuracy of radio telescope -	35"

Russia	Australia	Canada	China	Finland	Germany	Great Britain
Hungary	India	Italy	Japan	Kirgizia	Netherlands	Poland
Republic of South Africa	Spain	Sweden	Switzerland	Ukraine	United States	Uzbekistan

Planned launch date of the mission is **2007**.

Our proposal

In 2004-2005 we proposed a way to test GR predictions with Radioastron:

Since angular resolution of Radioastron at 1.3 cm is around 8 uas and the size of darkness (shadow) could help us to evaluate a charge, while shape could help us to evaluate a spin (good!)

The shortest wavelength is 1.3 cm (it is too long to detect shadow) (not good for Radioastron!)

So, we propose to test GR predictions about shape and size of BH images with observations. Astronomy is dealing with images. Therefore, establishing the correspondence of theoretical image and reconstructed image using observational data is an aim for further observations.

ELSEVIER

Measuring the black hole parameters in the galactic center with RADIOASTRON

A.F. Zakharov [a,b,c,*], A.A. Nucita [d], F. DePaolis [d], G. Ingrosso [d]

[a] *Institute of Theoretical and Experimental Physics, 25, B. Cheremushkinskaya st., Moscow 117259, Russia*
[b] *Space Research Centre of Lebedev Physics Institute, Moscow, Russia*
[c] *Joint Institute for Nuclear Research, Dubna, Russia*
[d] *Dipartimento di Fisica, Universita di Lecce and INFN, Sezione di Lecce, Italy*

Abstract

Recently, Holz and Wheeler (2002) [ApJ 578, 330] considered a very attracting possibility to detect retro-MACHOs, i.e., retro-images of the Sun by a Schwarzschild black hole. In this paper, we discuss glories (mirages) formed near rapidly rotating Kerr black hole horizons and propose a procedure to measure masses and rotation parameters analyzing these forms of mirages. In some sense that is a manifestation of gravitational lens effect in the strong gravitational field near black hole horizon and a generalization of the retro-gravitational lens phenomenon. We analyze the case of a Kerr black hole rotating at arbitrary speed for some selected positions of a distant observer with respect to the equatorial plane of a Kerr black hole. Some time ago Falcke, Melia, Agol (2000) [ApJ 528, L13S] suggested to search shadows at the Galactic Center. In this paper, we present the boundaries for shadows. We also propose to use future radio interferometer RADIOASTRON facilities to measure shapes of mirages (glories) and to evaluate the black hole spin as a function of the position angle of a distant observer.
© 2005 Elsevier B.V. All rights reserved.

PACS: 97.60.L; 04.70; 95.30.S; 04.20; 98.62.S

Keywords: Black hole physics; Gravitational lenses; Microlensing

1. Introduction

* Corresponding author. Tel.:+7 095 1299759; fax: +7 095 8839601.
E-mail address: zakharov@itep.ru (A.F. Zakharov).

Recently Holz and Wheeler (2002) have suggested that a Schwarzschild black hole may form retro-images (called retro-MACHOs) if it is illuminated by the Sun. We analyze a rapidly rotating

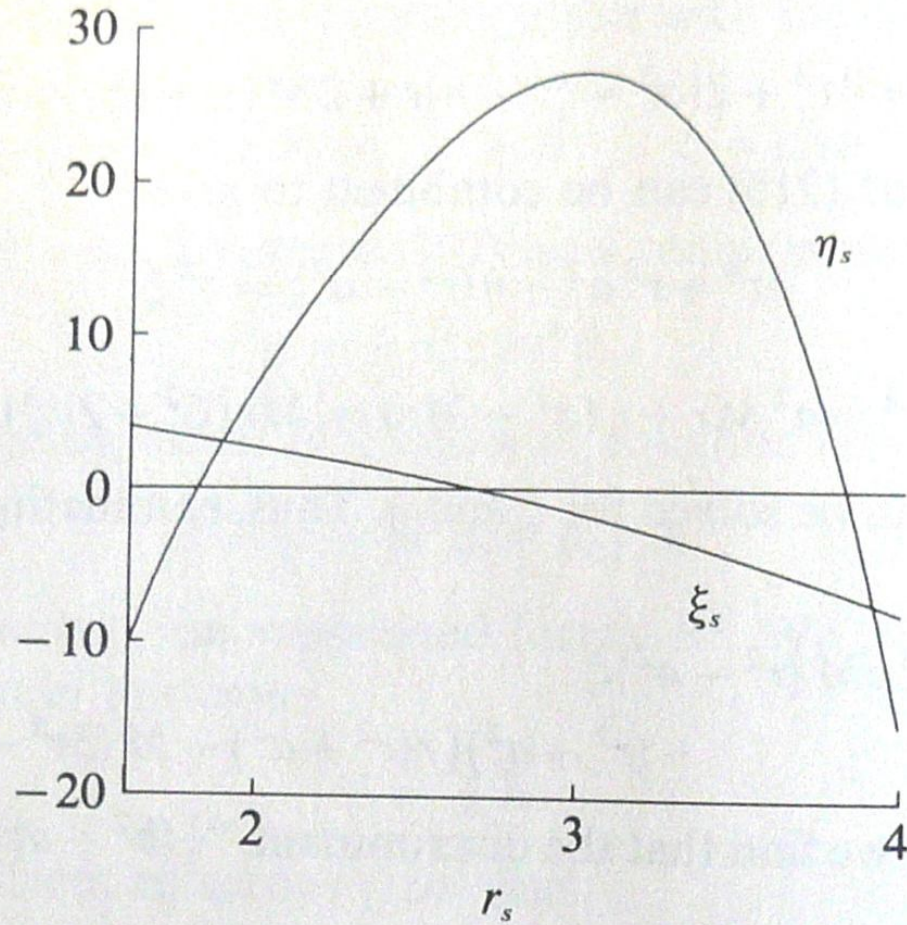# The Mathematical Theory of Black Holes

S. Chandrasekhar

FIG. 34. The locus (ξ_s, η_s) determining the constants of the motion for three-dimensional orbits of constant radius described around a Kerr black-hole with $a = 0.8$. The unit of length along the abscissa is M.
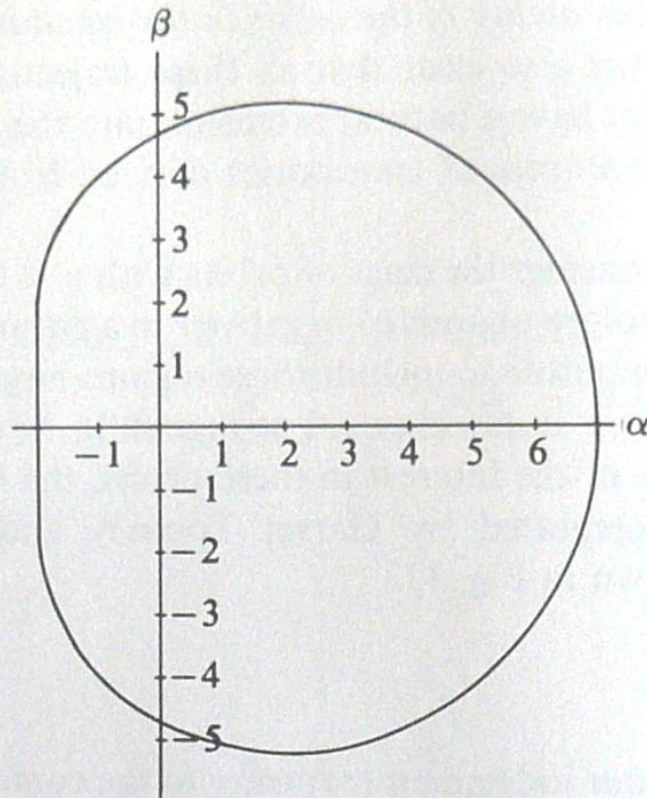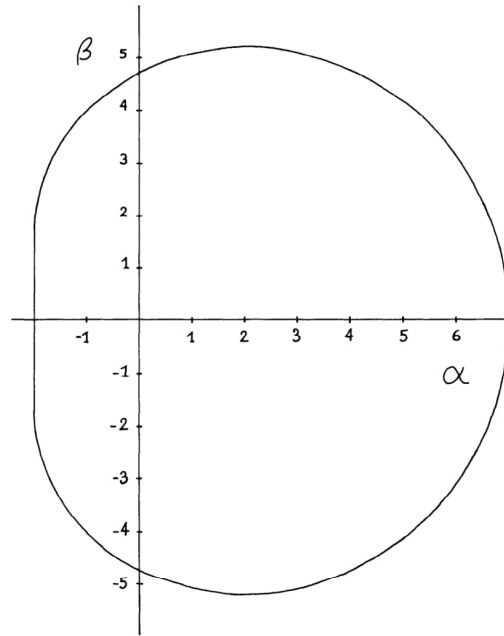
FIG. 38. The apparent shape of an extreme ($a = M$) Kerr black-hole as seen by a distant observer in the equatorial plane, if the black hole is in front of a source of illumination with an angular size larger than that of the black hole. The unit of length along the coordinate axes α and β (defined in equation (241) is M.

black hole from infinity, the apparent shape will be determined by

$$(\alpha, \beta) = [\xi, \sqrt{\eta(\xi)}].$$

(242)

Figure 6. The apparent shape of an extreme ($a = m$) Kerr black hole as seen by a distant observer in the equatorial plane, if the black hole is in front of a source of illumination with an angular size larger than that of the black hole.

is largest there and because of the gravitational focusing effects associated with the bending of the rays toward the equatorial plane. Note that the radiation comes out along the flat portion of the apparent boundary of the extreme black hole as plotted in Figure 6.

D.   Geometrical Optics

A detailed calculation of the brightness distribution coming from a source near a Kerr black hole requires more of geometrical optics than the calculation of photon trajectories. I will now review some techniques which are useful in making astrophysical calculations in connection with black holes.

The fundamental principle can be expressed as the conservation of photon density in phase space along each photon trajectory. A phase space element $d^3x\, d^3p$, the product of a proper spatial volume element and a physical momentum-space volume element in a local observer's frame of reference, is a Lorentz invariant, so the particular choice of local observer is arbitrary. The density $N(x^a, p^{(\beta)})$ is defined

Types of unbound geodesics in the Kerr metric

A. F. Zakharov

Institute of Theoretical and Experimental Physics, Academy of Sciences of the USSR, Moscow

Sets of constants of motion of a particle that correspond to different types of r-motion are considered. The topology of these sets is determined and a number of constants characterizing these sets are found.

INTRODUCTION

An important problem in the study of unbound motion of particles in the Kerr metric is the description of the set of constants of motion for which a particle traveling from infinity goes below the horizon of a black hole. We shall give a qualitative description of this set and also of the set of constants of motion for which the particle asymptotically approaches a sphere placed around the black hole, and the sets of constants of motion for which the particle departs to infinity. The solution of this problem is important in connection with the accretion of noninteracting particles on a rotating black hole.

It is well-known that Kepler orbits are characterized by two constants (E and L), since we can identify orbits that can transform into one another by rotations through the Euler angles. Hence, orbits in the Schwarzschild metric are also characterized by two constants. It turns out that a change in the radial coordinate in the Kerr metric is determined by only three constants in the case of moving particles (because the particle mass characterizes the connection between the affine parameter and the proper time of the particle, and the affine parameter can be chosen to be the proper time of the particle), and two constants in the case of the motion of photons (because of the photon energy characterizes the set of different affine parameters in the equation for the change in the r coordinate.)

1. BASIC NOTATION

The equation of motion for the radial variable in the Kerr metric is[1]

$$\rho^4 (dr/d\tau)^2 = R(r), \tag{1}$$

$$R(r) = r^4 + (a^2 - \xi^2 - \eta) r^2 + 2M [\eta + (\xi - a)^2] r - a^2 \eta \quad \text{(Photons)},$$

$$R(r) = r^4 + (a^2 - \xi^2 - \eta) r^2$$
$$+ 2M [\eta + (\xi - a)^2] r - a^2 \eta - r^2 \Delta / E \quad \text{(Particles)},$$

where

$$\rho^2 = r^2 + a^2 \cos^2 \theta, \quad \Delta = r^2 - 2Mr + a^2, \quad a - S/M. \tag{2}$$

The constants S and M refer to the black hole, namely, S is the angular momentum and M the mass of the black hole. The constants E, ξ, and η refer to the particle, namely, E is its energy at infinity, $\xi = L_z/E$ (L_z is the angular momentum of the particle about the axis of rotation of the black hole), and $\eta = Q/E^2$ (Q is given by

$$Q = p_\theta^2 + \cos^2 \theta [a^2 (\mu^2 - E^2) + \sin^{-2} \theta L_z^2],$$

and μ is the mass of the particle). It is readily verified that

the radial motion of the particle depends on the following constants:

$$\hat{a} = a/M, \quad \hat{E} = E/\mu, \quad \hat{\xi} = \xi/M, \quad \hat{\eta} = \eta/M^2.$$

The radial motion of photons does not depend on the constant $\hat{E}$. Instead of the coordinate r, we now introduce $\hat{r} = r/M$. (The symbol $\wedge$ will be omitted henceforth.) Thus, the character of motion in the r-coordinate for given value of a is determined by the three constants E, ξ, η in the case of a moving particle, and by the two constants ξ and η in the case of photons.

Depending on the multiplicities of the roots of the polynomial $R(r)$ (for $r \geq r_g$), we can have three types of motion in the r-coordinate,[2] namely:

(1) the polynomial $R(r)$ has no roots (for $r \geq r_g$). The particle then falls into the black hole;

(2) the polynomial $R(r)$ has roots and $r_{max} > r_g$ (r_{max} is the maximum root); for $(\partial R/\partial r)(r_{max}) \neq 0$ we then have, $(\partial R/\partial r)(r_{max}) > 0$, and the particle departs to infinity after approaching the black hole;

(3) the polynomial $R(r)$ has a root and $R(r_{max}) = (\partial R/\partial r)(r_{max}) = 0$; the particle now takes an infinite proper time to approach the sphere of radius r_{max}.

2. DESCRIPTION OF THE SET OF CONSTANTS CORRESPONDING TO DIFFERENT TYPES OF MOTION

We shall now examine the sets of constants of motion E, ξ, and η corresponding to different types of particles motion for a given black-hole rotation parameter $a = \text{const}$. Let us cut the space E,ξ,η with the plane $E = \text{const} \geq 1$ and describe in this slice the set of constants corresponding to different types of motion. It then turns out that the boundary of the set of constants corresponding to the second type of motion for $\eta \geq 0$ is the set of constants for which the motion belongs to the third type. We shall look upon this set as the graph of the function $\eta = \eta(\xi)$. We note that the set of these constants as functions $\xi(r)$ and $\eta(r)$ was examined by Chandrasekhar[1]. Let us describe some of the properties of the function $\eta(\xi)$. If the motion of the particle is of the third type, we have

$$R(r) = 0, \quad (\partial R/\partial r)(r) = 0 \tag{3}$$

for $\eta \geq 0, r \geq r_g$.

Thus, to obtain the function $\eta(\xi)$, we must eliminate r from (3). Assuming that (3) provides an implicit specification of $r(\xi)$ and $\eta(\xi)$, we find that

$$d\eta/d\xi (-\Delta) = 2\xi r^2 - 4(\xi - a) r, \tag{4}$$

$$d\eta/d\xi (-2r+2) + (dr/d\xi)(\partial^2 R/\partial r^2) = 4\xi r - 4(\xi - a)$$

for $r \geq r_g, \eta \geq 0$. We note that, for $\Delta > 0$ and $\partial^2 R / \partial r^2 \neq 0$, the implicit function theorem shows that $r(\xi)$ and $\eta(\xi)$ are single-valued functions. Analysis similar to that given in Ref. 3 then shows that, when $a \neq 1$ or $\xi \neq 2$, we have $\partial^2 R / \partial r^2 > 0$. When $a = 1$ and $\xi = 2$, we find from (3) that $\Delta = 0$. When $a = 1$, it is readily verified that the set corresponding to the third type of motion includes the straight segments $[\xi = 2, 0 \leq \eta \leq (3E^4 - 4E^2 + 1)/(E^2(E^2 - 1))]$ (Ref. 4) (for photons, $\xi = 2, 0 \leq \eta \leq 3$, by analogy with Refs. 5 and 6). It can also be shown that the function $\eta(\xi)$ has one maximum and $r(\xi)$ is a monotonically decreasing function.[4] Thus, the set of constants corresponding to the first type of motion is bounded by the curve $\eta(\xi)$ for $\eta \geq 0$, as shown in Figs. 1 and 2. It is also readily shown that, when $\eta < 0$ and when η and ξ are such that the motion of the particle is possible, i.e.,

$$-[a(E^2-1)^{1/2}/E - |\xi|]^2 \leq \eta < 0, \quad |\xi| \leq a(E^2-1)^{1/2}/E,$$

the particle is also captured[2] (this set is illustrated in Fig. 2).

3. UNBOUND MOTION OF PHOTONS

Chandrasekhar[1] has shown that the condition for capture of a particle in the equatorial plane is the inequality

$$6 \cos [\arccos(-a)/3 + 2\pi/3]$$

$$-a \leq \xi \leq 6 \cos [\arccos(-a)/3] - a. \tag{5}$$

Thus, the functions of $r(\xi)$ and $\eta(\xi)$ are defined only for values satisfying the inequalities (5). We also note that the function $\eta(\xi)$ is a maximum for $\xi = -2a, r(-2a) = 3(\eta(-2a) = 27)$. This can be veri-
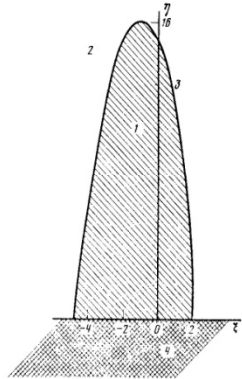

FIG. 1. Different types of particle motion for $E = 1$ and $a = 1$. Region 1—particle trapped, region 2—scattering; curve 3 corresponds to the third type of motion. Region 4 corresponds to values of the constants for which particle motion is impossible.
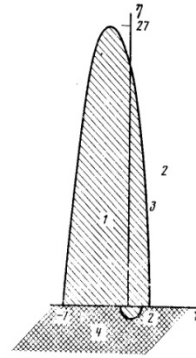

FIG. 2. Same as Fig. 1 for a massless particle and $a = 1$.

fied by direct evaluation of (3) and (4). Figure 2 shows a plot of the function $\eta(\xi)$ for $a = 1$.

4. MOTION OF PARTICLE OF ARBITRARY ENERGY

Consider a moving particle of arbitrary energy at infinity ($E > 1$). It can be verified that, if

$$\eta_{max} = \frac{-(\alpha^2 - 18\alpha - 27) + (\alpha^4 + 28\alpha^3 + 270\alpha^2 + 972\alpha + 729)^{1/2}}{2E^2\alpha},$$

$$r_{max} = (8\alpha^2/27 + \eta_{max}E^2\alpha(\alpha/3+1))^{1/2} - 2\alpha/3,$$

$$\xi_{max} = 2a/(r_{max}-2), \tag{6}$$

where $\alpha = (E^2 - 1)^{-1}$, these values ensure that $R(r)$ and $\partial R / \partial r$ vanish, i.e., they satisfy (3). We also note that, for values chosen in accordance with (6), the right-hand side of the first equation in (4) vanishes, i.e., these values correspond to the maximum of $\eta(\xi)$. The values η_{max} and r_{max} turn out to be equal to the corresponding values of these quantities for $a = 0$ (Schwarzschild metric).[7]

5. ONE CASE OF UNBOUND PARTICLE MOTION

Consider a case of unbound particle motion for $E = 1$. If the motion takes place in the equatorial plane, $\eta = 0$ (Ref. 8) and

$$R(r) = 2r^3 - \xi^2 r^2 + 2(a - \xi)^2 r. \tag{7}$$

The motion then belongs to the third type if $\xi^4 = 16(a - \xi)^2$, and $r = \xi^2/4$. It follows that there are only two values that correspond to the third type of motion in the equatorial plane, namely, $\xi = -2 - 2(1 + a)^{1/2}$ and $\xi = 2 + 2(1 - a)^{1/2}$. Thus, the domain of definition of $\eta(\xi)$ is the segment $[-2(1 + (1 + a)^{1/2}), 2(1 + (1 - a)^{1/2})]$. The domain of variation of the function $r(\xi)$ is the segment $[(1 + (1 - a)^{1/2})^2, (1 + (1 + a)^{1/2})^2]$. This follows from the fact that $r(\xi)$ is a monotonically decreasing function of ξ. When $a = 0$, we find that $\eta(\xi) = 16 - \xi^2$. When $E \to 1$, we
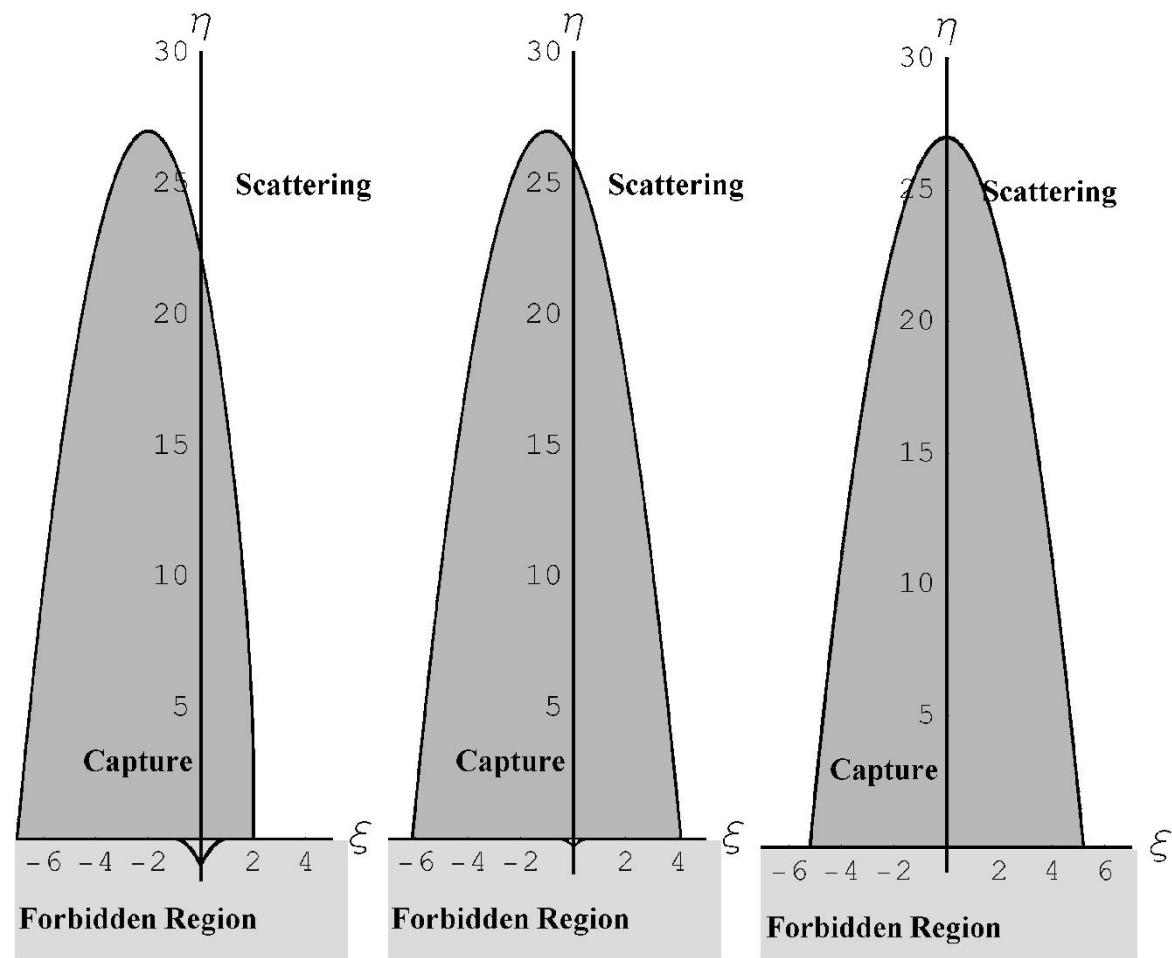
Fig. 1. Different types for photon trajectories and spin parameters ($a = 1., a = 0.5, a = 0.$). Critical curves separate capture and scatter regions. Here we show also the forbidden region corresponding to constants of motion $\eta < 0$ and $(\xi, \eta) \bar{\in} M$ as it was discussed in the text.
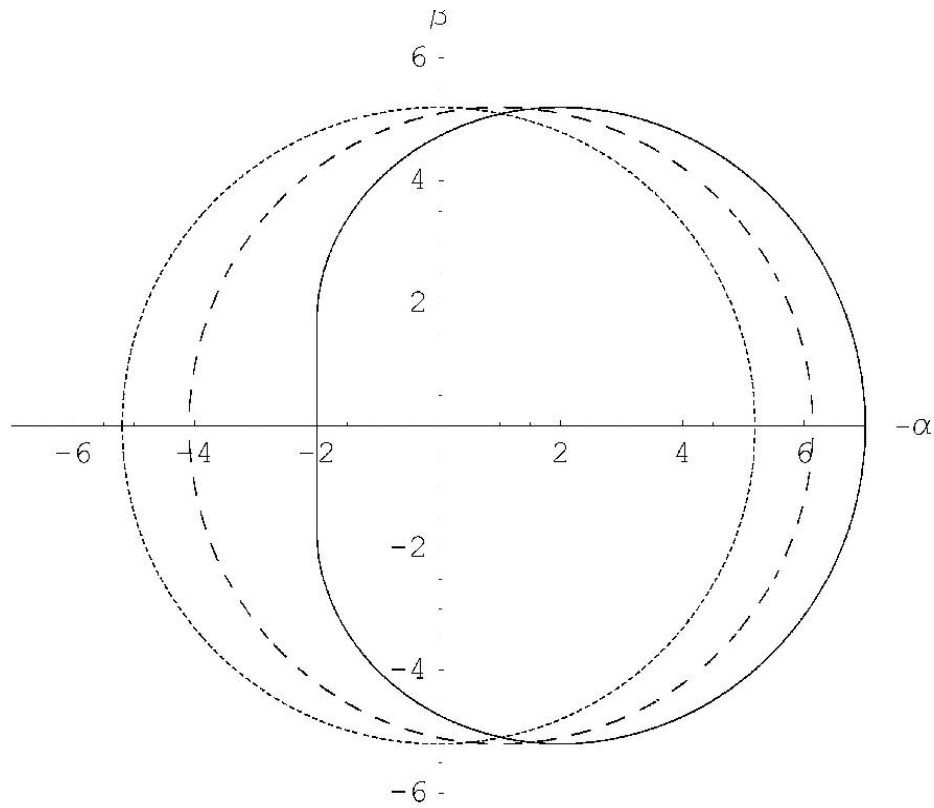
Fig. 2. Mirages around black hole for equatorial position of distant observer and different spin parameters. The solid line, the dashed line and the dotted line correspond to $a = 1, a = 0.5, a = 0$ correspondingly
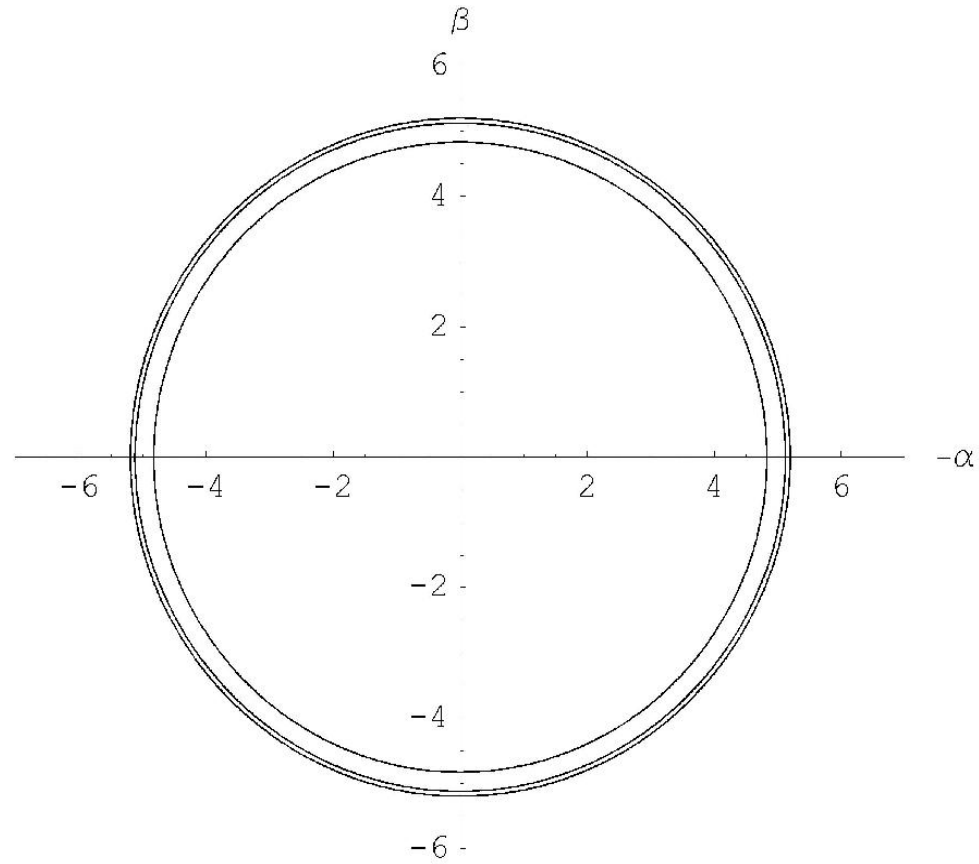
Fig. 3. Mirages around a black hole for the polar axis position of distant observer and different spin parameters ($a = 0, a = 0.5, a = 1$). Smaller radii correspond to greater spin parameters.
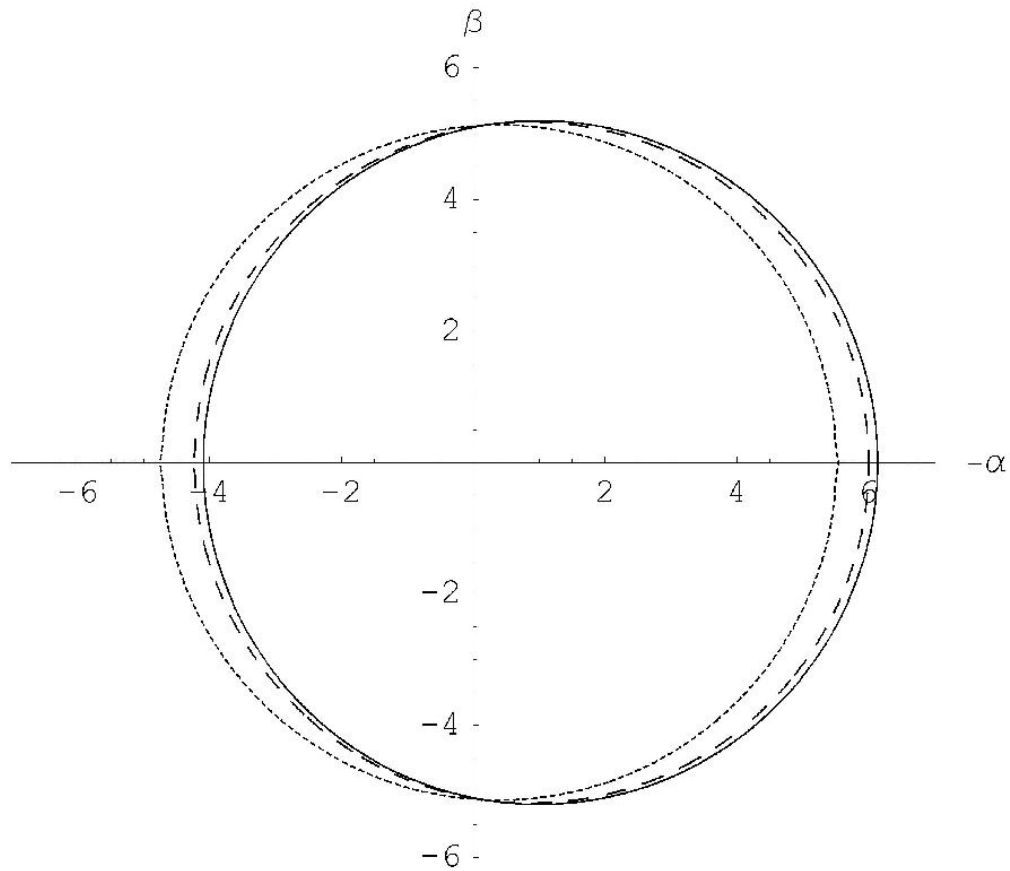
Fig. 4. Mirages around black hole for different angular positions of a distant observer and the spin $a = 0.5$. Solid, dashed and dotted lines correspond to $\theta_0 = \pi/2, \pi/3$ and $\pi/8$, respectively.
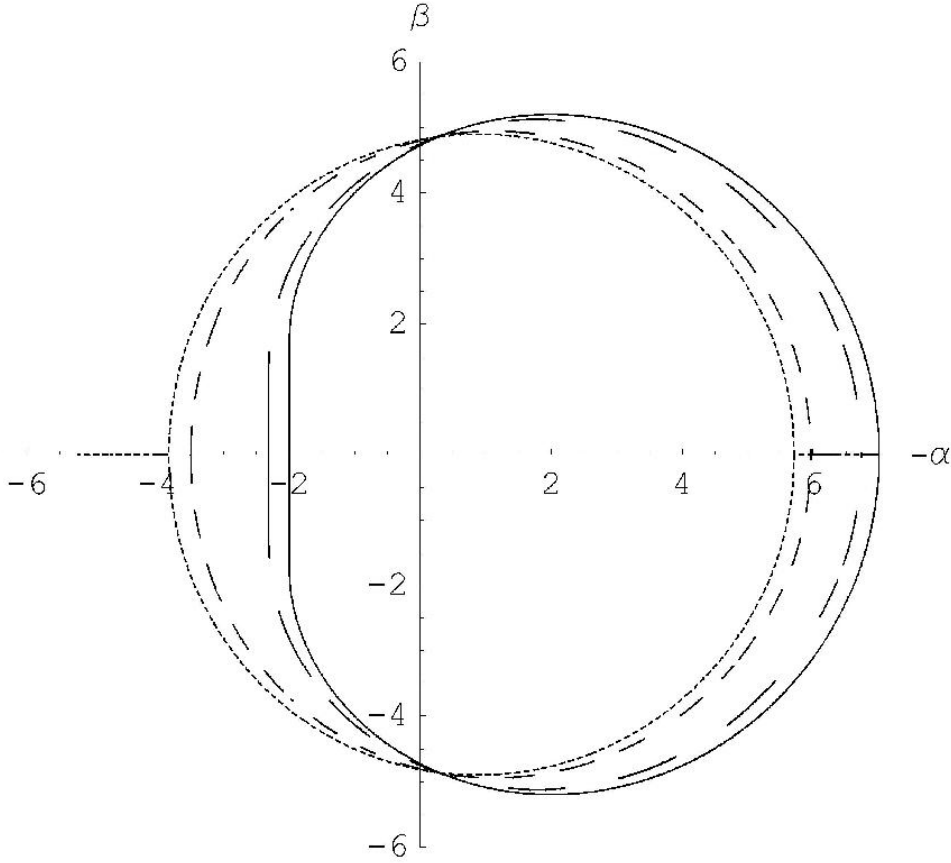
Fig. 5. Mirages around black hole for different angular positions of a distant observer and the spin $a = 1$. Solid, long dashed, short dashed and dotted lines correspond to $\theta_0 = \pi/2, \pi/3, \pi/6$ and $\pi/8$, respectively.

may not be sufficient to being detectable by RADIOASTRON. However, numerical simulations by Falcke et al. (2000, 2001) give hope that the luminosity could be not too small at least for arcs of images formed by co-rotating photons ($\alpha > 0$). Second, turbulent plasma could give essential broadening of observed images (Bower et al., 2004), the longest interferometer baseline $b_{max} \sim$ 350000 km (or for higher orbit $b_{max} \sim 3.2 \times 10^6$ km) and for this case we have similar to Bower et al. (2004) length scale in the scattering medium is $l = (D_{scattering}/D_{GC}) \times b_{max} \sim 4.4*10^3$ km (or $l = 4.4 \times 10^4$ km for the higher orbit). Thus, the scale could be less or more than the predicted and measured values of the inner scale, which are in the range 10^2–$10^{5.5}$ km (Wilkinson et al., 1994; Desai and Fey, 2001; Bower et al., 2004), thus the broadening the images could be essential but it is not very easy to calculate it in details for such parameters.

Recent observations of simultaneous X-ray and radio flares at 3 mm, 7 mm, 1.3 cm and 2 cm with the few-hundred second rise/fall timescales gave indirect evidences that X-ray and radio radiation from the close vicinity of Sgr A* was detected because of that is the most natural interpretation of these flares (Baganoff et al., 2001). However, another interpretations of these flares could not be ruled out and in this case an optical depth for radio waves at 1.3 cm wavelength toward Sgr A* may be not very small.

Few years ago a possibility to get images of nearby black holes in X-ray band was discussed by White (2000), Cash et al. (2000), moreover Cash et al. (2000) presented a laboratory demonstration of the X-ray interferometer. If the project will be realized, one could get X-ray images of black holes with 0.1×10^{-6} arcsec resolution, thus using this tool one could detect X-ray images around the Galactic Centre and around the black hole in M87 Galaxy.

One could mention also that if the emitting region has a degenerate position with respect to the line of sight (for example, the inclination angle of an accretion disk is $\gtrsim 85°$) strong bending effects found by Matt et al. (1993) and analyzed later by Zakharov and Repin (2003a) do

In spite of the difficulties of measuring the shapes of images near black holes is so attractive challenge to look at the "faces" of black holes because namely the mirages outline the "faces" and correspond to fully general relativistic description of a region near black hole horizon without any assumption about a specific model for astrophysical processes around black holes (of course we assume that there are sources illuminating black hole surroundings). No doubt that the rapid growth of observational facilities will give a chance to measure the mirage shapes using not only RADIOASTRON facilities but using also other instruments and spectral bands (for example, X-ray interferometer MAXIM (White, 2000; Cash et al., 2000) or sub-mm VLBI array (Miyoshi, 2004)). Astro Space Centre of Lebedev Physics Institute proposed except the RADIOASTRON mission and developed also space based interferometers (Millimetron and Sub-millimetron) for future observations in mm and sub-mm bands. These instruments could be used for the determination of shadow shapes.

References

Aschenbach, B., Grosso, N., Porquet, D., Predehl, P., 2004. A&A 417, 71.

Baganoff, F.K., et al., 2001. Nature 413, 45.

Beloborodov, A., 2002. ApJ 566, L85.

Bower, F.C., Falcke, H., Sault, R.J., Backer, D.C., 2002. ApJ 571, 843.

Bower, F.C., Wright, M.C.H., Falcke, H., Backer, D.C., 2003. ApJ 588, 331.

Bower, F.C., Falcke, H., Herrnstein, R.M., et al., 2004. Sciencexpress, Available from: <www.sciencexpress.org/1April2004/>.

Bozza, V., 2002. PRD 66, 103001.

Bozza, V., 2003. PRD 67, 103006.

Bozza, V., Mancini, L., 2004a. GRG 36, 435.

Bozza, V., Mancini, L., 2004b. Available from: <astro-ph/0404526>.

Carter, B., 1968. Phys. Rev. 174, 1559.

Cash, W., Shipley, A., Osterman, S., Joy, M., 2000. Nature 407, 160.

Ciufolini, I., Ricci, F., 2002. CQG 19, 3863.

Ciufolini, I., Ricci, F., 2003. gr-qc/0301030.

Chandrasekhar, S., 1983. Mathematical Theory of Black Holes. Clarendon Press, Oxford.

De Paolis, F., Geralico, A., Ingrosso, G., Nucita, A.A., 2003.

AFZ et al., NA (2005): "No doubt that the rapid growth of observational facilities will give a chance to
measure the mirage shapes… using… sub-mm VLBI array (Miyoshi, 2004))."

Shadows from Melia

**Astronomy
&
Astrophysics**
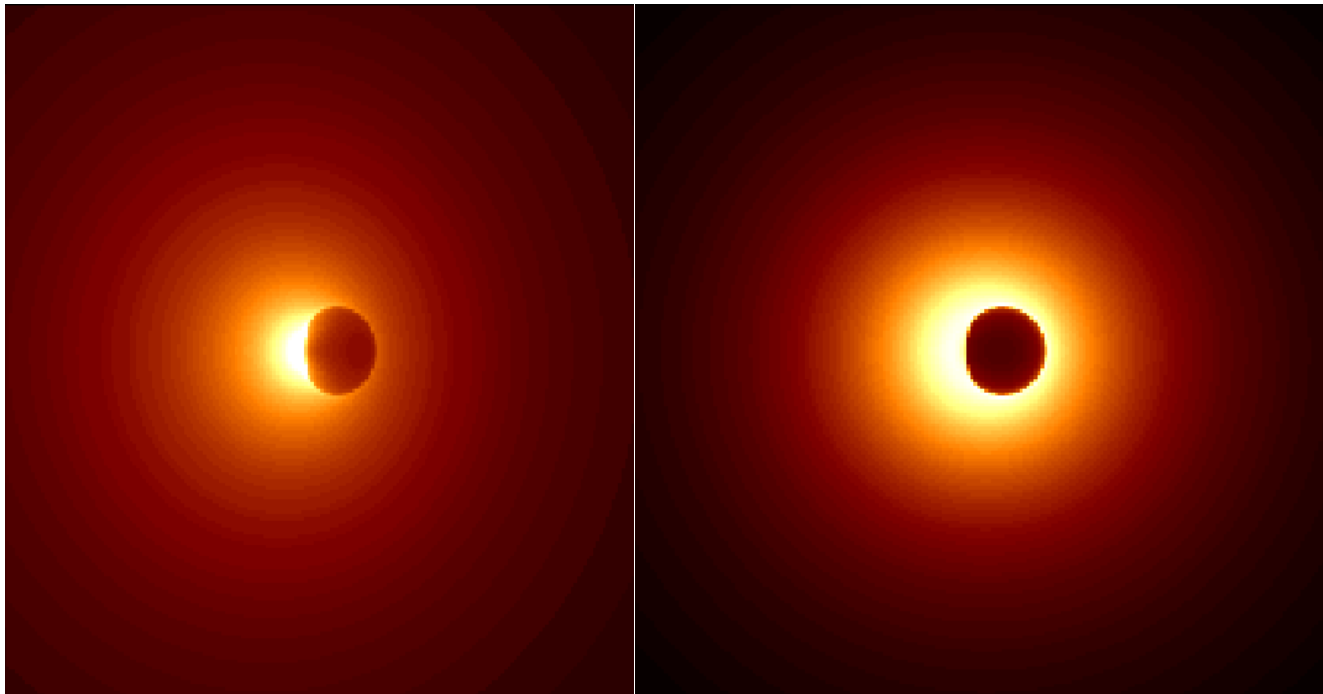
Direct measurements of black hole charge
with future astrometrical missions
(Research Note)

A. F. Zakharov[1,2,3,4], F. De Paolis[5], G. Ingrosso[5], and A. A. Nucita[5]

[1] National Astronomical Observatories of Chinese Academy of Sciences, 20A Datun Road, Chaoyang District, Beijing 100012, PR China
[2] Institute of Theoretical and Experimental Physics, 25 B. Cheremushkinskaya st., Moscow 117259, Russia
  e-mail: zakharov@itep.ru
[3] Astro Space Centre of Lebedev Physics Institute, 84/32, Profsoyuznaya st., Moscow 117810, Russia
[4] Joint Institute for Nuclear Research, Dubna, Russia
[5] Department of Physics, University of Lecce and INFN, Section of Lecce, via Arnesano, 73100 Lecce, Italy

ABSTRACT

Recently, Zakharov et al. (2005a, New Astron., 10, 479) considered the possibility of evaluating the spin parameter and the inclination angle for Kerr black holes in nearby galactic centers by using future advanced astrometrical instruments. A similar approach which uses the characteristic properties of gravitational retro-lensing images can be followed to measure the charge of a Reissner-Nordström black hole. Indeed, in spite of the fact that their formation might be problematic, charged black holes are objects of intensive investigations. From a theoretical point of view, it is well-known that a black hole is described by only three parameters, namely, its mass M, angular momentum J, and charge Q. Therefore, it would be important to have a method for measuring all these parameters, preferably by independent model of any. In this paper, we propose a procedure to measure the black hole charge by using the size of the retro-lensing images that can be revealed by future astrometrical missions. A discussion of the Kerr-Newmann black hole case is also offered.

Key words. black hole physics – astrometry – gravitation – gravitational lensing – galaxies: nuclei

1. Introduction

"Black holes have no hair" means that a black hole is characterized by only three parameters ("hairs"), its mass M, angular momentum J, and charge Q (see, e.g. Misner et al. 1973; Wald 1984 or Heusler 1998 for a more recent review). Therefore, in principle, charged black holes can be formed, although astrophysical conditions that lead to their formation may look rather problematic: see, for example, Zamir (1993); Ruffini et al. (1999); Ruffini et al. (2000); Lee et al. (2001); Perjes & Vasuth (2003); Ray et al. (2003); Moderski & Rogatko (2004); Vogt & Letelier (2004); Lemos & Weinberg (2004); Sereno (2004); Ghezzi & Letelier (2005). Nevertheless, one can not claim that their existence is forbidden by theoretical or observational arguments.

Charged black holes are also objects of intensive studies, since they are described by Reissner-Nordström geometry which is a static, spherically symmetrical solution of Yang-Mills-Einstein equations with fairly natural requirements on asymptotic behavior of the solutions (Gal'tsov & Ershov 1988; Gal'tsov et al. 1989; Gal'tsov & Ershov 1989; Lee et al. 1991). The Reissner-Nordström metric thus describes a spherically symmetric black hole with a color charge and (or) a magnetic monopole (see also Heusler 1998).

The formation of retro-lensing images (also known as mirage, shadows, or "faces" in the literature) due to the strong gravitational field effects near black holes has been investigated by several authors (Holz & Wheeler 2002; De Paolis et al. 2003; De Paolis et al. 2004; Zakharov et al. 2005a,b,c). The question that naturally arises is whether these images are observable or not. It has been shown that the retro-lensing image around the black hole at the Galactic Center (Sgr A^*) due to S_2 star is observable in the K-band (peaked at 2.2 μm) by the next generation infra-red space-based missions. The effects of retro-lensing image shapes due to black hole spin has also been investigated (De Paolis et al. 2004; Zakharov et al. 2005a,c,e).

In this paper we focus on the possibility of measuring the black hole charge as well, and we present an analytical dependence of mirage size on the black hole charge. Indeed, future space missions like Radioastron in radio band or MAXIM in X-ray band have angular resolution close to the shadow size for massive black holes in the center of our own and nearby galaxies.

$$R(r_{max}) = 0, \qquad \frac{\partial R}{\partial r}(r_{max}) = 0, \tag{6}$$

as it was done, for example, by Chandrasekhar (1983) to solve similar problems.

Introducing the notation $\xi^2 = l, Q^2 = q$, we obtain

$$R(r) = r^4 - lr^2 + 2lr - qr. \tag{7}$$

The discriminant Δ of the polynomial $R(r)$ has the form (as it was shown by Zakharov (1991a,b, 1994a)):

$$\Delta = 16l^3[l^2(1-q) + l(-8q^2 + 36q - 27) - 16q^3]. \tag{8}$$

The polynomial $R(r)$ thus has a multiple root if and only if

$$l^3[l^2(1-q) + l(-8q^2 + 36q - 27) - 16q^3] = 0. \tag{9}$$

Excluding the case $l = 0$, which corresponds to a multiple root at $r = 0$, we find that the polynomial $R(r)$ has a multiple root for $r \geq r_+$ if and only if

$$l^2(1-q) + l(-8q^2 + 36q - 27) - 16q^3 = 0. \tag{10}$$

If $q = 0$, we obtain the well-known result for a Schwarzschild black hole (Misner, Thorne and Wheeler 1973; Wald 1984; Lightman et al. 1975), $l = 27$, or $L_{cr} = 3\sqrt{3}$. If $q = 1$, then $l = 16$, or $L_{cr} = 4$, which also corresponds to numerical results given by Young (1976).

The photon capture cross section for an extreme charged black hole turns out to be considerably smaller than the capture cross section of a Schwarzschild black hole. The critical value of the impact parameter, characterizing the capture cross section for a Reissner - Nordström black hole, is determined by the equation (Zakharov 1991a,b, 1994a)

$$l = \frac{(8q^2 - 36q + 27) + \sqrt{(8q^2 - 36q + 27)^2 + 64q^3(1-q)}}{2(1-q)}. \tag{11}$$

As it was explained by Zakharov et al. (2005a,b) this leads to the formation of shadows described by the critical value of L_{cr} or, in other words, in the spherically symmetric case, shadows are circles with radii L_{cr}. Therefore, measuring the shadow size, one could evaluate the black hole charge in black hole mass units M.
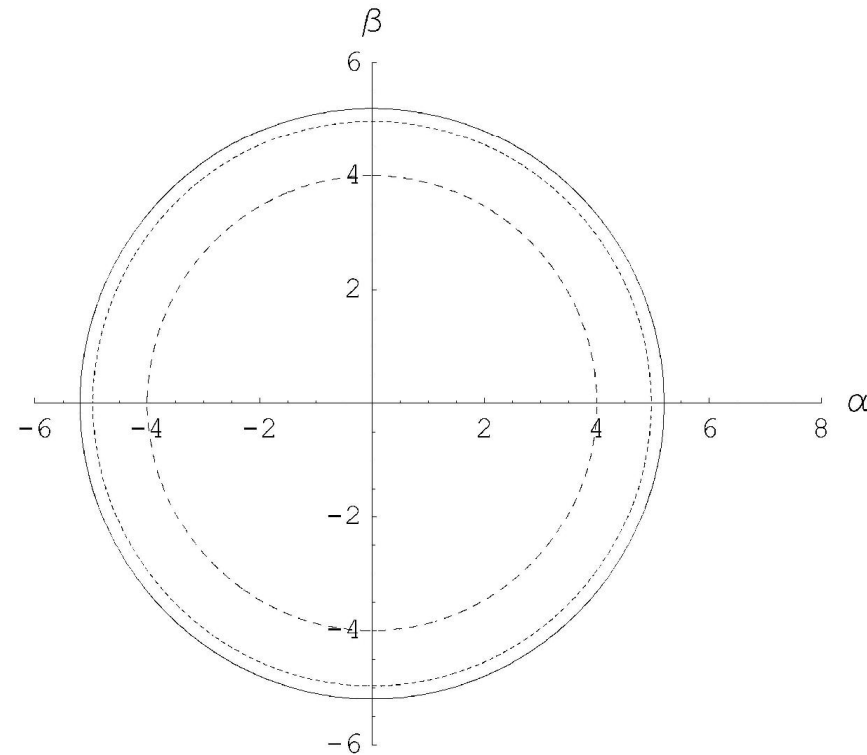

Fig. 1. Shadow (mirage) sizes are shown for selected charges of black holes $Q = 0$ (solid line), $Q = 0.5$ (short dashed line) and $Q = 1$ (long dashed line).

Jourdain: "For more than forty years I have been speaking prose while knowing nothing of it," (from "*Bourgeois Gentleman* or *The Middle-Class Aristocrat* ", J. B. Moliere)

We: "For many years we had speaking about BH's in Randall --- Sundrum model or in (beyond) Horndesky theory (scalar-tensor one) while knowing nothing of the theories…" (tidal charge or "charge" due to scalar-tensor theories)

In 2006 – 2007 we proposed to use space-ground interferometer Millimetron to observe shadows

Measuring the supermassive black hole parameters with space missions

Alexander F. Zakharov

National Astronomical Observatories of Chinese Academy of Sciences, Beijing 100012, China
ITEP, 25, B. Cheremushkinskaya st., Moscow 117259, Russia
BLTP, JINR, Dubna, Russia
email: zakharov@itep.ru

Abstract. Recent X-ray observations of microquasars and Seyfert galaxies reveal broad emission lines in their spectra, which can arise in the innermost parts of accretion disks. Recently Müller & Camenzind (2004) classified different types of spectral line shapes and described their origin. Zakharov (2006b) clarified their conclusions about an origin of doubled peaked and double horned line shapes in the framework of a radiating annulus model and discussed s possibility to evaluate black hole parameters analyzing spectral line shapes.

Keywords. Black holes – X-ray astronomy – supermassive black holes

There are a lot of papers discussing theoretical aspects of possible scenarios for generation of broad iron lines in AGNs, see for example, reviews by Fabian *et al.* (2000); Matt (2006). Moreover, an influence of microlensing on Fe K_α line shapes and spectra was discussed by Popovic *et al.* (2006); optical depths for these phenomena were calculated by Zakharov *et al.* (2004, 2005a,b). Formation of shadows (mirages) is another example when general relativistic effects are extremely important and in principle they could be detected with forthcoming interferometrical facilities such as Radioastron, Millimetron, MAXIM, as was shown by Zakharov *et al.* (2005c,d,e,f,g,h) (perspective studies of microlensing with Radioastron facilities were discussed (Zakharov (2006a)). Observations of shadows could give a real chance to observe "faces" of black holes of black holes and confirm general relativity predictions in the strong gravitational field, and to obtain new constraints on alternative theories of gravity.

Müller & Camenzind (2004) classified different types of spectral line shapes and described their origin. Zakharov (2006b) and Zakharov & Repin (2005, 2006) clarified their conclusions about an origin of doubled peaked and double horned line shapes. Based on results of numerical simulations we showed using a radiating annulus model that double peaked spectral lines arise for *almost any* locations of narrow emission rings (annuli) (except closest orbits as we could see below) although Müller & Camenzind (2004) concluded that such profiles arise for relatively flat spacetimes and typical radii for emission region about 25 r_g. We did not impose assumptions about an emissivity law; we only assume that the radiating region is a narrow circular ring (annulus). We used an approach which was discussed in details by Zakharov (1991a); Zakharov (1994a); Zakharov (1995, 2003, 2004, 2005); Zakharov & Repin (1999, 2002, 2003a,b,c, 2004a); Zakharov *et al.* (2003

Dark Matter
in Astro-
and Particle Physics

DARK 2004

Edited by H. V. Klapdor-Kleingrothaus
and R. Arnowitt

Springer

Shadow Shapes Around the Black Hole in the Galactic Centre

A.F. Zakharov[1,2,3], A.A. Nucita[4], F. DePaolis[4], and G. Ingrosso[4]

[1] Institute of Theoretical and Experimental Physics, B.Cheremushkinskaya st., 25, Moscow, 117259, Russia,
zakharov@itep.ru
[2] Space Research Centre of Lebedev Physics Institute, Moscow
[3] Joint Institute for Nuclear Research, Dubna
[4] Dipartimento di Fisica Universita di Lecce and INFN, Sezione di Lecce, Italy,
Achille.Nucita,Francesco.DePaolis,Gabriele.Ingrosso@le.infn.it

Abstract. Recently Holz & Wheeler [1] considered a very attracting possibility to detect retro-MACHOs, i.e. retro-images of the Sun by a Schwarzschild black hole. In this paper we discuss glories (mirages) formed near rapidly rotating Kerr black hole horizons and propose a procedure to measure masses and rotation parameters analyzing these forms of mirages. In some sense that is a manifestation of gravitational lens effect in the strong gravitational field near black hole horizon and a generalization of the retro-gravitational lens phenomenon. We analyze the case of a Kerr black hole rotating at arbitrary speed for some selected positions of a distant observer with respect to the equatorial plane of a Kerr black hole. We discuss glories (mirages) formed near rapidly rotating Kerr black hole horizons and propose a procedure to measure masses and rotation parameters analyzing these forms of mirages. Some time ago Falcke, Melia & Agol [2] suggested to search shadows at the Galactic Center. In this paper we present the boundaries for shadows calculated numerically. We also propose to use future radio interferometer RADIOASTRON facilities to measure shapes of mirages (glories) and to evaluate the black hole spin as a function of the position angle of a distant observer.

Recently Holz & Wheeler [1] have suggested that a Schwarzschild black hole may form retro-images (called retro-MACHOs) if it is illuminated by the Sun. We analyze a rapidly rotating Kerr black hole case for some selected positions of a distant observer with respect to the equatorial plane of the Kerr black hole. We discuss glories (mirages) formed near a rapidly rotating Kerr black hole horizon and propose a procedure to measure the mass and the black hole spin analyzing the mirage shapes. Since a source illuminating the black hole surroundings may be located in an arbitrary direction with respect to the observer line of sight, a generalization of the retro-gravitational lens idea suggested by Holz & Wheeler [1] is needed. A strong gravitational field approximation for a gravitational lens model was considered recently in several papers [3, 4, 5, 6, 7, 8, 10, 11, 12, 13, 14, 15]. However, if we consider the standard geometry for a gravitational lens model, namely if a gravitational lens is located between a source and observer, then the probability to have evidences for strong gravitational field effects is quite small, because

STUDIES OF RELATIVISTIC EFFECTS
WITH RADIOASTRON SPACE MISSION

A. F. Zakharov

National Astronomical Observatories of Chinese Academy of Sciences,
20A Datun Road, Chaoyang District, Beijing, 100012, China
Russian Scientific Centre – Institute of Theoretical and Experimental Physics, 117259, Moscow, Russia
Bogoliubov Laboratory for Theoretical Physics, JINR, 141980 Dubna, Russia
Center of Advanced Mathematics and Physics, National University of Science and Technology,
Rawalpindi, Pakistan

SUMMARY: In the review we discuss possible studies of GR phenomena such as gravitational microlensing and shadow analysis with the forthcoming RadioAstron space mission. It is well-known that gravitational lensing is a powerful tool in the investigation of the distribution of matter, including that of dark matter (DM). Typical angular distances between images and typical time scales depend on the gravitational lens masses. For the microlensing, angular distances between images or typical astrometric shifts are about $10^{-5} - 10^{-6}$ as[1]. Such an angular resolution will be reached with the space–ground VLBI interferometer, Radioastron. The basic targets for microlensing searches should be bright point-like radio sources at cosmological distances. In this case, an analysis of their variability and a reliable determination of microlensing could lead to an estimation of their cosmological mass density. Moreover, one could not exclude the possibility that non-baryonic dark matter could also form microlenses if the corresponding optical depth were high enough. It is known that in gravitationally lensed systems, the probability (the optical depth) to observe microlensing is relatively high; therefore, for example, such gravitationally lensed objects, like CLASS gravitational lens B1600+434, appear the most suitable to detect astrometric microlensing, since features of photometric microlensing have been detected in these objects. However, to directly resolve these images and to directly detect the apparent motion of the knots, the Radioastron sensitivity would have to be improved, since the estimated flux density is below the sensitivity threshold, alternatively, they may be observed by increasing the integration time, assuming that a radio source has a typical core – jet structure and microlensing phenomena are caused by the superluminal apparent motions of knots. In the case of a confirmation (or a disproval) of claims about microlensing in gravitational lens systems, one can speculate about the microlens contribution to the gravitational lens mass. Astrometric microlensing due to Galactic Macho's action is not very important because of low optical depths and long typical time scales. Therefore, the launch of the space interferometer Radioastron will give excellent new facilities to investigate microlensing in the radio band, allowing the possibility not only to resolve microimages but also to observe astrometric microlensing. Shadows around supermassive black holes can be detected with the RadioAstron space interferometer.

Key words. Gravitational lensing – quasars: general – dark matter – Relativity

---

[1] In this paper as means arcsec.

hole (Zakharov et al. 2005a), the mirage is deformed depending on the black hole spin a and on the angle of the line of sight, but its size is almost the same. In the case of a Reissner-Nordström black hole its charge changes the size of the shadows up to 30% for the extreme charge case. Therefore, the charge of the black hole can be measured by observing the shadow size, if the other black hole parameters are known with sufficient precision. In general, one could say that measuring the mirage shape (in size) allows to evaluate all the black hole "hairs".

Few years ago the possibility of observing images of distant sources around black holes in the X-ray band by means of a X-ray interferometer was discussed by White (2000), Cash et al. (2000). Indeed, the aim of the MAXIM project is to realize a space based X-ray interferometer capable of observing with angular resolution as small as 0.1 μas.

In spite of the difficulties of measuring the shapes of shadow images, to look at black hole "faces" is an attractive challenge since the mirages outline the "faces" and correspond to fully general relativistic description of the region nearby the black hole horizon without any assumption about a specific model for astrophysical processes around black holes (of course, we assume that there are sources illuminating black hole surroundings). There is no doubt that the rapid improvement of observational facilities will enable to measure the mirage shapes using not only RadioAstron facilities but also other instruments and spectral bands, like the X-ray interferometer MAXIM, the RadioAstron mission or other space based interferometers in millimeter and sub-millimeter bands.

One could mention here that the Astro Space Centre of Lebedev Physics Institute proposed the Millimetron mission as a successor of the RadioAstron (the estimated year for a launch of the Millimetron mission is 2016). The cryogenic telescope will act at mm and sub-mm wavelength bands and the ground-space interferometer Millimetron–ALMA will have angular resolution about 10^{-9} as at 0.3 mm wavelength. In this case, the interferometer will provide a possibility of a clear reconstruction of the shadow shapes with the interferometer.

7. CONCLUSIONS

Firstly, one should point out that gravitationally lensed systems are the most promising objects to be used in a microlensing search. Astrometric microlensing could be detected in a gravitational lens system such as B1600+434, if the proper motion of source, lens and an observer are generated mostly by a superluminal motion of knots in the jet (superluminal motion in a jet was found with HALCA in the quasar PKS 1622-297 (Wajima 2005)). But in this case, based on flux density estimates (Koopmans and de Bruyn 2000), one could say that the sensitivity of the RadioAstron interferometer should be improved by a factor of 10.

Assuming there is microlensing of the core in the B1600+434 system for example, the astrometric microlensing should be about $20 - 40$ μas (Treyer and Wambsganss, 2004). The RadioAstron interferometer will have enough sensitivity to detect such an astrometric displacement.

Secondly, in principle, microlensing of distant sources could be the only tool available for determination of the Ω_L using the microlensing event rate. To resolve Ω_L problem with the RadioAstron interferometer one should analyze variabilities of compact sources with a core size $\lesssim 40$ μas and with high enough flux densities (about $\gtrsim 20$ mJy at the 6 cm wavelength, and about $\gtrsim 100$ mJy at the 1.35 cm wavelength) to fit the most reliable model for variabilities of the sources such as scintillations and microlensing. The fraction of the suitable extragalactic targets for the VSOP and RadioAstron missions is about 13% – 14% (Moellenbrock et al. 1996, Hirabayashi et al. 2000, Scott et al. 2004, Kovalev et al. 2005). If the analysis indicates that other explanations (such as scintillations) are more likely than microlensing, and future observations with the Radioastron interferometer show no astrometric microlensing features, one could conclude that the Hawkins hypothesis should be ruled out. However, if an essential fraction of variability could be fitted by microlensing, the sources should be adopted as the highest priority targets for future astrometric microlensing searches.

Therefore, one could say that astrometric microlensing (or direct image resolution with Radioastron interferometer) is the crucial test to confirm (or rule out) the microlens hypothesis for gravitationally lensed systems and for point-like distant objects.

Astrometric microlensing due to Macho's action in our Galaxy is not very important for observations with the space interferometer Radioastron, since event probabilities are low and typical time scales are longer than an estimated life-time of the Radioastron space mission.

We conclude that after the RadioAstron launch, we will have the first opportunity to detect microlensing directly. To make use of this opportunity, perspective targets need to be carefully evaluated in advance using both observational data and theoretical analysis. In the radio band, the number of point-like bright sources at cosmological distances and gravitationally lensed systems with point-like components demonstrating microlens signatures is not very high and the sources should be analyzed carefully in the search for candidates, for which the microlensing model fits the data better than alternative theories.

Constraints on a charge in the Reissner-Nordström metric for the black hole at the Galactic Center

Alexander F. Zakharov[*]

North Carolina Central University, Durham, North Carolina 27707, USA; Institute of Theoretical and Experimental Physics, Moscow 117218, Russia; Joint Institute for Nuclear Research, Dubna 141980, Russia; Institute for Computer Aided Design of RAS, 123056 Moscow, Russia; and National Research Nuclear University (NRNU MEPHI), 115409 Moscow, Russia

Using an algebraic condition of vanishing discriminant for multiple roots of fourth-degree polynomials, we derive an analytical expression of a shadow size as a function of a charge in the Reissner-Nordström (RN) metric [1,2]. We consider shadows for negative tidal charges and charges corresponding to naked singularities $q = Q^2/M^2 > 1$, where Q and M are black hole charge and mass, respectively, with the derived expression. An introduction of a negative tidal charge q can describe black hole solutions in theories with extra dimensions, so following the approach we consider an opportunity to extend the RN metric to negative Q^2, while for the standard RN metric Q^2 is always non-negative. We found that for $q > 9/8$, black hole shadows disappear. Significant tidal charges $q = -6.4$ (suggested by Bin-Nun [3–5]) are not consistent with observations of a minimal spot size at the Galactic Center observed in mm-band; moreover, these observations demonstrate that a Reissner-Nordström black hole with a significant charge $q \approx 1$ provides a better fit of recent observational data for the black hole at the Galactic Center in comparison with the Schwarzschild black hole.

PACS numbers: 04.80.Cc, 04.20.-q, 04.50.Gh, 04.70.Bw

I. INTRODUCTION

Soon after the discovery of general relativity (GR), the first solutions corresponding to spherical symmetric black holes were found [1,2,6]; however, initially people were rather sceptical about possible astronomical applications of the solutions corresponding to black holes [7] (see also, for instance, one of the first textbooks on GR [8]). Even after an introduction to the black hole concept by Wheeler [9] (he used the term in his public lecture in 1967 [10]), we did not know too many examples where we really need GR models with strong gravitational fields that arise near black hole horizons to explain observational data. The cases where we need strong field approximation are very important since they give an opportunity to check GR predictions in a strong field limit; therefore, one could significantly constrain alternative theories of gravity.

One of the most important options to test gravity in the strong field approximation is analysis of relativistic line shape as it was shown in [11], with assumptions that a line emission is originated at a circular ring area of a flat accretion disk. Later on, such signatures of the Fe $K\alpha$ line have been found in the active galaxy MCG-6-30-15 [12]. Analyzing the spectral line shape, the authors concluded the emission region is so close to the black hole horizon that one has to use Kerr metric approximation [13] to fit observational data [12]. Results of simulations of iron $K\alpha$ line formation are given in [14,15] (where we used our

approach [16]); see also [17] for a more recent review of the subject.

Now there are two basic observational techniques to investigate a gravitational potential at the Galactic Center, namely, (a) monitoring the orbits of bright stars near the Galactic Center to reconstruct a gravitational potential [18] (see also a discussion about an opportunity to evaluate black hole dark matter parameters in [19] and an opportunity to constrain some class of an alternative theory of gravity [20]) and (b) measuring in mm band, with VLBI technique, the size and shape of shadows around the black hole, giving an alternative possibility to evaluate black hole parameters. The formation of retro-lensing images (also known as mirages, shadows, or "faces" in the literature) due to the strong gravitational field effects nearby black holes has been investigated by several authors [21–24].

Theories with extra dimensions admit astrophysical objects (supermassive black holes in particular) which are rather different from standard ones. Tests have been proposed when it would be possible to discover signatures of extra dimensions in supermassive black holes since the gravitational field may be different from the standard one in the GR approach. So, gravitational lensing features are different for alternative gravity theories with extra dimensions and general relativity.

Recently, Bin-Nun [3–5] discussed the possibility that the black hole at the Galactic Center is described by the tidal Reissner-Nordström metric which may be admitted by the Randall-Sundrum II braneworld scenario [25]. Bin-Nun suggested an opportunity of evaluating the black hole

[*]zakharov@itep.ru

$$\text{Dis}(s_1, s_2, s_3, s_4) = \begin{vmatrix} 1 & 1 & 1 & 1 \\ X_1 & X_2 & X_3 & X_4 \\ X_1^2 & X_2^2 & X_3^2 & X_4^2 \\ X_1^3 & X_2^3 & X_3^3 & X_4^3 \end{vmatrix}^2$$

$$= \begin{vmatrix} 4 & p_1 & p_2 & p_3 \\ p_1 & p_2 & p_3 & p_4 \\ p_2 & p_3 & p_4 & p_5 \\ p_3 & p_4 & p_5 & p_6 \end{vmatrix}. \qquad (20)$$

Expressing the polynomials $p_k (1 \le k \le 6)$ in terms of the polynomials $s_k (1 \le k \le 4)$ and using Newton's equations

we calculate the polynomials and discriminant of the family X_1, X_2, X_3, X_4 in roots of the polynomial $R(r)$; we obtain

$$p_1 = s_1 = 0, \qquad p_2 = -2s_2, \qquad p_3 = 3s_3,$$
$$p_4 = 2s_2^2 - 4s_4, \qquad p_5 = -5s_3 s_2,$$
$$p_6 = -2s_2^3 + 3s_3^2 + 6s_4 s_2, \qquad (21)$$

where $s_1 = 0, s_2 = -l, s_3 = -2l, s_4 = -ql$, corresponding to the polynomial $R(r)$ in Eq. (8). The discriminant Dis of the polynomial $R(r)$ has the form

$$\text{Dis}(s_1, s_2, s_3, s_4) = \begin{vmatrix} 4 & 0 & 2l & -6l \\ 0 & 2l & -6l & 2l(l+2q) \\ 2l & -6l & 2l(l+2q) & -10l^2 \\ -6l & 2l(l+2q) & -10l^2 & 2l^2(l+6+3q) \end{vmatrix}$$
$$= 16l^3[l^2(1-q) + l(-8q^2 + 36q - 27) - 16q^3]. \qquad (22)$$

The polynomial $R(r)$ thus has a multiple root if and only if

$$l^3[l^2(1-q) + l(-8q^2 + 36q - 27) - 16q^3] = 0. \quad (23)$$

Excluding the case $l = 0$, which corresponds to a multiple root at $r = 0$, we find that the polynomial $R(r)$ has a multiple root for $r \ge r_+$ if and only if

$$l^2(1-q) + l(-8q^2 + 36q - 27) - 16q^3 = 0. \qquad (24)$$

If $q = 0$, we obtain the well-known result for a Schwarzschild black hole [38,39,49], $l_{cr} = 27$, or $\xi_{cr} = 3\sqrt{3}$ [where l_{cr} is the positive root of Eq. (24)]. If $q = 1$, then $l = 16$, or $\xi_{cr} = 4$, which also corresponds to numerical results given in paper [50]. The photon capture cross section for an extreme charged black hole turns out to be considerably smaller than the capture cross section of a Schwarzschild black hole. The critical value of the impact parameter, characterizing the capture cross section for a RN black hole, is determined by the equation

$$l_{cr} = \frac{(8q^2 - 36q + 27) + \sqrt{D_1}}{2(1-q)}, \qquad (25)$$

where $D_1 = (8q^2 - 36q + 27)^2 + 64q^3(1-q) = -512(q - \frac{9}{8})^3$. It is clear from the last relation that there are circular unstable photon orbits only for $q \le \frac{9}{8}$ (see also results in [37] about the same critical value). Substituting Eq. (25) into the expression for the coefficients of the polynomial $R(r)$ it is easy to calculate the radius of the unstable circular photon orbit (which is the same as the minimum periastron

distance). The orbit of a photon moving from infinity with the critical impact parameter, determined in accordance with Eq. (25) spirals into circular orbit. To find a radius of photon unstable orbit we will solve Eq. (7) substituting l_{cr} in the relation. From trigonometric formula for roots of cubic equation we have

$$r_{\text{crit}} = 2\sqrt{\frac{l_{cr}}{6}} \cos\frac{\alpha}{3}, \qquad (26)$$
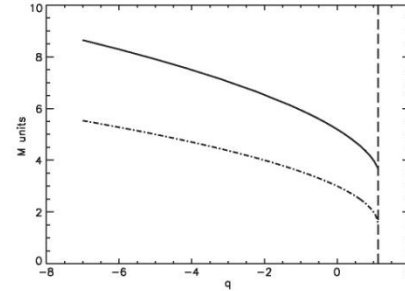
where

FIG. 1. Shadow (mirage) radius (solid line) and radius of the last circular unstable photon orbit (dot-dashed line) in M units as a function of q. The critical value $q = 9/8$ is shown with dashed vertical line.

Unstable photon orbits but not shadows could exist for naked singularities with $1 < Q^2 < 9/8$, while in paper arxiv:1802.08060[astro-ph.HE], the authors presented an example of naked singularities with a shadows.

Shadows as a tool to evaluate black hole parameters and a dimension of spacetime

Alexander F. Zakharov [a,b,*], Francesco De Paolis [c], Gabriele Ingrosso [c], Achille A. Nucita [c]

[a] Institute of Theoretical and Experimental Physics, 25, B. Cheremushkinskaya St., Moscow 117259, Russia
[b] Bogoliubov Laboratory of Theoretical Physics, Joint Institute for Nuclear Research, Dubna, Russia
[c] Dipartimento di Fisica Universita di Salento and INFN, Sezione di Lecce, Italy

ARTICLE INFO

Article history:
Available online xxxx

ABSTRACT

Shadow formation around supermassive black holes were simulated. Due to enormous progress in observational facilities and techniques of data analysis researchers approach to opportunity to measure shapes and sizes of the shadows at least for the closest supermassive black hole at the Galactic Center. Measurements of the shadow sizes around the black holes can help to evaluate parameters of black hole metric. Theories with extra dimensions (Randall–Sundrum II braneworld approach, for instance) admit astrophysical objects (supermassive black holes, in particular) which are rather different from standard ones. Different tests were proposed to discover signatures of extra dimensions in supermassive black holes since the gravitational field may be different from the standard one in the general relativity (GR) approach. In particular, gravitational lensing features are different for alternative gravity theories with extra dimensions and general relativity. Therefore, there is an opportunity to find signatures of extra dimensions in supermassive black holes. We show how measurements of the shadow sizes can put constraints on parameters of black hole in spacetime with extra dimensions.

© 2011 Elsevier B.V. All rights reserved.

Contents

1. Introduction

There are not too many observational signatures of black holes where we actually need a strong gravitational field approximation to explain observational data. For many years bright examples

* Corresponding author at: Institute of Theoretical and Experimental Physics, 25, B. Cheremushkinskaya St., Moscow 117259, Russia.
   E-mail address: zakharov@itep.ru (A.F. Zakharov).

Some time ago Bin-Nun (2010) discussed an opportunity that the black hole at the Galactic Center is described by the tidal Reissner-- Nordstrom metric which may be admitted by the Randall--Sundrum II braneworld scenario. Bin-Nun suggested an opportunity of evaluating the black hole metric analyzing (retro-)lensing of bright stars around the black hole in the Galactic Center. Doeleman et al. (2008) evaluated a shadow size for the black hole at the Galactic Center. Measurements of the shadow size around the black hole may help to evaluate parameters of black hole metric Zakharov et al (2005). We derive an analytic expression for the black hole shadow size as a function of charge for the tidal Reissner-- Nordstrom metric. We conclude that observational data concerning shadow size measurements are not consistent with significant negative charges, in particular, the significant negative charge $Q/(4M^2)=-1.6$ (discussed by Bin-Nun (2010) is practically ruled out with a very probability (the charge is roughly speaking is beyond 9 σ confidence level, but a negative charge is beyond 3 σ confidence level).

LETTERS

Event-horizon-scale structure in the supermassive black hole candidate at the Galactic Centre

Sheperd S. Doeleman[1], Jonathan Weintroub[2], Alan E. E. Rogers[1], Richard Plambeck[3], Robert Freund[4], Remo P. J. Tilanus[5,6], Per Friberg[5], Lucy M. Ziurys[4], James M. Moran[2], Brian Corey[1], Ken H. Young[2], Daniel L. Smythe[1], Michael Titus[1], Daniel P. Marrone[7,8], Roger J. Cappallo[1], Douglas C.-J. Bock[9], Geoffrey C. Bower[3], Richard Chamberlin[10], Gary R. Davis[5], Thomas P. Krichbaum[11], James Lamb[12], Holly Maness[3], Arthur E. Niell[1], Alan Roy[11], Peter Strittmatter[4], Daniel Werthimer[13], Alan R. Whitney[1] & David Woody[12]

The cores of most galaxies are thought to harbour supermassive black holes, which power galactic nuclei by converting the gravitational energy of accreting matter into radiation[1]. Sagittarius A* (Sgr A*), the compact source of radio, infrared and X-ray emission at the centre of the Milky Way, is the closest example of this phenomenon, with an estimated black hole mass that is 4,000,000 times that of the Sun[2,3]. A long-standing astronomical goal is to resolve structures in the innermost accretion flow surrounding Sgr A*, where strong gravitational fields will distort the appearance of radiation emitted near the black hole. Radio observations at wavelengths of 3.5 mm and 7 mm have detected intrinsic structure in Sgr A*, but the spatial resolution of observations at these wavelengths is limited by interstellar scattering[4–7]. Here we report observations at a wavelength of 1.3 mm that set a size of 37^{+16}_{-10} microarcseconds on the intrinsic diameter of Sgr A*. This is less than the expected apparent size of the event horizon of the presumed black hole, suggesting that the bulk of Sgr A* emission may not be centred on the black hole, but arises in the surrounding accretion flow.

The proximity of Sgr A* makes the characteristic angular size scale of the Schwarzschild radius ($R_{Sch} = 2GM/c^2$) larger than for any other black hole candidate. At a distance of ~8 kpc (ref. 8), the Sgr A* Schwarzschild radius is 10 μas, or 0.1 astronomical unit (AU). Multi-wavelength monitoring campaigns[9–11] indicate that activity on scales of a few R_{Sch} in Sgr A* is responsible for observed short-term variability and flaring from radio to X-rays, but direct observations of structure on these scales by any astronomical technique has not been possible. Very-long-baseline interferometry (VLBI) at 7 mm and 3.5 mm wavelength shows the intrinsic size of Sgr A* to have a wavelength dependence, which yields an extrapolated size at 1.3 mm of 20–40 μas (refs 6, 7). VLBI images at wavelengths longer than 1.3 mm, however, are dominated by interstellar scattering effects that broaden images of Sgr A*. Our group has been working to extend VLBI arrays to 1.3 mm wavelength, to reduce the effects of interstellar scattering, and to utilize long baselines to increase angular resolution with a goal of studying the structure of Sgr A* on scales commensurate with the putative event horizon of the black hole. Previous pioneering VLBI work at 1.4 mm wavelength

uncertainties resulted in a range for the derived size of 50–170 μas (ref. 12).

On 10 and 11 April 2007, we observed Sgr A* at 1.3 mm wavelength with a three-station VLBI array consisting of the Arizona Radio Observatory 10-m Submillimetre Telescope (ARO/SMT) on Mount Graham in Arizona, one 10-m element of the Combined Array for Research in Millimeter-wave Astronomy (CARMA) in Eastern California, and the 15-m James Clerk Maxwell Telescope (JCMT) near the summit of Mauna Kea in Hawaii. A hydrogen maser time standard and high-speed VLBI recording system were installed at both the ARO/SMT and CARMA sites to support the observation. The JCMT partnered with the Submillimetre Array (SMA) on Mauna Kea, which housed the maser and the VLBI recording system and provided a maser-locked receiver reference to the JCMT. Two 480-MHz passbands sampled to two-bit precision were recorded at each site, an aggregate recording rate of 3.84×10^9 bits per second (Gbit s^{-1}). Standard VLBI practice is to search for detections over a range of interferometer delay and delay rate. Six bright quasars were detected with high signal to noise on all three baselines allowing array geometry, instrumental delays and frequency offsets to be accurately calibrated. This calibration greatly reduced the search space for detections of Sgr A*. All data were processed on the Mark4 correlator at the MIT Haystack Observatory in Massachusetts.

On both 10 and 11 April 2007, Sgr A* was robustly detected on the short ARO/SMT–CARMA baseline and the long ARO/SMT–JCMT baseline. On neither day was Sgr A* detected on the CARMA–JCMT baseline, which is attributable to the sensitivity of the CARMA station being about a third that of the ARO/SMT (owing to weather, receiver temperature and aperture efficiency). Table 1 lists the Sgr A* detections on the ARO/SMT–JCMT baseline. The high signal to noise ratio, coupled with the tight grouping of residual delays and delay rates, makes the detections robust and unambiguous.

There are too few visibility measurements to form an image by the usual Fourier transform techniques; hence, we fit models to the visibilities (shown in Fig. 1). We first modelled Sgr A* as a circular Gaussian brightness distribution, for which one expects a Gaussian relationship between correlated flux density and projected baseline length. The weighted least-squares best-fit model (Fig. 1) corre-
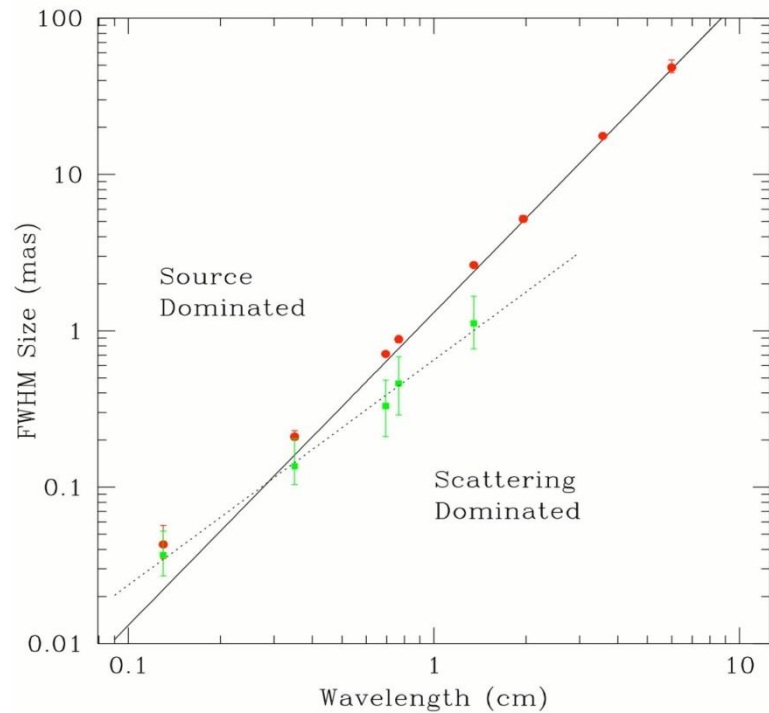
Fig 2

Figure 2 Observed and intrinsic size of Sgr A* as a function of wavelength. Red circles show major-axis observed sizes of Sgr A* from VLBI observations (all errors 3σ). Data from wavelengths of 6 cm to 7 mm are from ref. 13, data at 3.5 mm are from ref. 7, and data at 1.3 mm are from the observations reported here. The solid line is the best-fit λ^2 scattering law from ref. 13, and is derived from measurements made at $\lambda > 17$ cm. Below this line, measurements of the intrinsic size of Sgr A* are dominated by scattering effects, while measurements that fall above the line indicate intrinsic structures that are larger than the scattering size (a 'source-dominated' regime). Green points show derived major-axis intrinsic sizes from 2 cm $< \lambda <$ 1.3 mm and are fitted with a λ^α power law ($\alpha = 1.44 \pm 0.07$, 1σ) shown as a dotted line. When the 1.3-mm point is removed from the fit, the power-law exponent becomes $\alpha = 1.56 \pm 0.11$ (1σ).
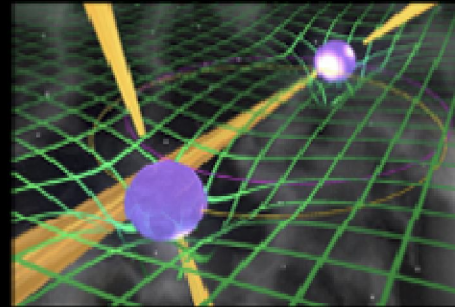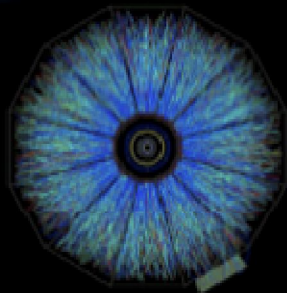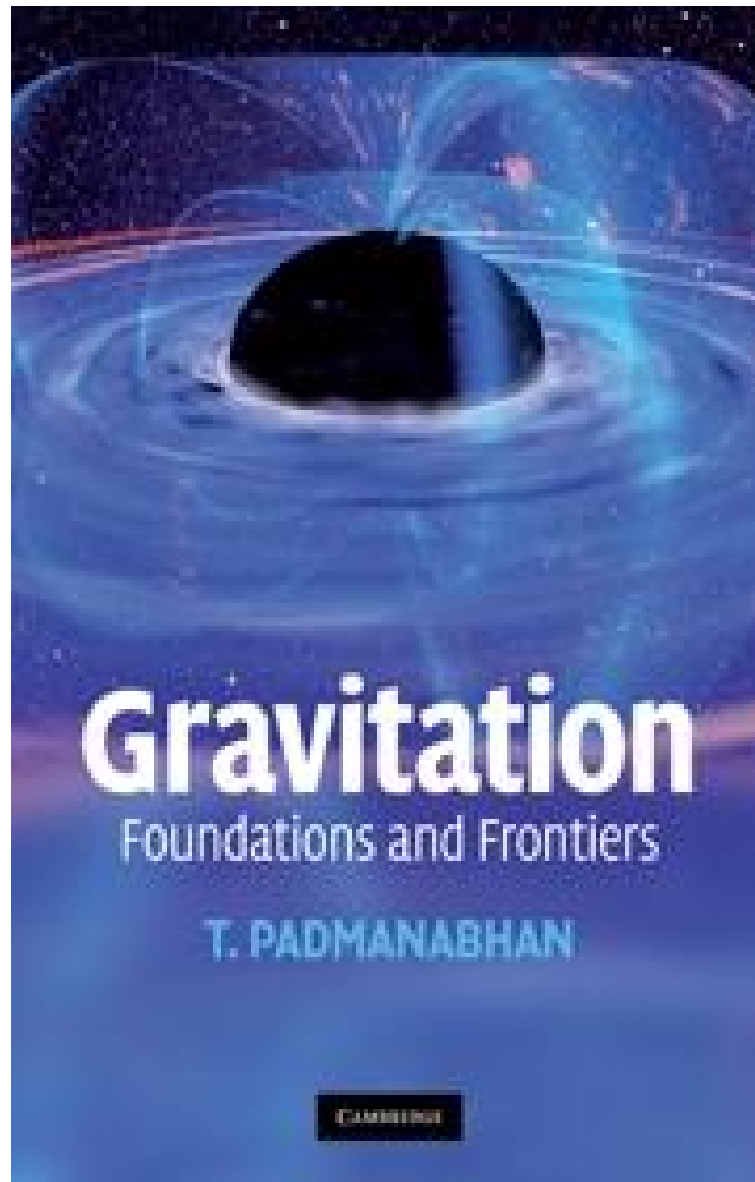
Gravitation
Foundations and Frontiers

T. PADMANABHAN

NATURE | NEWS

Young black hole had monstrous growth spurt

Super-massive object found in early Universe tests theories of cosmic evolution.

Davide Castelvecchi

25 February 2015

Print

Zhaoyu Li/SHAO

An artist's impression of a quasar with a supermassive black hole at its heart in the distant Universe.

A black hole that grew to gargantuan size in the Universe's first billion years is by far the largest yet spotted from such an early date, researchers have announced. The object, discovered by astronomers in 2013, is 12 billion times as massive as the Sun, and six times greater than its largest-known contemporaries. Its existence poses a challenge for theories of the evolution of black holes, stars and galaxies, astronomers say.

Light from the black hole took 12.9 billion years to reach Earth, so astronomers see the object as it was 900 million years after the Big Bang. That "is actually a very short time" for a black hole to have grown so large, says astronomer Xue-Bing Wu of Peking University in Beijing. He led an international collaboration that describes the discovery in *Nature*[1].

For its age, this black hole "is really much more massive than anything else we have seen so far", says Christian Veillet, director of the Large Binocular Telescope Observatory in Tucson, Arizona.

Interstellar

Figure 13. Inset: paint-swatch accretion disk with inner and outer radii $r = 9.26M$ and $r = 18.70M$ before being placed around a black hole. Body: this paint-swatch disk, now in the equatorial plane around a black hole with $a/M = 0.999$, as viewed by a camera at $r_c = 74.1M$ and $\theta_c = 1.511$ (86.56°), ignoring frequency shifts, associated colour and brightness changes, and lens flare. (Figure from *The Science of Interstellar* [40], used by permission of W. W. Norton & Company, Inc, and created by our Double Negative team, $^{\text{TM}}$ & © Warner Bros. Entertainment Inc. (s15)). This image may be used under the terms of the Creative Commons Attribution-NonCommercial-NoDerivs 3.0 (CC BY-NC-ND 3.0) license. Any further distribution of these images must maintain attribution to the author(s) and the title of the work, journal citation and DOI. You may not use the images for commercial purposes and if you remix, transform or build upon the images, you may not distribute the modified images.

itself. This entire image comes from light rays emitted by the disk's bottom face: the wide bottom portion of the image, from rays that originate behind the hole, and travel under the hole and back upward to the camera; the narrow top portion, from rays that originate on the disk's front underside and travel under the hole, upward on its back side, over its top, and down to the camera—making one full loop around the hole.

There is a third disk image whose bottom portion is barely visible near the shadow's edge. That third image consists of light emitted from the disk's top face, that travels around the hole once for the visible bottom part of the image, and one and a half times for the unresolved top part of the image.

In the remainder of this section 4 we deal with a moderately realistic accretion disk—but a disk created for *Interstellar* by Double Negative artists rather than created by solving astrophysical equations such as [32]. In appendix A.6 we give some details of how this and other Double Negative accretion disk images were created. This artists' *Interstellar* disk was chosen to be very anemic compared to the disks that astronomers see around black holes and that astrophysicists model—so the humans who travel near it will not get fried by x-rays and gamma-rays. It is physically thin and marginally optically thick and lies in the black hole's equatorial plane. It is not currently accreting onto the black hole, and it has cooled to a position-independent temperature $T = 4500$ K, at which it emits a black-body spectrum.

Figure 14 shows an image of this artists' disk, generated with a gravitational lensing geometry and computational procedure identical to those for our paint-swatch disk, figure 13
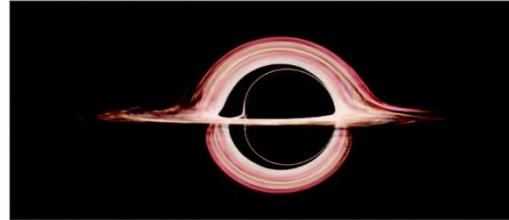
Figure 14. A moderately realistic accretion disk, created by Double Negative artists and gravitationally lensed by the same black hole with $a/M = 0.999$ as in figure 13 and with the same geometry.

(no frequency shifts or associated colour and brightness changes; no lens flare). Christopher Nolan and Paul Franklin decided that the flattened left edge of the black-hole shadow, and the multiple disk images alongside that left edge, and the off-centred disk would be too confusing for a mass audience. So—although *Interstellar*'s black hole had to spin very fast to produce the huge time dilations seen in the movie—for visual purposes Nolan and Franklin slowed the spin to $a/M = 0.6$, resulting in the disk of figure 15(a).

4.1.2. Colour and brightness changes due to frequency shifts.
The influences of Doppler and gravitational frequency shifts on the appearance of this disk are shown in figures 15(b) and (c).

Since the left side of the disk is moving toward the camera and the right side away with speeds of roughly $0.55c$, their light frequencies get shifted blueward on the left and redward on the right—by multiplicative factors of order 1.5 and 0.4 respectively when one combines the Doppler shift with a $\sim 20\%$ gravitational redshift. These frequency changes induce changes in the disk's perceived *colours* (which we compute by convolving the frequency-shifted spectrum with the sensitivity curves of motion picture film) and also induce changes in the disk's perceived *brightness*; see appendix A.6 for some details.

In figure 15(b), we have turned on the colour changes, but not the corresponding brightness changes. As expected, the disk has become blue on the left and red on the right.

In figure 15(c), we have turned on both the colour and the brightness changes. Notice that the disk's left side, moving toward the camera, has become very bright, while the right side, moving away, has become very dim. This is similar to astrophysically observed jets, emerging from distant galaxies and quasars; one jet, moving toward Earth is typically bright, while the other, moving away, is often too dim to be seen.

### 4.2. Lens flare and the accretion disk in the movie Interstellar

Christopher Nolan, the director and co-writer of *Interstellar*, and Paul Franklin, the visual effects supervisor, were committed to make the film as scientifically accurate as possible—within constraints of not confusing his mass audience unduly and using images that are exciting and fresh. A fully realistic accretion disk, figure 15(c), that is exceedingly lopsided, with the hole's shadow barely discernible, was obviously unacceptable.

Schwarzschild black hole images: $\theta=85$ **deg**
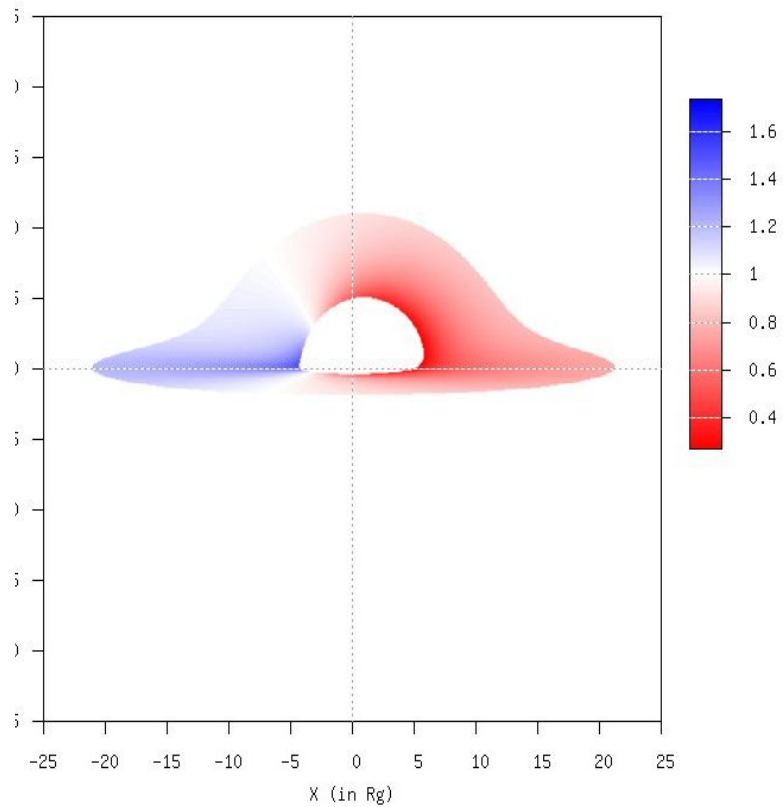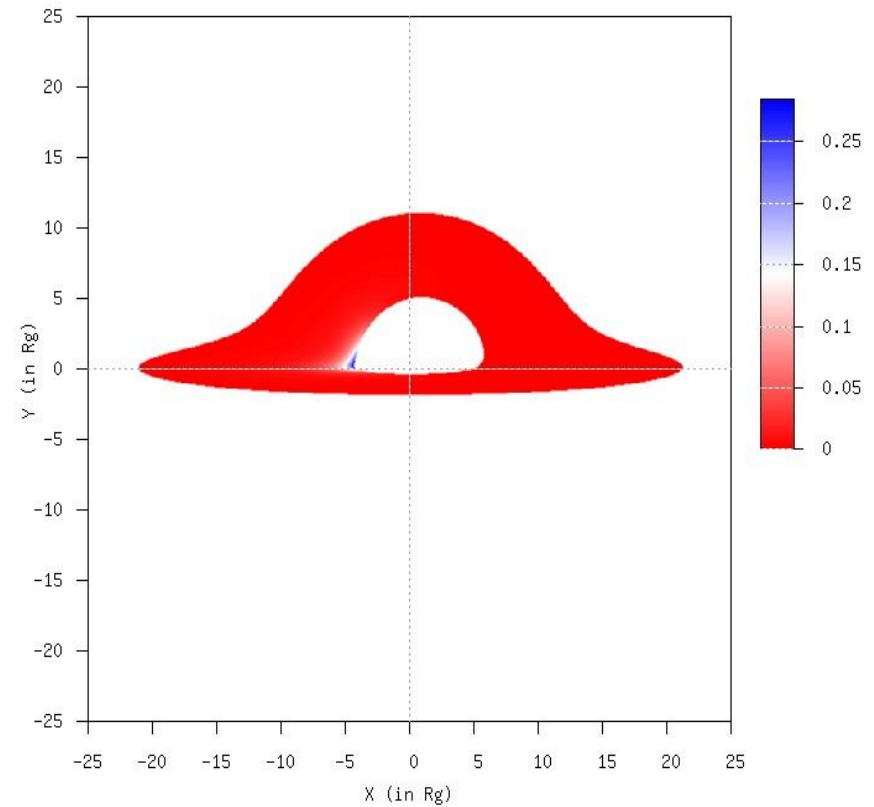
- Redshift map
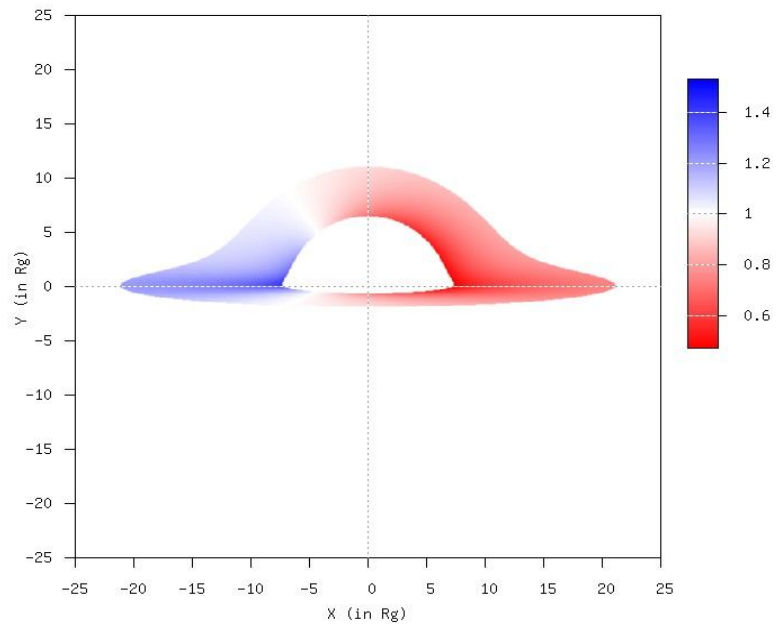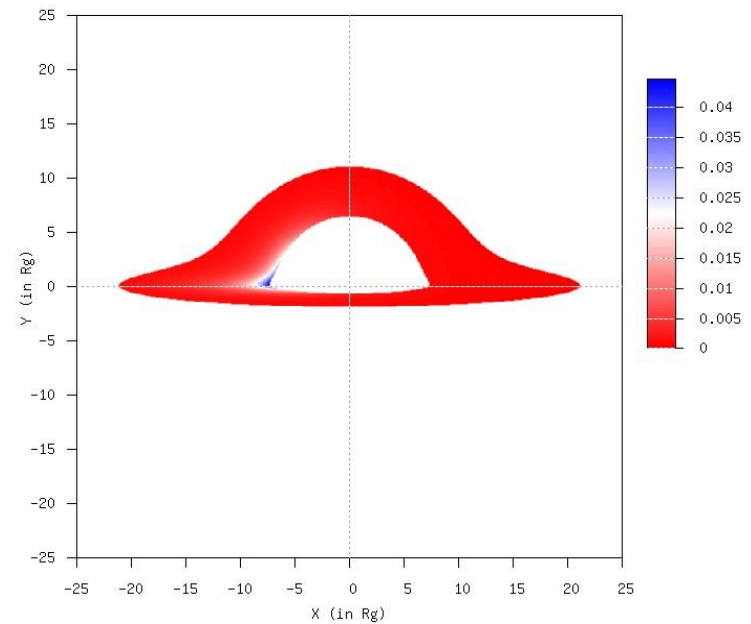
- Intensity map

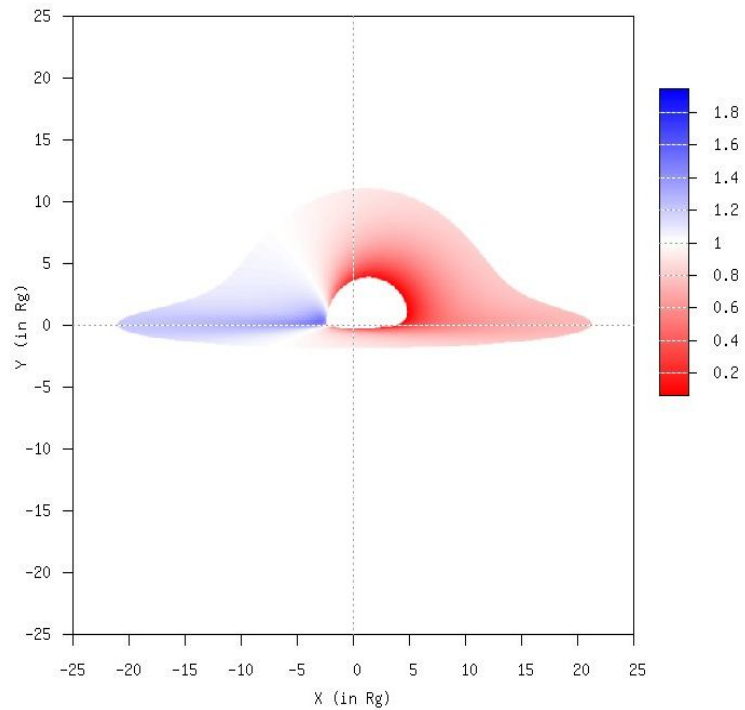# Kerr black hole images (*a*=0.75): θ=**85 deg**
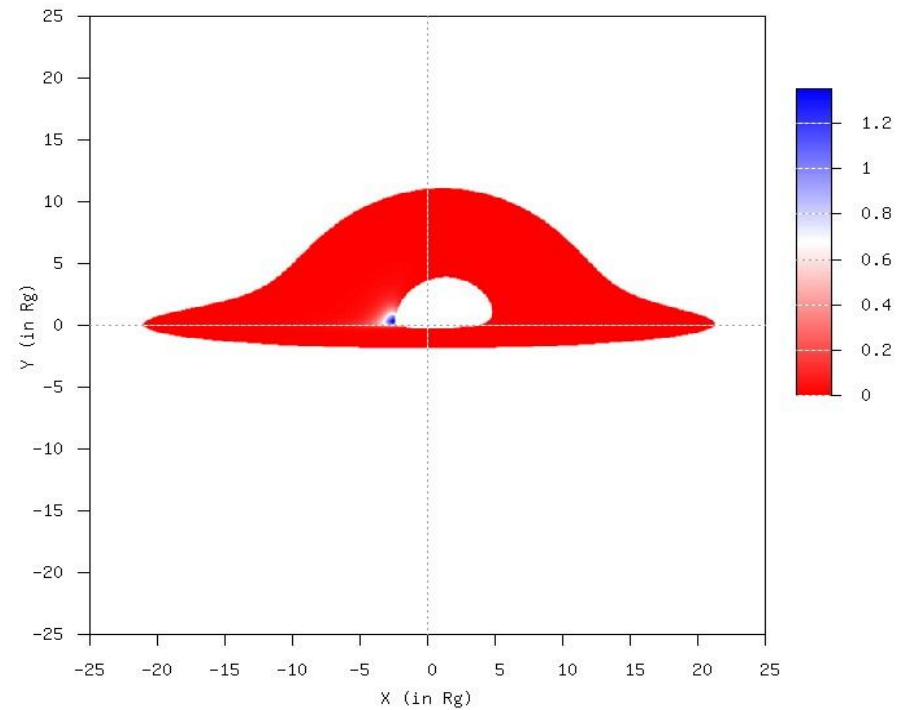
- Redshift map

- Intensity map

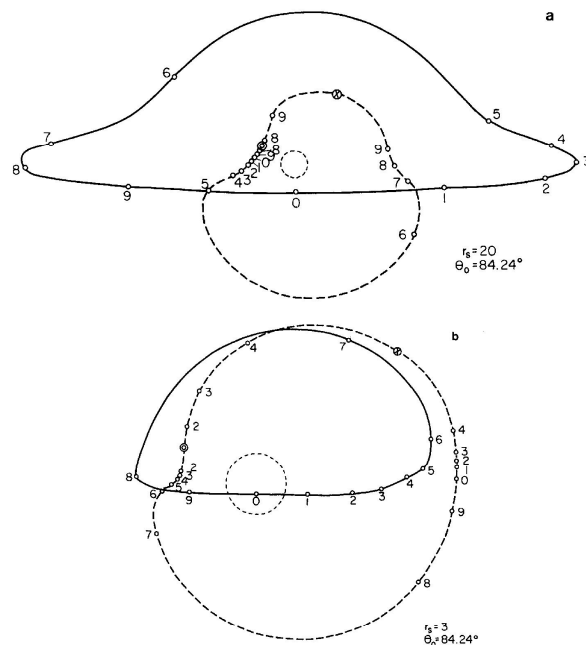# Kerr black hole images (*a*=0.99): θ=**85 deg**

- Redshift map

- Intensity map

FIG. 8.—Apparent positions of the two brightest images as functions of time for two orbital radii and an observer at a polar angle $\theta_0 = 84°24$. The small, dashed circle in each plot is the locus $\alpha^2 + \beta^2 = 1$ and gives the scale of the plot. The direct image moves along the solid line; the one-orbit image, along the dashed line. Ticks mark the positions of the images at 10 equally spaced times. A pair of one-orbit images appears to be created at the points ⊚ and annihilated at the points ⊗. See text.

fore of α) and the variation in surface brightness increase more rapidly for the one-orbit image than for the direct image as we consider stars of progressively smaller orbital radii.

As the apparent position of the image seen by the distant observer changes, so does the corresponding direction of emission in the local rest frame of the star. If the instantaneous direction of emission of the beam of radiation which reaches the observer is represented by a point in figure 3 (for $r_s = 1.5$), this point moves along the cos $\theta_0 =$ const. curve corresponding to the given type of image in the direction indicated by the arrows. Creation of pairs of images on the one-orbit curves is at the points marked ⊚; destruction, at points ⊗. For $r_s = 1.5$ there is no retrograde image and, hence, no creation and destruction of images for observers with $\theta_0 \lesssim 40°$.

When r_s is not much larger than unity, the images move very slowly on the parts of the curves nearest the backward ϕ-direction and very rapidly on the remainder of the

EHT team: "Similarly, for the EHT, the data we take only tells us only a piece of the story, as there are an infinite number of possible images that are perfectly consistent with the data we measure. But not all images are created equal— some look more like what we think of as images than others. To chose the best image, we essentially take all of the infinite images that explain our telescope measurements, and rank them by how reasonable they look. We then choose the image (or set of images) that looks most reasonable. "

Measurements

Infinite Number of Possibilities
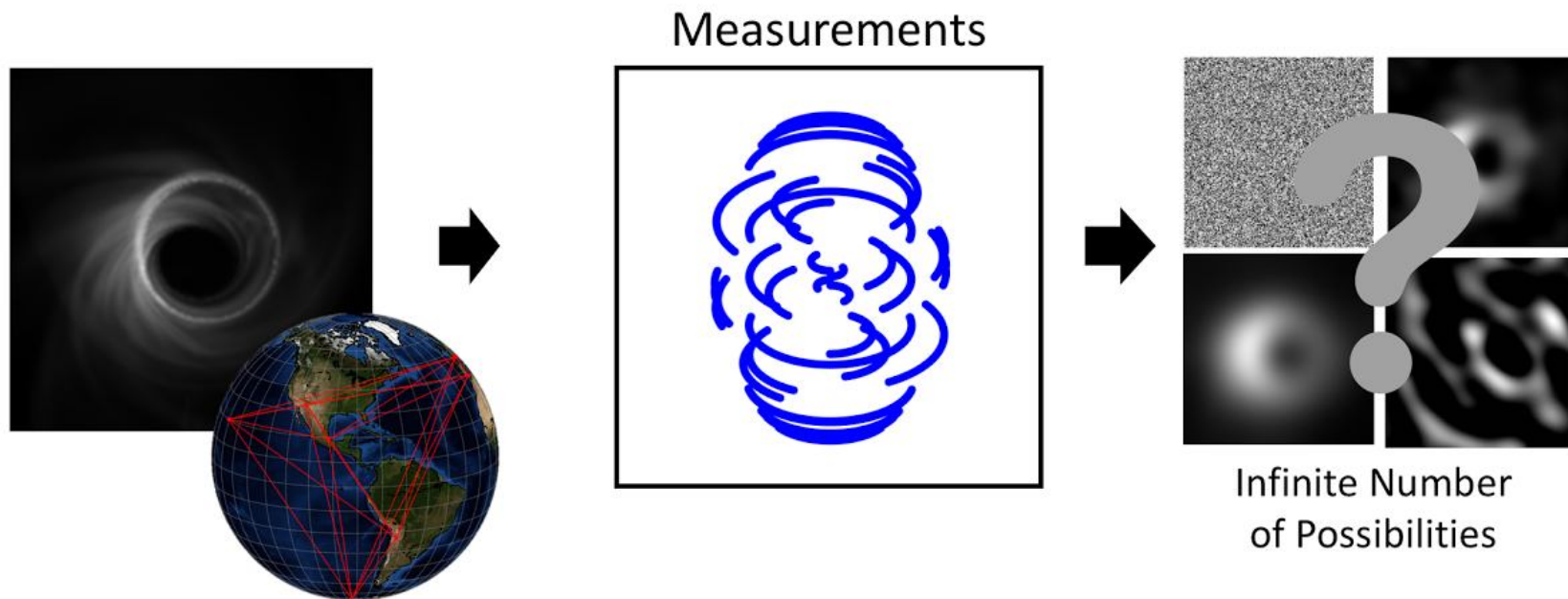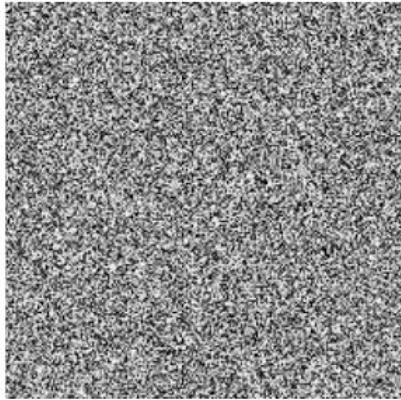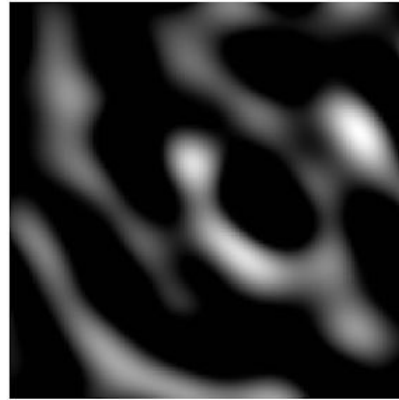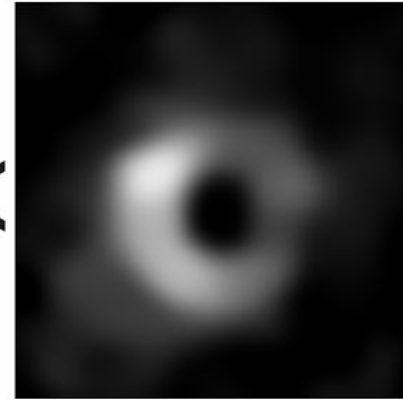
Unlikely < More Likely < Very Likely ✓
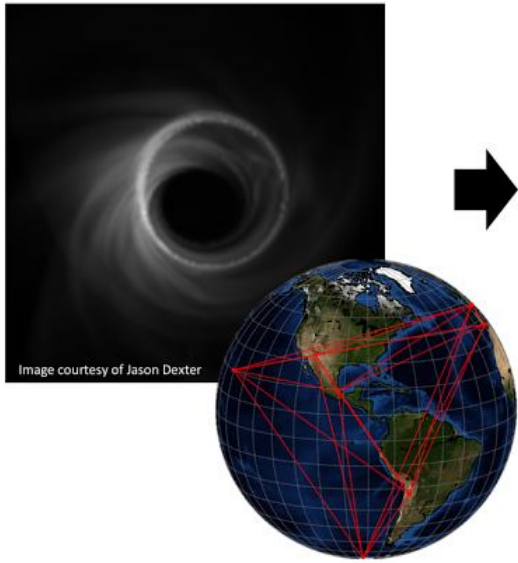
Measurements

Reconstruction

Image courtesy of Jason Dexter
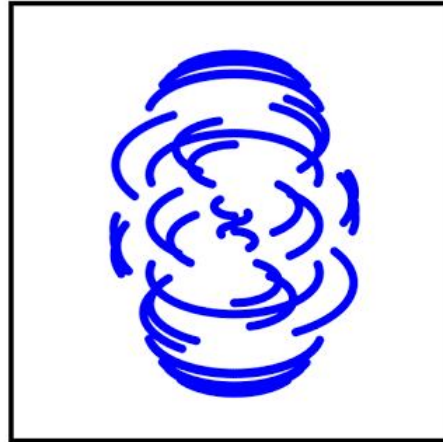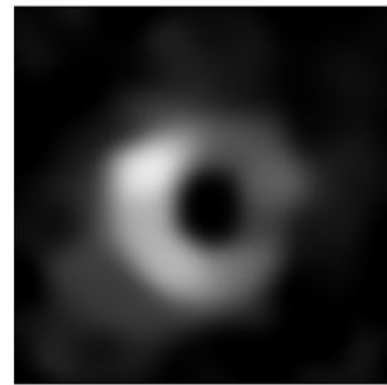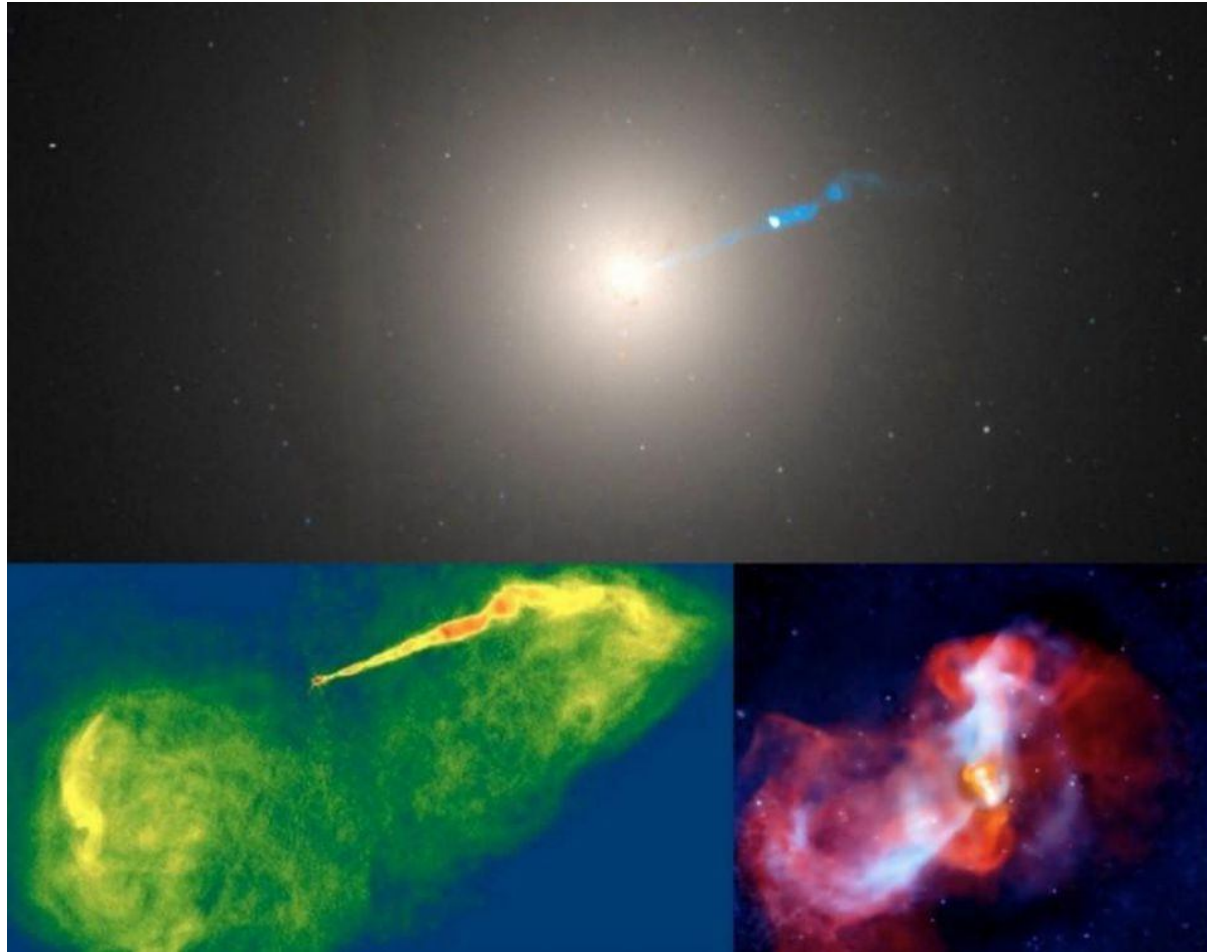
EHT results in brief

- **First M87 Event Horizon Telescope Results. I. The Shadow of the Supermassive Black Hole, ApJL 875 L1.**

- To image and study this phenomenon, we have assembled the Event Horizon Telescope, a global very long baseline interferometry array observing at a wavelength of 1.3 mm. This allows us to reconstruct event-horizon-scale images of the supermassive black hole candidate in the center of the giant elliptical galaxy M87. We have resolved the central compact radio source as an asymmetric bright emission ring with a diameter of 42±3 μas. derive a central mass of $M_{BH}=(6.5\pm0.7)\times10^9 M_{Sun}$.

- In many AGNs, collimated relativistic plasma jets (Bridle & Perley 1984; Zensus 1997) launched by the central black hole contribute to the observed emission. These jets may be powered either by magnetic fields threading the event horizon,

- extracting the rotational energy from the black hole (Blandford & Znajek 1977), or from the accretion flow (Blandford & Payne 1982). The near-horizon emission from low-luminosity active galactic nuclei (LLAGNs; Ho 1999) is produced by

- synchrotron radiation that peaks from the radio through the far infrared. This emission may be produced either in the accretion flow (Narayan et al. 1995), the jet (Falcke et al. 1993), or both (Yuan et al. 2002).
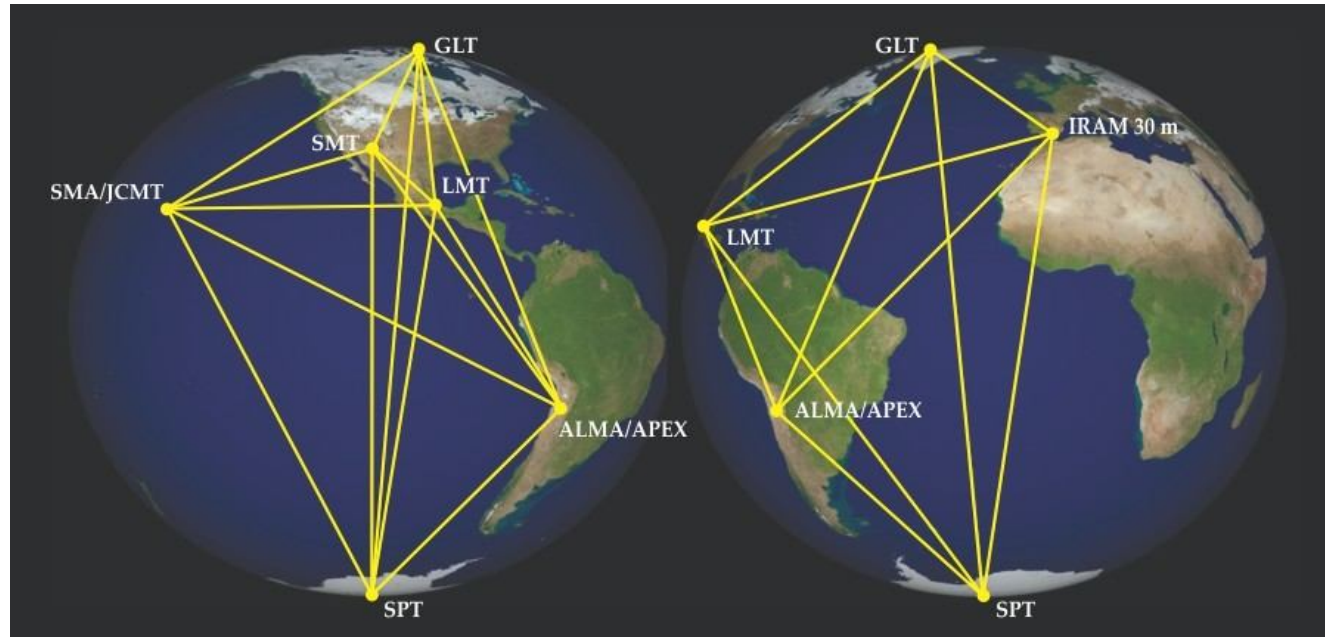
*Figure 2. **The Event Horizon Telescope** is a global array of millimeter telescopes (see http://eventhorizontelescope.org/array) that aims to take the first pictures of black holes. (Courtesy of Dan Marrone/University of Arizona.)*

Event Horizon Telescope (EHT)
A Global Network of Radio Telescopes

2018 Observatories

ALMA		Atacama Large Millimeter/submillimeter Array — CHAJNANTOR PLATEAU, CHILE
APEX		Atacama Pathfinder EXperiment — CHAJNANTOR PLATEAU, CHILE
30-M		IRAM 30-M Telescope — PICO VELETA, SPAIN
JCMT		James Clerk Maxwell Telescope — MAUNAKEA, HAWAII
LMT		Large Millimeter Telescope — SIERRA NEGRA, MEXICO
SMA		Submillimeter Array — MAUNAKEA, HAWAII
SMT		Submillimeter Telescope — MOUNT GRAHAM, ARIZONA
SPT		South Pole Telescope — SOUTH POLE STATION
GLT		The Greenland Telescope — THULE AIR BASE, GREENLAND, DENMARK

Observing in 2020

Kitt Peak		Kitt Peak 12-meter Telescope — KITT PEAK, ARIZONA, USA
NOEMA		NOEMA Observatory — PLATEAU DE BURE, FRANCE

Map labels: GLT, NOEMA, 30-M, SMT, Kitt Peak, JCMT, SMA, LMT, ALMA, APEX, SPT

NSF · AUI · NRAO

M87* black hole appearance in 2009-2017

MODELS

2009 2011 2012 2013

IMAGE

2017

40 μas

CARMA
SMT
JCMT

SMA
CSO
JCMT
CARMA
SMT

SMA
CARMA
SMT

SMA
JCMT
CARMA
SMT
APEX

SMA
JCMT
SMT
LMT
IRAM 30m
ALMA
APEX
SPT

Credit: M. Wielgus, D. Pesce
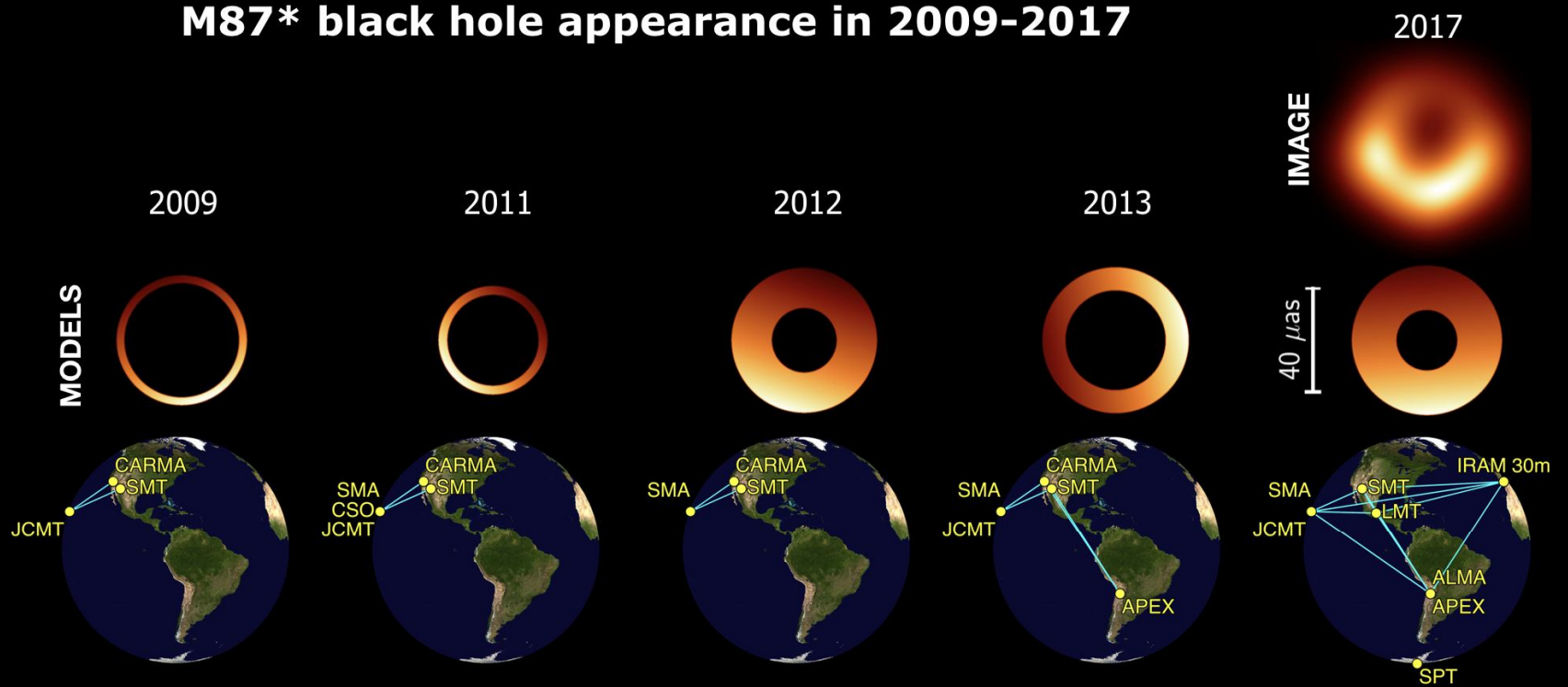
Event Horizon Telescope

Credit: M. Wielgus, D. Pesce
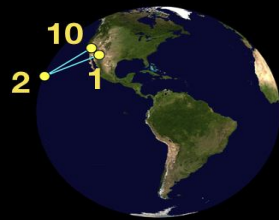
Event Horizon Telescope

2009-2012

2013

2017
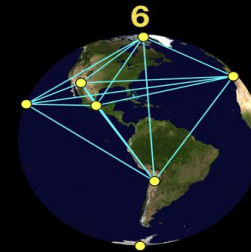
2018

2021

The EHT array observing M87*

1. **Mt Graham, Arizona, USA**
   SMT: Submillimeter Telescope (since 2009)
2. **Maunakea, Hawai'i, USA**
   JCMT: James Clerk Maxwell Telescope (since 2009)
   SMA: Submillimeter Array (since 2011)
   CSO: Caltech Submillimeter Observatory (2011)
3. **Atacama, Chile**
   APEX: Atacama Pathfinder Experiment (since 2013)
   ALMA: Atacama Large Millimeter/submillimeter Array (since 2017)
4. **Sierra Negra, Mexico**
   LMT: Large Millimeter Telescope Alfonso Serrano (since 2017)
5. **Pico Veleta, Spain**
   IRAM 30m: IRAM 30-meter telescope (since 2017)
6. **Thule, Greenland**
   GLT: Greenland Telescope (since 2018)
7. **Plateau de Bure, France**
   NOEMA: NOrthern Extended Millimeter Array (since 2021)
8. **Kitt Peak, Arizona, USA**
   KP: ARO 12m Radio Telescope (since 2021)

9. **South Pole**
   SPT: South Pole Telescope (since 2017, not directly observing M87*)
10. **Cedar Flat, California, USA**
    CARMA: Combined Array for Research in Millimeter-wave Astronomy (2009-2013)

Model Comparison and Parameter Estimation

Table 1
Parameters of M87*

Parameter	Estimate
Ring diameter [a] d	$42 \pm 3\ \mu$as
Ring width [a]	$<20\ \mu$as
Crescent contrast [b]	$>10:1$
Axial ratio [a]	$<4:3$
Orientation PA	$150°$–$200°$ east of north
$\theta_g = GM/Dc^2$ [c]	$3.8 \pm 0.4\ \mu$as
$\alpha = d/\theta_g$ [d]	$11^{+1.1}_{-0.3}$
M [c]	$(6.5 \pm 0.7) \times 10^9\ M_\odot$

Parameter	Prior Estimate
D [e]	(16.8 ± 0.8) Mpc
M(stars) [e]	$6.2^{+1.1}_{-0.6} \times 10^9\ M_\odot$
M(gas) [e]	$3.5^{+0.9}_{-0.3} \times 10^9\ M_\odot$

Notes.
[a] Derived from the image domain.
[b] Derived from crescent model fitting.
[c] The mass and systematic errors are averages of the three methods (geometric models, GRMHD models, and image domain ring extraction).
[d] The exact value depends on the method used to extract d, which is reflected in the range given.
[e] Rederived from likelihood distributions (Paper VI).

procedure, we infer values of θ_g and α for regularized maximum likelihood and CLEAN reconstructed images.

Combining results from all methods, we measure emission region diameters of $42 \pm 3\ \mu$as, angular sizes of the gravitational radius $\theta_g = 3.8 \pm 0.4\ \mu$as, and scaling factors in the range $\alpha = 10.7$–11.5, with associated errors of $\sim 10\%$. For the distance of 16.8 ± 0.8 Mpc adopted here, the black hole mass is $M = (6.5 \pm 0.7) \times 10^9\ M_\odot$; the systematic error refers to the 68% confidence level and is much larger than the statistical error of $0.2 \times 10^9\ M_\odot$. Moreover, by tracing the peak of the emission in the ring we can determine the shape of the image and obtain a ratio between major and minor axis of the ring that is $\lesssim 4:3$; this corresponds to a $\lesssim 10\%$ deviation from circularity in terms of root-mean-square distance from an average radius.

Table 1 summarizes the measured parameters of the image features and the inferred black hole properties based on data from all bands and all days combined. The inferred black hole mass strongly favors the measurement based on stellar dynamics (Gebhardt et al. 2011). The size, asymmetry, brightness contrast, and circularity of the reconstructed images and geometric models, as well as the success of the GRMHD simulations in describing the interferometric data, are consistent with the EHT images of M87* being associated with strongly lensed emission from the vicinity of a Kerr black hole.

8. Discussion

A number of elements reinforce the robustness of our image

our measurement of the black hole mass in M87* is not inconsistent with all of the prior mass measurements, this allows us to conclude that the null hypothesis of the Kerr metric (Psaltis et al. 2015; Johannsen et al. 2016), namely, the assumption that the black hole is described by the Kerr metric, has not been violated. Fourth, the observed emission ring reconstructed in our images is close to circular with an axial ratio $\lesssim 4:3$; similarly, the time average images from our GRMHD simulations also show a circular shape. After associating to the shape of the shadow a deviation from the circularity—measured in terms of root-mean-square distance from an average radius in the image—that is $\lesssim 10\%$, we can set an initial limit of order four on relative deviations of the quadrupole moment from the Kerr value (Johannsen & Psaltis 2010). Stated differently, if Q is the quadrupole moment of a Kerr black hole and ΔQ the deviation as deduced from circularity, our measurement—and the fact that the inclination angle is assumed to be small—implies that $\Delta Q/Q \lesssim 4$ ($\Delta Q/Q = \varepsilon$ in Johannsen & Psaltis 2010).

Finally, when comparing the visibility amplitudes of M87* with 2009 and 2012 data (Doeleman et al. 2012; Akiyama et al. 2015), the overall radio core size at a wavelength of 1.3 mm has not changed appreciably, despite variability in total flux density. This stability is consistent with the expectation that the size of the shadow is a feature tied to the mass of the black hole and not to properties of a variable plasma flow.

It is also straightforward to reject some alternative astrophysical interpretations. For instance, the image is unlikely to be produced by a jet-feature as multi-epoch VLBI observations of the plasma jet in M87 (Walker et al. 2018) on scales outside the horizon do not show circular rings. The same is typically true for AGN jets in large VLBI surveys (Lister et al. 2018). Similarly, were the apparent ring a random alignment of emission blobs, they should also have moved away at relativistic speeds, i.e., at $\sim 5\ \mu$as day^{-1} (Kim et al. 2018b), leading to measurable structural changes and sizes. GRMHD models of hollow jet cones could show under extreme conditions stable ring features (Pu et al. 2017), but this effect is included to a certain extent in our Simulation Library for models with $R_{high} > 10$. Finally, an Einstein ring formed by gravitational lensing of a bright region in the counter-jet would require a fine-tuned alignment and a size larger than that measured in 2012 and 2009.

At the same time, it is more difficult to rule out alternatives to black holes in GR, because a shadow can be produced by any compact object with a spacetime characterized by unstable circular photon orbits (Mizuno et al. 2018). Indeed, while the Kerr metric remains a solution in some alternative theories of gravity (Barausse & Sotiriou 2008; Psaltis et al. 2008), non-Kerr black hole solutions do exist in a variety of such modified theories (Berti et al. 2015). Furthermore, exotic alternatives to black holes, such as naked singularities (Shaikh et al. 2019), boson stars (Kaup 1968; Liebling & Palenzuela 2012), and gravastars (Mazur & Mottola 2004; Chirenti & Rezzolla 2007), are admissible solutions within GR and provide concrete, albeit

As it was explained by Zakharov et al. (2005a,b) this leads to the formation of shadows described by the critical value of L_{cr} or, in other words, in the spherically symmetric case, shadows are circles with radii L_{cr}. Therefore, measuring the shadow size, one could evaluate the black hole charge in black hole mass units M.
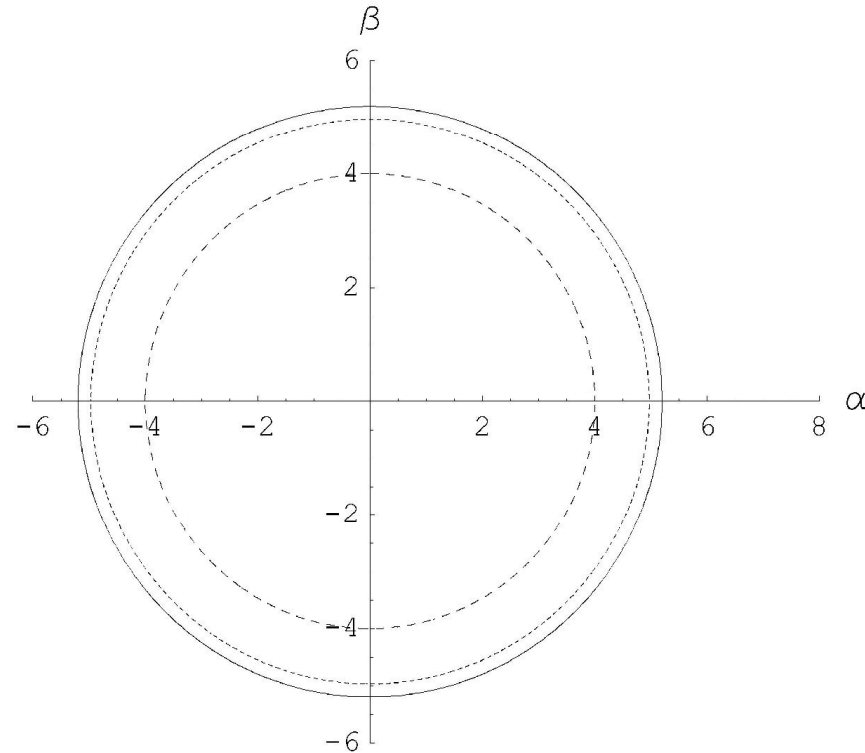

Fig. 1. Shadow (mirage) sizes are shown for selected charges of black holes $Q = 0$ (solid line), $Q = 0.5$ (short dashed line) and $Q = 1$ (long dashed line).

Constraints on black-hole charges with the 2017 EHT observations of M87*

Prashant Kocherlakota[1], Luciano Rezzolla,[1–3] Heino Falcke,[4] Christian M. Fromm,[5,6,1] Michael Kramer,[7]
Yosuke Mizuno,[8,9] Antonios Nathanail,[9,10] Héctor Olivares,[4] Ziri Younsi,[11,9] Kazunori Akiyama,[12,13,5] Antxon Alberdi,[14]
Walter Alef,[7] Juan Carlos Algaba,[15] Richard Anantua,[5,6,16] Keiichi Asada,[17] Rebecca Azulay,[18,19,7] Anne-Kathrin Baczko,[7]
David Ball,[20] Mislav Baloković,[5,6] John Barrett,[12] Bradford A. Benson,[21,22] Dan Bintley,[23] Lindy Blackburn,[5,6]
Raymond Blundell,[6] Wilfred Boland,[24] Katherine L. Bouman,[5,6,25] Geoffrey C. Bower,[26] Hope Boyce,[27,28]
Michael Bremer,[29] Christiaan D. Brinkerink,[4] Roger Brissenden,[5,6] Silke Britzen,[7] Avery E. Broderick,[30–32]
Dominique Broguiere,[29] Thomas Bronzwaer,[4] Do-Young Byun,[33,34] John E. Carlstrom,[35,22,36,37] Andrew Chael,[38,39]
Chi-kwan Chan,[20,40] Shami Chatterjee,[41] Koushik Chatterjee,[42] Ming-Tang Chen,[26] Yongjun Chen (陈永军),[43,44]
Paul M. Chesler,[5] Ilje Cho,[33,34] Pierre Christian,[45] John E. Conway,[46] James M. Cordes,[41] Thomas M. Crawford,[22,35]
Geoffrey B. Crew,[12] Alejandro Cruz-Osorio,[9] Yuzhu Cui,[47,48] Jordy Davelaar,[49,16,4] Mariafelicia De Laurentis,[50,9,51]
Roger Deane,[52–54] Jessica Dempsey,[23] Gregory Desvignes,[55] Sheperd S. Doeleman,[5,6] Ralph P. Eatough,[56,7]
Joseph Farah,[6,5,57] Vincent L. Fish,[12] Ed Fomalont,[58] Raquel Fraga-Encinas,[4] Per Friberg,[23] H. Alyson Ford,[59]
Antonio Fuentes,[14] Peter Galison,[5,60,61] Charles F. Gammie,[62,63] Roberto García,[29] Olivier Gentaz,[29] Boris Georgiev,[31,32]
Ciriaco Goddi,[4,64] Roman Gold,[65,30] José L. Gómez,[14] Arturo I. Gómez-Ruiz,[66,67] Minfeng Gu (顾敏峰),[43,68]
Mark Gurwell,[6] Kazuhiro Hada,[47,48] Daryl Haggard,[27,28] Michael H. Hecht,[12] Ronald Hesper,[69] Luis C. Ho (何子山),[70,71]
Paul Ho,[17] Mareki Honma,[47,48,72] Chih-Wei L. Huang,[17] Lei Huang (黄磊),[43,68] David H. Hughes,[66] Shiro Ikeda,[13,73–75]
Makoto Inoue,[17] Sara Issaoun,[4] David J. James,[5,6] Buell T. Jannuzi,[20] Michael Janssen,[7] Britton Jeter,[31,32]
Wu Jiang (江悟),[43] Alejandra Jimenez-Rosales,[4] Michael D. Johnson,[5,6] Svetlana Jorstad,[76,77] Taehyun Jung,[33,34]
Mansour Karami,[30,31] Ramesh Karuppusamy,[7] Tomohisa Kawashima,[78] Garrett K. Keating,[6] Mark Kettenis,[79]
Dong-Jin Kim,[7] Jae-Young Kim,[33,7] Jongsoo Kim,[33] Junhan Kim,[20,25] Motoki Kino,[13,80] Jun Yi Koay,[17] Yutaro Kofuji,[47,72]
Patrick M. Koch,[17] Shoko Koyama,[17] Carsten Kramer,[29] Thomas P. Krichbaum,[7] Cheng-Yu Kuo,[81,17] Tod R. Lauer,[82]
Sang-Sung Lee,[33] Aviad Levis,[25] Yan-Rong Li (李彦荣),[83] Zhiyuan Li (李志远),[84,85] Michael Lindqvist,[46] Rocco Lico,[14,7]
Greg Lindahl,[6] Jun Liu (刘俊),[7] Kuo Liu,[7] Elisabetta Liuzzo,[86] Wen-Ping Lo,[17,87] Andrei P. Lobanov,[7] Laurent Loinard,[88,89]
Colin Lonsdale,[12] Ru-Sen Lu (路如森),[43,44,7] Nicholas R. MacDonald,[7] Jirong Mao (毛基荣),[90–92] Nicola Marchili,[86,7]
Sera Markoff,[42,93] Daniel P. Marrone,[20] Alan P. Marscher,[76] Iván Martí-Vidal,[18,19] Satoki Matsushita,[17]
Lynn D. Matthews,[12] Lia Medeiros,[94,20] Karl M. Menten,[7] Izumi Mizuno,[23] James M. Moran,[5,6] Kotaro Moriyama,[12,47]
Monika Moscibrodzka,[4] Cornelia Müller,[7,4] Gibwa Musoke,[42,4] Alejandro Mus Mejías,[18,19] Hiroshi Nagai,[13,48]
Neil M. Nagar,[95] Masanori Nakamura,[96,17] Ramesh Narayan,[5,6] Gopal Narayanan,[97] Iniyan Natarajan,[54,52,98]
Joseph Neilsen,[99] Roberto Neri,[29] Chunchong Ni,[31,32] Aristeidis Noutsos,[7] Michael A. Nowak,[100] Hiroki Okino,[47,72]
Gisela N. Ortiz-León,[7] Tomoaki Oyama,[47] Feryal Özel,[20] Daniel C. M. Palumbo,[5,6] Jongho Park,[17] Nimesh Patel,[6]
Ue-Li Pen,[30,101–103] Dominic W. Pesce,[5,6] Vincent Piétu,[29] Richard Plambeck,[104] Aleksandar PopStefanija,[97]
Oliver Porth,[42,9] Felix M. Pötzl,[7] Ben Prather,[62] Jorge A. Preciado-López,[30] Dimitrios Psaltis,[20] Hung-Yi Pu,[105,17,30]
Venkatessh Ramakrishnan,[95] Ramprasad Rao,[26] Mark G. Rawlings,[23] Alexander W. Raymond,[5,6] Angelo Ricarte,[5,6]
Bart Ripperda,[106,16] Freek Roelofs,[4] Alan Rogers,[12] Eduardo Ros,[7] Mel Rose,[20] Arash Roshanineshat,[20] Helge Rottmann,[7]
Alan L. Roy,[7] Chet Ruszczyk,[12] Kazi L. J. Rygl,[86] Salvador Sánchez,[107] David Sánchez-Arguelles,[66,67] Mahito Sasada,[47,108]
Tuomas Savolainen,[109,110,7] F. Peter Schloerb,[97] Karl-Friedrich Schuster,[29] Lijing Shao,[7,71] Zhiqiang Shen (沈志强),[43,44]
Des Small,[79] Bong Won Sohn,[33,34,111] Jason SooHoo,[12] He Sun (孙赫),[25] Fumie Tazaki,[47] Alexandra J. Tetarenko,[112]
Paul Tiede,[31,32] Remo P. J. Tilanus,[4,64,113,20] Michael Titus,[12] Kenji Toma,[114,115] Pablo Torne,[7,107] Tyler Trent,[20]
Efthalia Traianou,[7] Sascha Trippe,[116] Ilse van Bemmel,[79] Huib Jan van Langevelde,[79,117] Daniel R. van Rossum,[4]
Jan Wagner,[7] Derek Ward-Thompson,[118] John Wardle,[119] Jonathan Weintroub,[5,6] Norbert Wex,[7] Robert Wharton,[7]
Maciek Wielgus,[5,6] George N. Wong,[62] Qingwen Wu (吴庆文),[120] Doosoo Yoon,[42] André Young,[4] Ken Young,[6]
Feng Yuan (袁峰),[43,68,121] Ye-Fei Yuan (袁业飞),[122] J. Anton Zensus,[7] Guang-Yao Zhao,[14] and Shan-Shan Zhao[43]

(EHT Collaboration)

[1]*Institut für Theoretische Physik, Goethe-Universität,*
Max-von-Laue-Strasse 1, 60438 Frankfurt, Germany
[2]*Frankfurt Institute for Advanced Studies, Ruth-Moufang-Strasse 1, 60438 Frankfurt, Germany*
[3]*School of Mathematics, Trinity College, Dublin 2, Ireland*
[4]*Department of Astrophysics, Institute for Mathematics, Astrophysics and Particle Physics (IMAPP),*
Radboud University, P.O. Box 9010, 6500 GL Nijmegen, Netherlands
[5]*Black Hole Initiative at Harvard University, 20 Garden Street, Cambridge, Massachusetts 02138, USA*
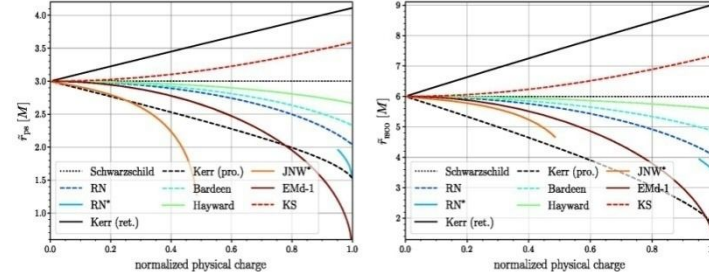
FIG. 1. Left: variation in the photon sphere radii for the single-charge nonrotating solutions as a function of the normalized physical charge. Right: The same as in the left panel but for the ISCO radii. We include also, for comparison, the variation in the Kerr equatorial prograde and retrograde photon sphere and ISCO radii in the left and right panels respectively.

depend exclusively on the g_{tt} component of the metric when expressed using an areal radial coordinate $\tilde{r}$ (see, e.g., [28,36]). To gauge the effect of spin, we also show the variation in the locations of the equatorial prograde and retrograde circular photon orbits and the ISCOs in the Kerr black-hole spacetime, expressed in terms of the Cartesian Kerr-Schild radial coordinate r_{CKS}, which, in the equatorial plane, is related to the Boyer-Lindquist radial coordinate used elsewhere in this work r simply via [90]

$$r_{CKS} = \sqrt{r^2 + a^2}. \tag{15}$$

It is apparent from Fig. 1 that the maximum deviation in the photon-sphere size from the Schwarzschild solution occurs for the EMd-1 black hole and is $\approx 75\%$, while the size of the prograde equatorial circular photon orbit for Kerr deviates by at most $\approx 50\%$. Similarly, the maximum variation in the ISCO size also occurs for the EMd-1 solution and is $\approx 73\%$, while the prograde equatorial ISCO for Kerr can differ by $\approx 66\%$.

V. CHARGE CONSTRAINTS FROM THE EHT M87* OBSERVATIONS

We first consider compact objects with a single "charge," and report in the left panel of Fig. 2 the variation in the shadow radius for various spherically symmetric black hole solutions, as well as for the RN and JNW naked singularities.[3] More specifically, we consider the black-hole

---

[3]While the electromagnetic and scalar charge parameters for the RN and JNW spacetimes are allowed to take values $\bar{q} > 1$ and $0 < \hat{\nu} := 1 - \bar{\nu} < 1$ respectively, they do not cast shadows for $\bar{q} > \sqrt{9/8}$ and $0.5 \leq \hat{\nu} < 1$ (see, e.g., Sec. IV D of [36] and references therein).

solutions given by Reissner-Nordström (RN) [62], Bardeen [63,75], Hayward [64,91], Kazakov-Solodhukin (KS) [66], and also the asymptotically-flat Einstein-Maxwell-dilaton (EMd-1) with $\phi_\infty = 0$ and $\alpha_1 = 1$ [67,68,88] solution (see Sec. IV of [36] for further details on these solutions). For each of these solutions we vary the corresponding charge (in units of M) in the allowed range, i.e., RN: $0 < \bar{q} \leq 1$; Bardeen: $0 < \bar{q}_m \leq \sqrt{16/27}$; Hayward: $0 < \bar{l} \leq \sqrt{16/27}$; Frolov: $0 < \bar{l} \leq \sqrt{16/27}$, $0 < \bar{q} \leq 1$; KS: $0 < \bar{l}$; EMd-1: $0 < \bar{q} < \sqrt{2}$, but report the normalized value in the figure so that all curves are in a range between 0 and 1. The figure shows the variation in the shadow size of KS black holes over the parameter range $0 < \bar{l} < \sqrt{2}$. Note that the shadow radii tend to become smaller with increasing physical charge, but also that this is not universal behavior, since the KS black holes have increasing shadow radii (the singularity is smeared out on a surface for this solution, which increases in size with increasing $\bar{l}$).

Overall, it is apparent that the regular Bardeen, Hayward, and Frolov black-hole solutions are compatible with the present constraints. At the same time, the Reissner-Nordström and Einstein-Maxwell-dilaton 1 black-hole solutions, for certain values of the physical charge, produce shadow radii that lie outside the 1-σ region allowed by the 2017 EHT observations, and we find that these solutions are now constrained to take values in, $0 < \bar{q} \lesssim 0.90$ and $0 < \bar{q} \lesssim 0.95$ respectively. Furthermore, the Reissner-Nordström naked singularity is entirely eliminated as a viable model for M87* and the Janis-Newman-Winicour naked singularity parameter space is restricted further by this measurement to $0 < \hat{\nu} \lesssim 0.47$. Finally, we also find that the KS black hole is also restricted to have charges in the range $\bar{l} < 1.53$. In addition, note that the nonrotating Einstein-Maxwell-dilaton 2 (EMd-2) solution [70]—which depends on two
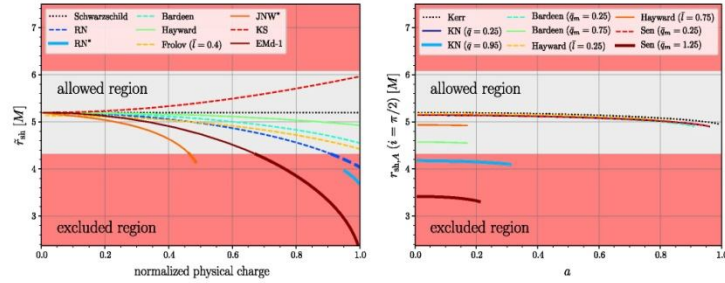
FIG. 2. Left: shadow radii $\bar{r}_{sh}$ for various spherically symmetric black-hole solutions, as well as for the JNW and RN naked singularities (marked with an asterisk), as a function of the physical charge normalized to its maximum value. The gray/red shaded regions refer to the areas that are 1-σ consistent/inconsistent with the 2017 EHT observations and highlight that the latter set constraints on the physical charges (see also Fig. 3 for the EMd-2 black hole). Right: shadow areal radii $r_{sh,A}$ as a function of the dimensionless spin a for four families of black-hole solutions when viewed on the equatorial plane ($i = \pi/2$). Also in this case, the observations restrict the ranges of the physical charges of the Kerr-Newman and the Sen black holes (see also Fig. 3).

independent charges—can also produce shadow radii that are incompatible with the EHT observations; we will discuss this further below. The two EMd black-hole solutions (1 and 2) correspond to fundamentally different field contents, as discussed in [70].

We report in the right panel of Fig. 2 the shadow areal radius $r_{sh,A}$ for a number of stationary black holes, such as Kerr [72], Kerr-Newman (KN) [73], Sen [74], and the rotating versions of the Bardeen and Hayward black holes [75]. The data refers to an observer inclination angle of $i = \pi/2$, and we find that the variation in the shadow size with spin at higher inclinations (of up to $i = \pi/100$) is at most about 7.1% (for $i = \pi/2$, this is 5%); of course, at zero-spin the shadow size does not change with inclination. The shadow areal radii are shown as a function of the dimensionless spin of the black hole $a := J/M^2$, where J is its angular momentum, and for representative values of the additional parameters that characterize the solutions. Note that—similar to the angular momentum for a Kerr black hole—the role of an electric charge or the presence of a de Sitter core (as in the case of the Hayward black holes) is to reduce the apparent size of the shadow. Furthermore, on increasing the spin parameter, we recover the typical trend that the shadow becomes increasingly noncircular, as encoded, e.g., in the distortion parameter δ_{sh} defined in [57,83] (see Appendix). Also in this case, while the regular rotating Bardeen and Hayward solutions are compatible with the present constraints set by the 2017 EHT observations, the Kerr-Newman and Sen families of black holes can produce shadow areal radii that lie outside of the 1-σ region allowed by the observations.

To further explore the constraints on the excluded regions for the Einstein-Maxwell-dilaton 2 and the Sen black holes, we report in Fig. 3 the relevant ranges for these two solutions. The Einstein-Maxwell-dilaton 2 black holes are nonrotating but have two physical charges expressed by the coefficients $0 < \bar{q}_e < \sqrt{2}$ and $0 < \bar{q}_m < \sqrt{2}$, while the Sen black holes spin (a) and have an additional electromagnetic charge $\bar{q}_m$. Also in this case, the gray/red shaded regions refer to the areas that are consistent/inconsistent with the 2017 EHT observations. The figure shows rather easily that for these two black-hole families there are large
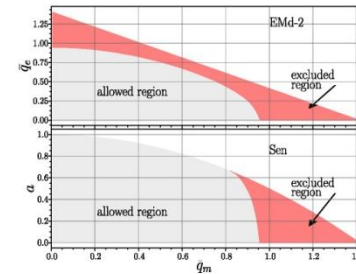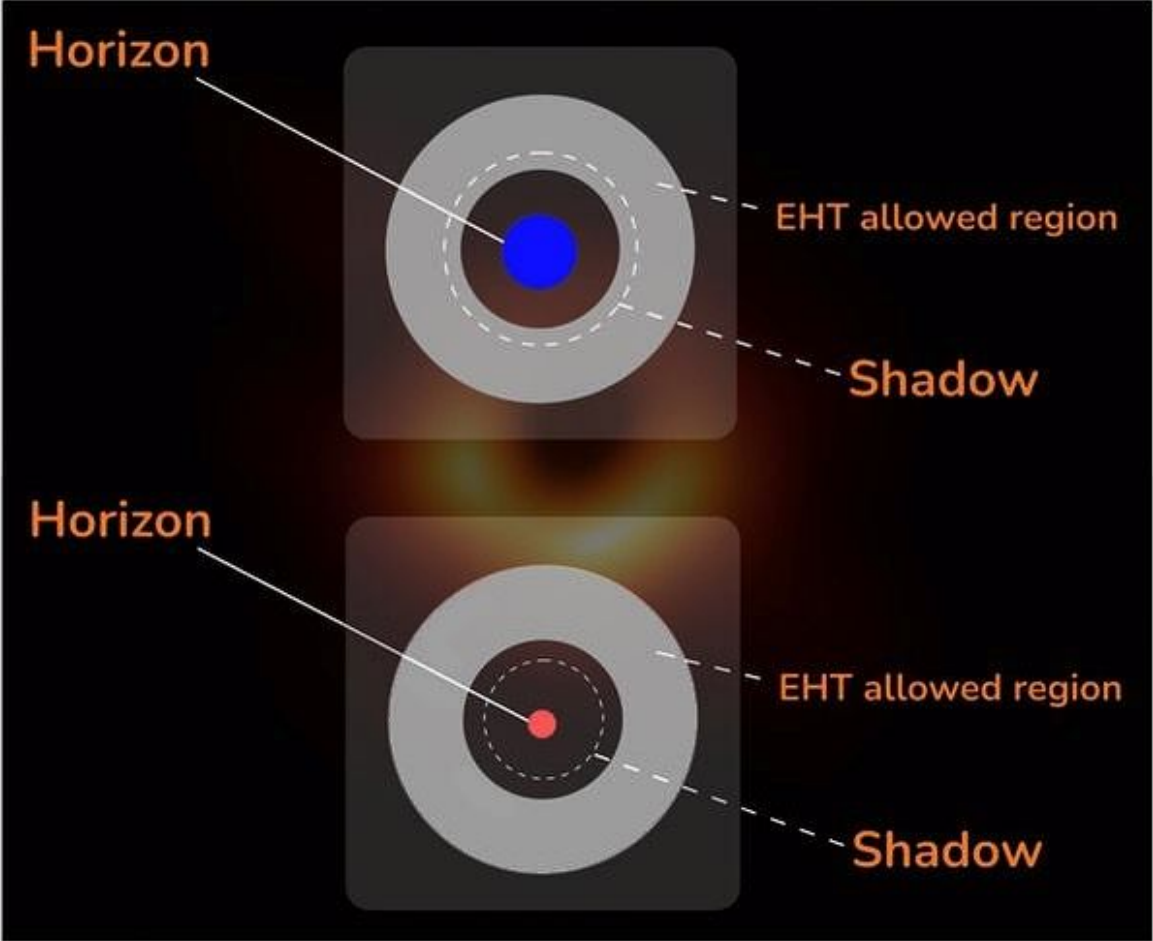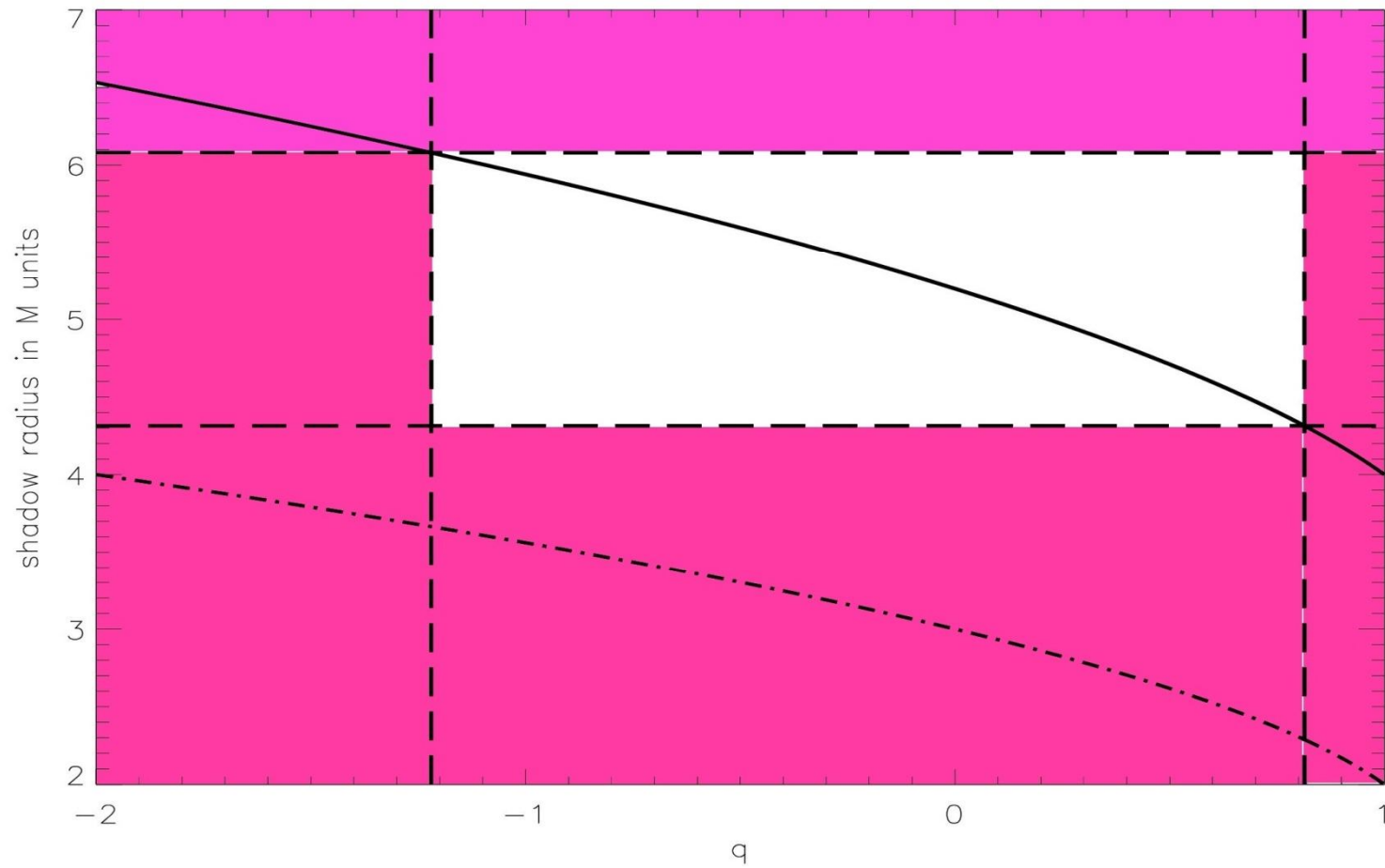

FIG. 3. Constraints set by the 2017 EHT observations on the nonrotating Einstein-Maxwell-dilaton 2 and on the rotating Sen black holes. Also in this case, the gray/red shaded regions refer to the areas that are 1-σ consistent/inconsistent with the 2017 EHT observations).

arxiv:2108.01533

First M87 Event Horizon Telescope Results. VII.
Polarization of the Ring

The Event Horizon Telescope Collaboration

(See the end matter for the full list of authors.)

Abstract

In 2017 April, the Event Horizon Telescope (EHT) observed the near-horizon region around the supermassive black hole at the core of the M87 galaxy. These 1.3 mm wavelength observations revealed a compact asymmetric ring-like source morphology. This structure originates from synchrotron emission produced by relativistic plasma located in the immediate vicinity of the black hole. Here we present the corresponding linear-polarimetric EHT images of the center of M87. We find that only a part of the ring is significantly polarized. The resolved fractional linear polarization has a maximum located in the southwest part of the ring, where it rises to the level of ~15%. The polarization position angles are arranged in a nearly azimuthal pattern. We perform quantitative measurements of relevant polarimetric properties of the compact emission and find evidence for the temporal evolution of the polarized source structure over one week of EHT observations. The details of the polarimetric data reduction and calibration methodology are provided. We carry out the data analysis using multiple independent imaging and modeling techniques, each of which is validated against a suite of synthetic data sets. The gross polarimetric structure and its apparent evolution with time are insensitive to the method used to reconstruct the image. These polarimetric images carry information about the structure of the magnetic fields responsible for the synchrotron emission. Their physical interpretation is discussed in an accompanying publication.

Unified Astronomy Thesaurus concepts: Polarimetry (1278); Radio interferometry (1346); Very long baseline interferometry (1769); Supermassive black holes (1663); Active galactic nuclei (16); Low-luminosity active galactic nuclei (2033); Astronomy data modeling (1859); Galaxy accretion disks (562); Galaxies: individual: M87

1. Introduction

The Event Horizon Telescope (EHT) Collaboration has recently reported the first images of the event-horizon-scale structure around the supermassive black hole in the core of the massive elliptical galaxy M87, one of its two main targets.[130] The EHT images of M87's core at 230 GHz (1.3 mm wavelength) revealed a ring-like structure whose diameter of 42 μas, brightness temperature, shape, and asymmetry are interpreted as synchrotron emission from relativistic electrons gyrating around magnetic field lines in close vicinity to the event horizon. We have described the details of the EHT's instrumentation, data calibration pipelines, data analyses and imaging procedures, and the theoretical interpretation of these first images in a series of publications (Event Horizon Telescope Collaboration et al. 2019a, 2019b, 2019c, 2019d, 2019e, 2019f, hereafter Papers I, II, III, IV, V, VI, respectively).

In this Letter, we present the first *polarimetric* analysis of the 2017 EHT observations of M87 and the first images of the linearly polarized radiation surrounding the M87 black hole shadow. These polarimetric images provide essential new information about the structure of magnetic field lines near the event horizon of M87's central supermassive black hole, and they put tight constraints on the theoretical interpretations of the nature of the ring and of relativistic jet-launching theories. The theoretical implications of these images and the constraints that they place on the magnetic field structure and accretion state of the black hole are discussed in an accompanying work (Event Horizon Telescope Collaboration et al. 2021, hereafter Paper VIII). Readers interested in the details of the data reduction, methodology, and validation can find a detailed index of this Letter in Section 1.2. Readers primarily interested in the results may skip directly to Section 5 and to subsequent discussion and conclusions in Section 6.

1.1. Previous Polarimetric Observations of the M87 Jet

The giant elliptical galaxy Messier 87 (M87, NGC 4486) is the central member of the Virgo cluster of galaxies and hosts a low-luminosity radio source (Virgo A, 3C 274, B1228+126). M87 is nearby and bright, and at its center is one of the best-studied active galactic nuclei (AGNs). M87 was the first galaxy in which an extragalactic jet (first described as a "narrow ray") extending from the nucleus was discovered (Curtis 1918). This kiloparsec-scale jet is visible, with remarkably similar morphology, at all wavelengths from radio to X-ray. The optical radiation from the jet on kpc scales was found to be linearly polarized by Baade (1956), which was confirmed by Hiltner (1959), suggesting that the emission mechanism is synchrotron radiation.

The central engine that powers the jet contains one of the most massive black holes known, measured from the central stellar velocity dispersion (Gebhardt et al. 2011; $M = (6.6 \pm 0.4) \times 10^9 M_\odot$) and directly from the size of the observed emitting

---

[127] NASA Hubble Fellowship Program, Einstein Fellow.
[128] EACOA Fellow.
[129] UKRI Stephen Hawking Fellow.
[130] The other primary target being the black hole in Sgr A* in the center of the Milky Way.

First M87 Event Horizon Telescope Results. VIII.
Magnetic Field Structure near The Event Horizon

The Event Horizon Telescope Collaboration
(See the end matter for the full list of authors.)

Abstract

Event Horizon Telescope (EHT) observations at 230 GHz have now imaged polarized emission around the supermassive black hole in M87 on event-horizon scales. This polarized synchrotron radiation probes the structure of magnetic fields and the plasma properties near the black hole. Here we compare the resolved polarization structure observed by the EHT, along with simultaneous unresolved observations with the Atacama Large Millimeter/submillimeter Array, to expectations from theoretical models. The low fractional linear polarization in the resolved image suggests that the polarization is scrambled on scales smaller than the EHT beam, which we attribute to Faraday rotation internal to the emission region. We estimate the average density $n_e \sim 10^{4-7}\,\mathrm{cm}^{-3}$, magnetic field strength $B \sim$ 1–30 G, and electron temperature $T_e \sim (1\text{–}12) \times 10^{10}$ K of the radiating plasma in a simple one-zone emission model. We show that the net azimuthal linear polarization pattern may result from organized, poloidal magnetic fields in the emission region. In a quantitative comparison with a large library of simulated polarimetric images from general relativistic magnetohydrodynamic (GRMHD) simulations, we identify a subset of physical models that can explain critical features of the polarimetric EHT observations while producing a relativistic jet of sufficient power. The consistent GRMHD models are all of magnetically arrested accretion disks, where near-horizon magnetic fields are dynamically important. We use the models to infer a mass accretion rate onto the black hole in M87 of $(3\text{–}20) \times 10^{-4}\,M_\odot\,\mathrm{yr}^{-1}$.

Unified Astronomy Thesaurus concepts: Accretion (14); Black holes (162); Event horizons (479); Jets (870); Kerr black holes (886); Magnetic fields (994); Magnetohydrodynamics (1964); Plasma astrophysics (1261); Polarimetry (1278); Radiative transfer (1335); Radio jets (1347); Relativistic jets (1390)

1. Introduction

The Event Horizon Telescope (EHT) Collaboration has recently published total intensity images of event-horizon-scale emission around the supermassive black hole in the core of the M87 galaxy (M87*; Event Horizon Telescope Collaboration et al. 2019a, 2019b, 2019c, 2019d, hereafter EHTC I, EHTC II, EHTC III, EHTC IV). The data reveal a $42 \pm 3~\mu$as diameter ring-like structure that is broadly consistent with the shadow of a black hole as predicted by Einstein's Theory of General Relativity (Event Horizon Telescope Collaboration et al. 2019e, 2019f; hereafter EHTC V, EHTC VI). The brightness temperature of the ring at 230 GHz ($\gtrsim 10^{10}$ K) is naturally explained by synchrotron emission from relativistic electrons gyrating around magnetic field lines. The ring brightness asymmetry results from light bending and Doppler beaming due to relativistic rotation of the matter around the black hole.

M87* is best known for launching a kpc-scale FR-I type relativistic jet, whose kinetic power is estimated to be $\sim 10^{42-44}$ erg s^{-1} (e.g., Stawarz et al. 2006; de Gasperin et al. 2012). The structure of the relativistic jet has been resolved and studied at radio to X-ray wavelengths (e.g., Di Matteo et al. 2003; Harris et al. 2009; Kim et al. 2018; Walker et al. 2018).

The published EHT image of M87* together with multi-wavelength observations are consistent with the picture that the supermassive black hole in M87 is surrounded by a relativistically hot, magnetized plasma (Rees et al. 1982; Narayan & Yi 1995; Narayan et al. 1995; Yuan & Narayan 2014; Reynolds et al. 1996; Yuan et al. 2002; Di Matteo et al. 2003). However, it is not clear whether the compact ring emission is produced by plasma that is inflowing (in a thick accretion flow), outflowing (at the jet base or in a wind), or both. Furthermore, the total intensity EHT observations also could not constrain the structure of magnetic fields in the observed emission region. In order to find out which physical scenario is realized in M87*, additional information is necessary.

Event Horizon Telescope Collaboration et al. (2021, hereafter EHTC VII) reports new results from the polarimetric EHT 2017 observations of M87*. The polarimetric images of M87* are reproduced in Figure 1. These images reveal that a significant fraction of the ring emission is linearly polarized, as expected for synchrotron radiation. The EHT polarimetric measurements are consistent with unresolved observations of the radio core at the same frequency with the Submillimeter Array (SMA; Kuo et al. 2014) and the Atacama Large Millimeter/submillimeter Array (ALMA; Goddi et al. 2021). They also provide a detailed view of the polarized emission region on event-horizon scales near the black hole. Polarized synchrotron radiation traces the underlying magnetic field

---

[126] NASA Hubble Fellowship Program, Einstein Fellow.
[127] EACOA Fellow.
[128] UKRI Stephen Hawking Fellow.

• Conclusions

- GR predicted a structure of darkness, while in observations one sees a distribution of brightness due to synchrotron emission and there are a number of accretion model.

- EHT team showed that shapes and sizes of shadow weakly depend on assumptions about accretion flows.

- AZ et al. (2004-2019):VLBI systems in mm and sub-mm bands could detect mirages ("faces") around supermassive black holes (for BH@ M87 and BH@GC in particular).

- VLBI systems in mm band detected a shadow around supermassive black hole for BH@ M87 .

- Shapes of images give an important information about BH parameters (including their charge).

- A significant tidal charge of the BH at GC (and at M87) is excluded by observations.

- Quantum (tidal) charges could be constrainted at M87* (and at Sgr A*)

- We hope the EHT team will release a new image of the SMBH@GC shortly at 1.3 mm wavelength shortly.

- Thanks for your kind attention!

-

- H. Falcke, S. Markoff, Toward the event horizon—the supermassive black hole in the Galactic Center, Classical and Quantum Gravity, 30, Issue 24, 244003 (2013)

- The review has quoted two our papers